Improved Energy Calibration for BGO Calorimeter in DAMPE

Cong ZHAO（赵聪）

University of Science and Technology of China

DAMPE Electron Analysis Meeting

Hefei, Feb. 9–13, 2026

Outline

- Overview
- Fluorescence Position-Independent Calibration
- MIPs Calibration
- Dynode Ratio Calibration of PMTs
- The Response to Cosmic-Ray Electron Candidates

Energy Measurement of Unit

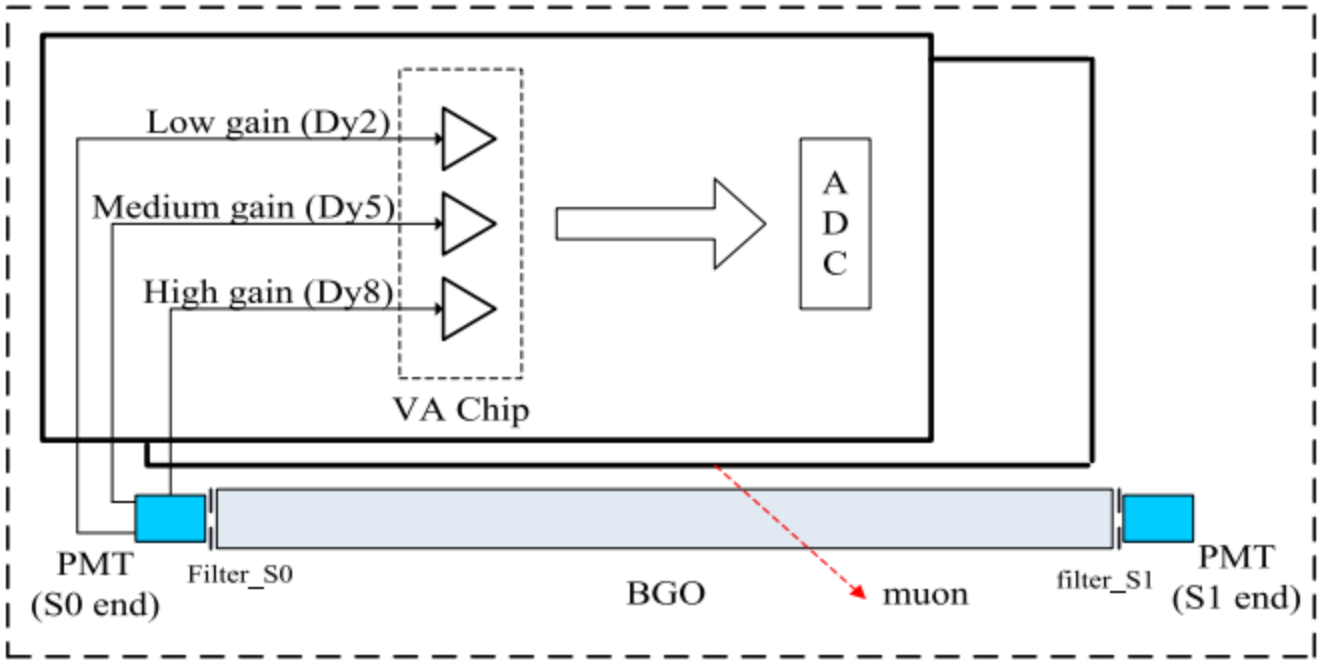

Two-end readout:

S0 end (Positive): higher energy precision

S1 end (Negative): higher energy upper limits

Multi-dynode PMT readout:
Dy8: High gain
Dy5: Medium gain
Dy2: Low gain

Dual-end multi-dynode readout

Energy Calibration Process

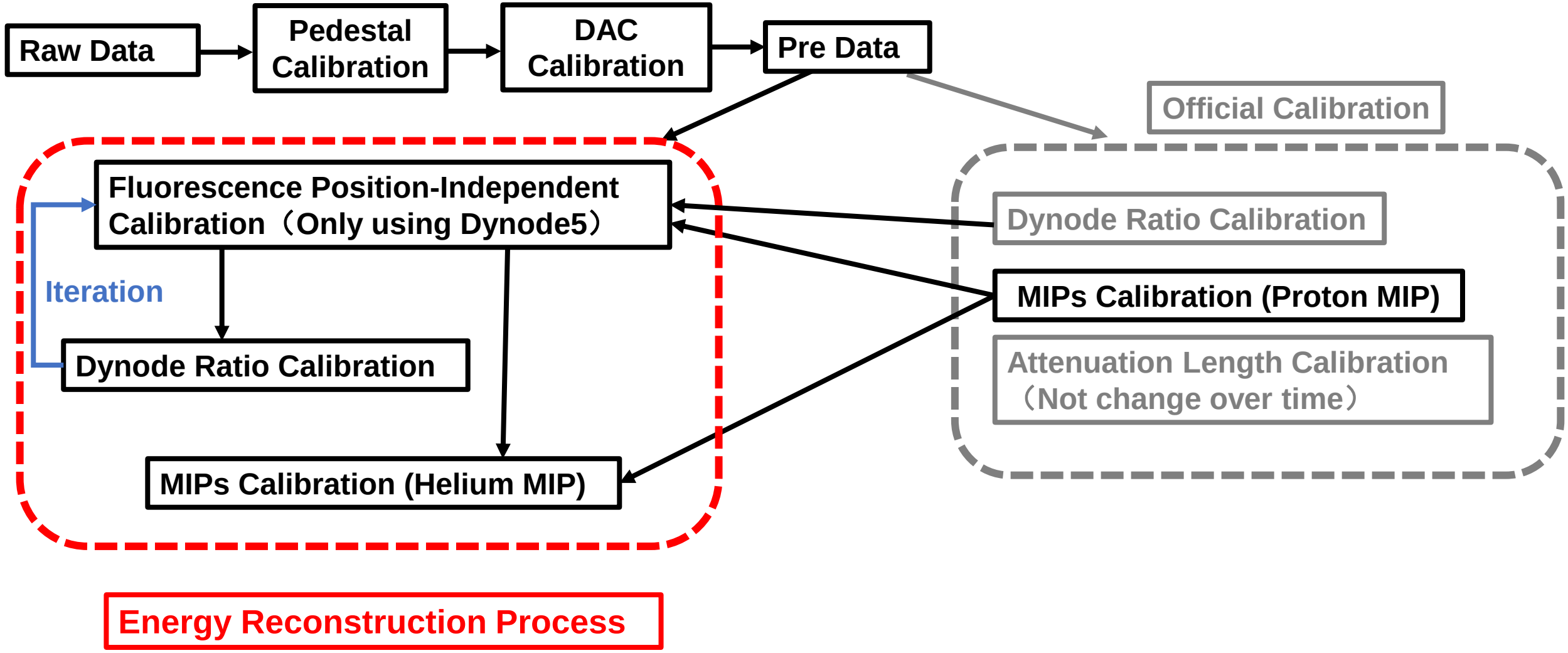

Fluorescence Position-Independent Calibration

Why only Dy5?

Why only use signals read out from both ends with Dy5?

- a narrower distribution
- a more linear behavior
- a negligible impact of MIP

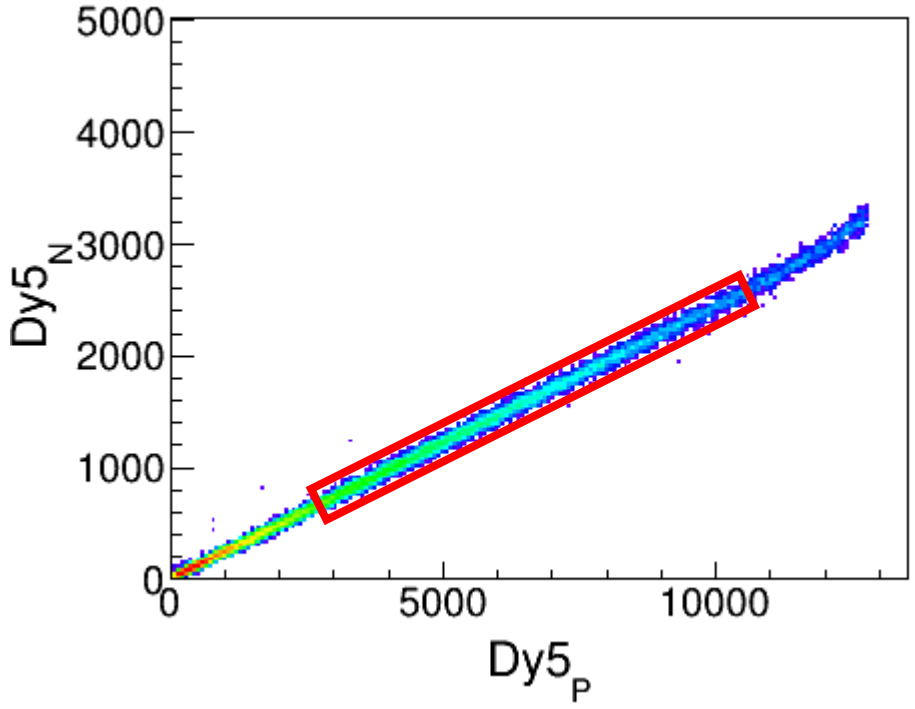

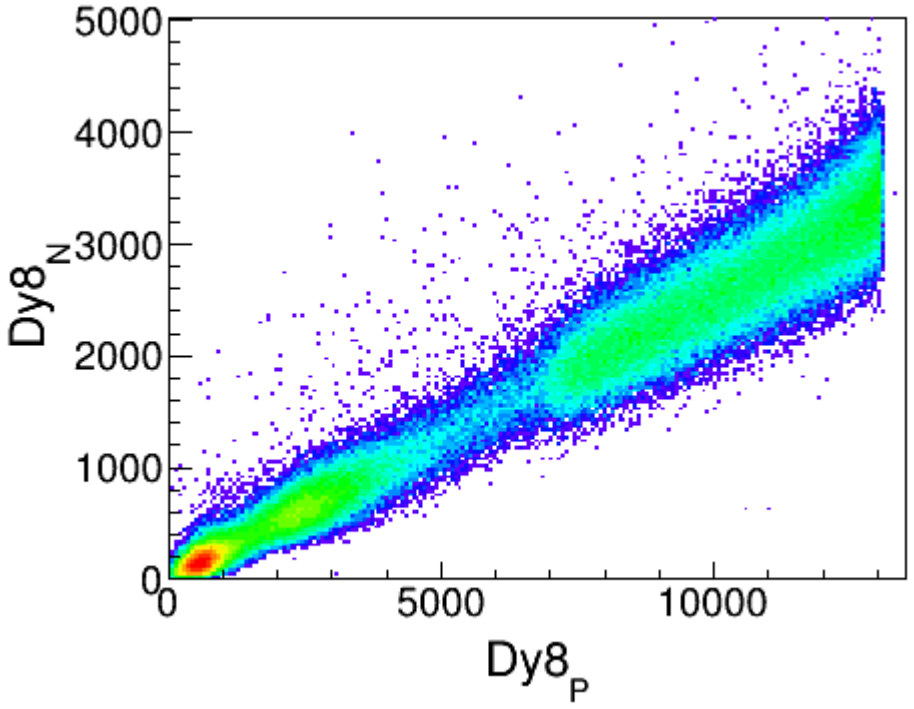

Traditional Method

Attenuation Length Calibration

Assumption: light attenuation follows an exponential law.

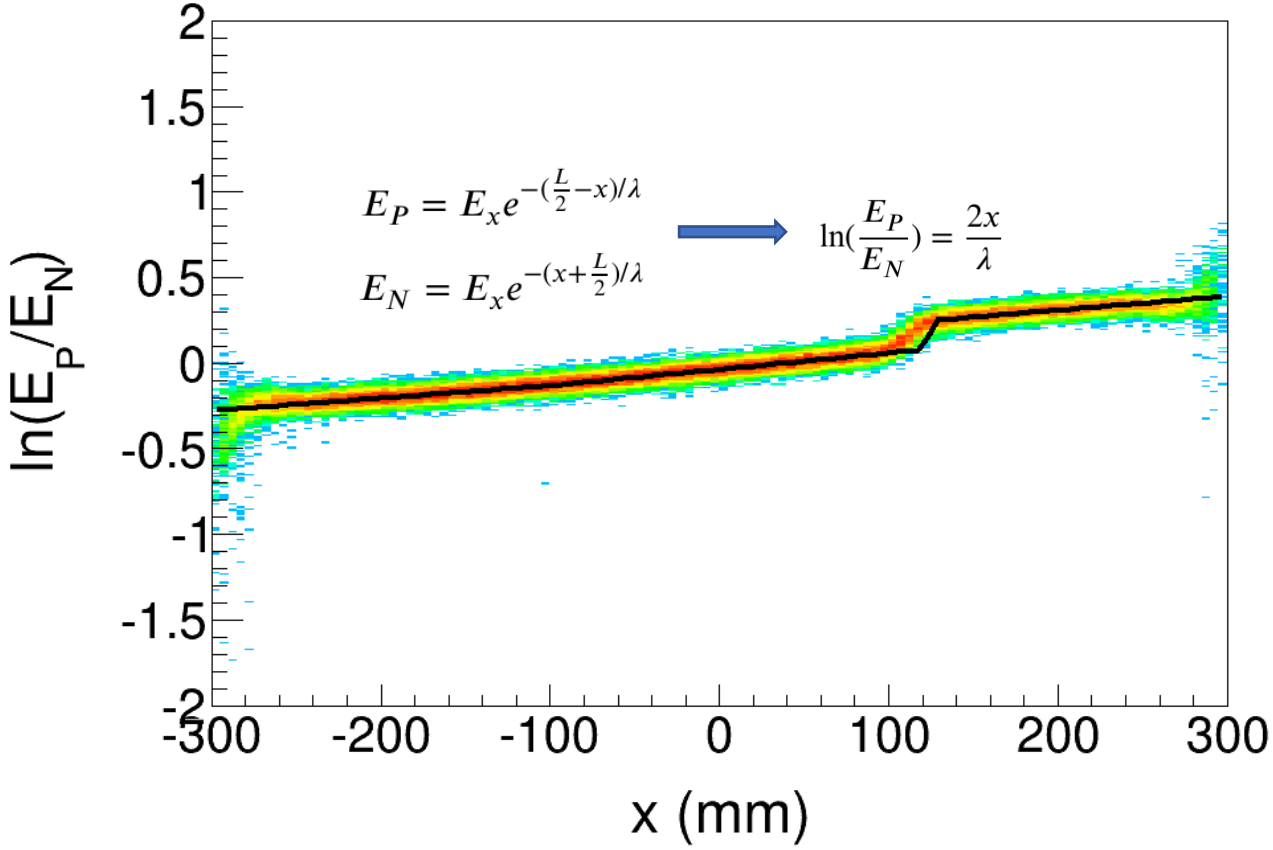

The linear fit function, even with segmentation and stepwise approaches, cannot fully describe $\ln(E_P/E_N)$.

Traditional Method

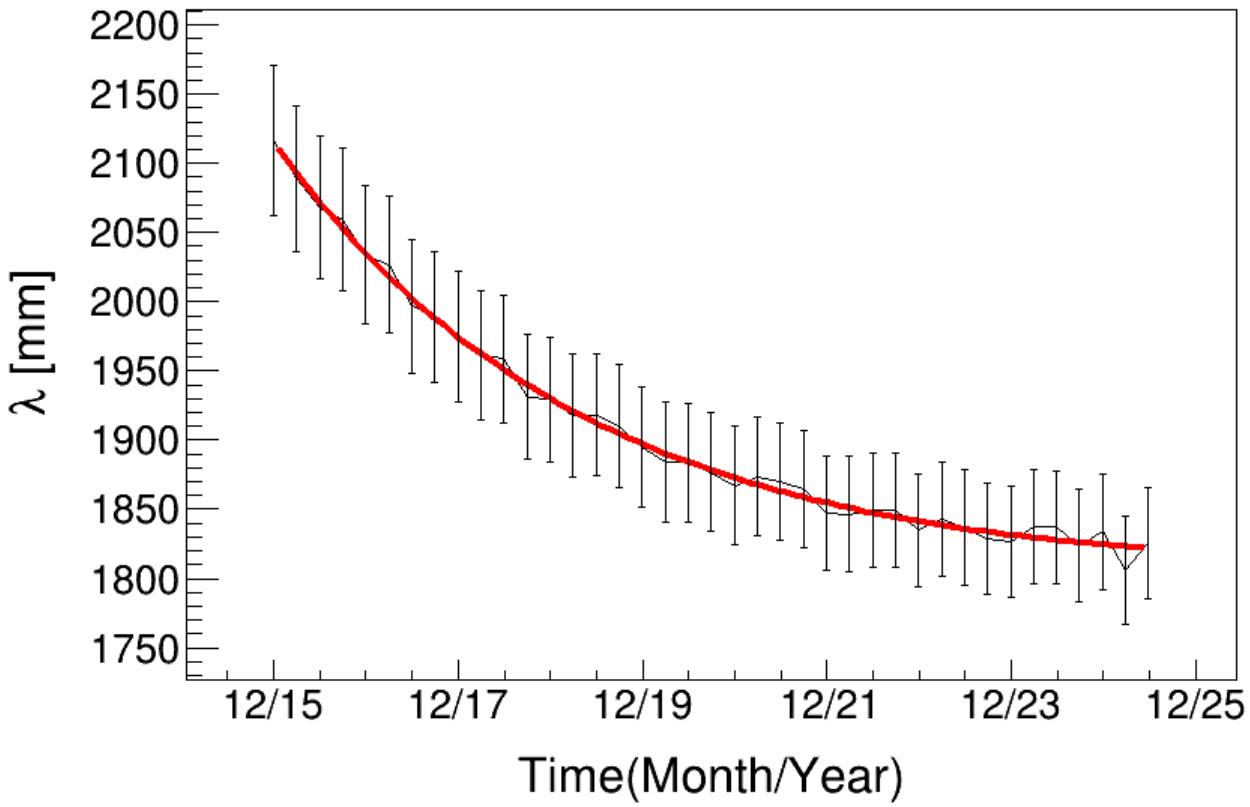

Energy Correction by Attenuation Length:

$$E_{P,x} = E_p \times e^{(\frac{L}{2}-x)/\lambda}$$

$$E_{N,x} = E_N \times e^{(x+\frac{L}{2})/\lambda}$$

$$E_{C,x} = \sqrt{E_P \times E_N}, \textbf{\textit{Position Independent}}$$

The fluorescence attenuation length can be used to monitor the temporal variation in the performance of each crystal, verifying that all crystals remain within the designated normal operating condition.

New Method

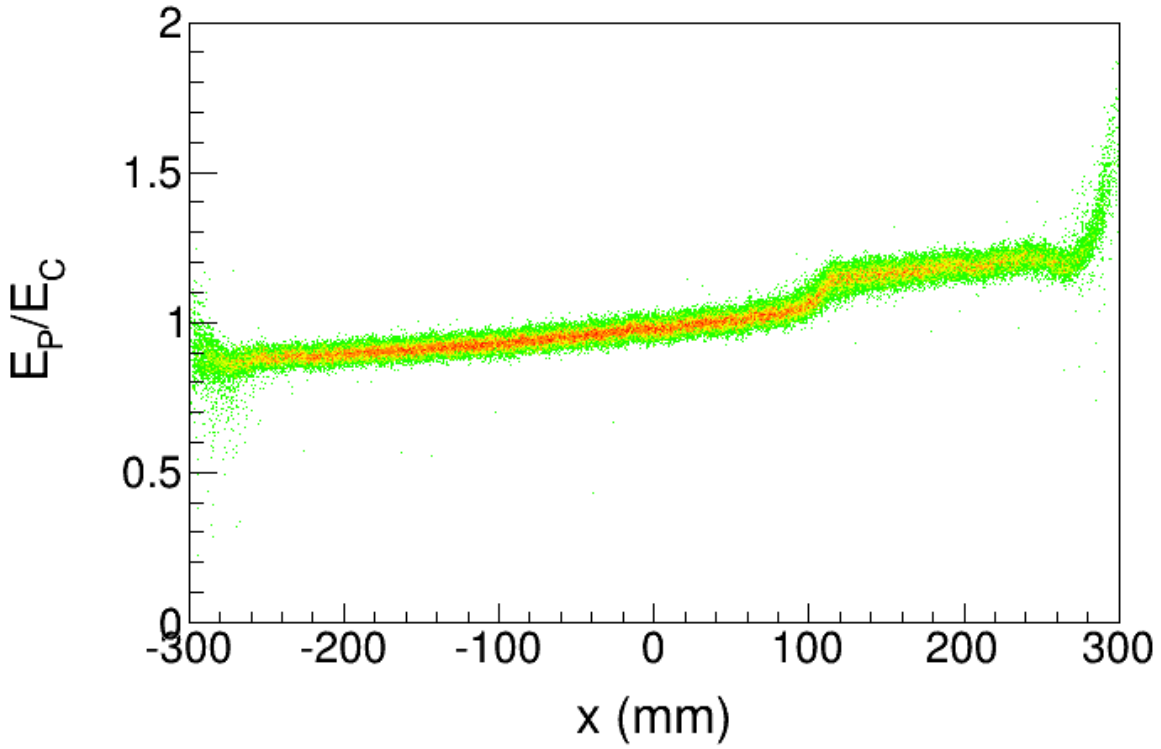

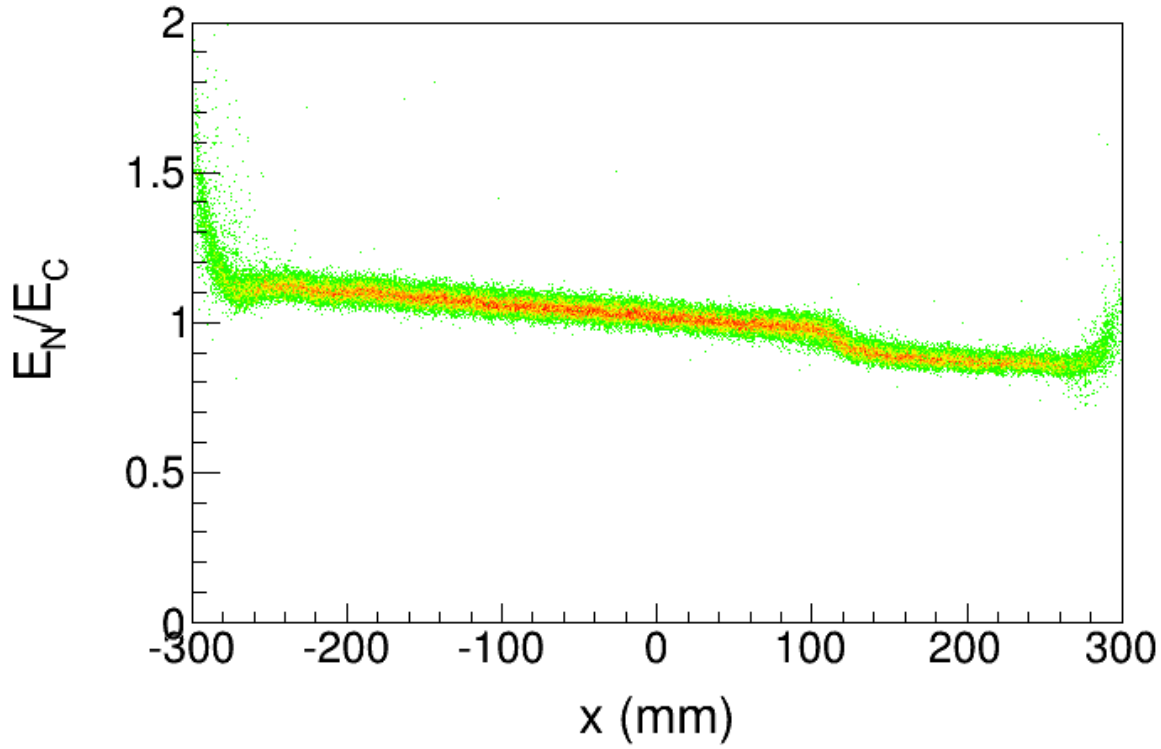

Instead of calibrating the attenuation length, E_P and E_N are corrected to E_C, relying on the stability of the E_C.

Stability of the E_C for Proton MIPs

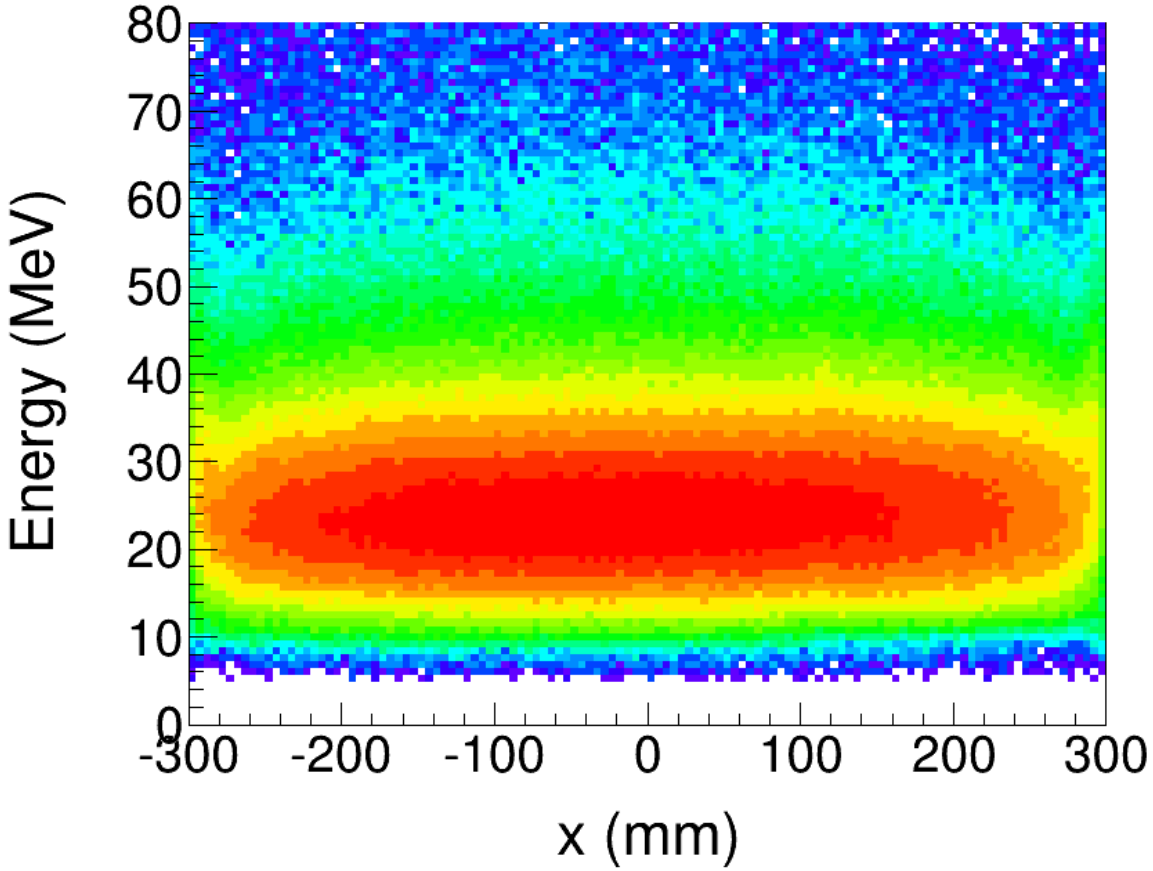

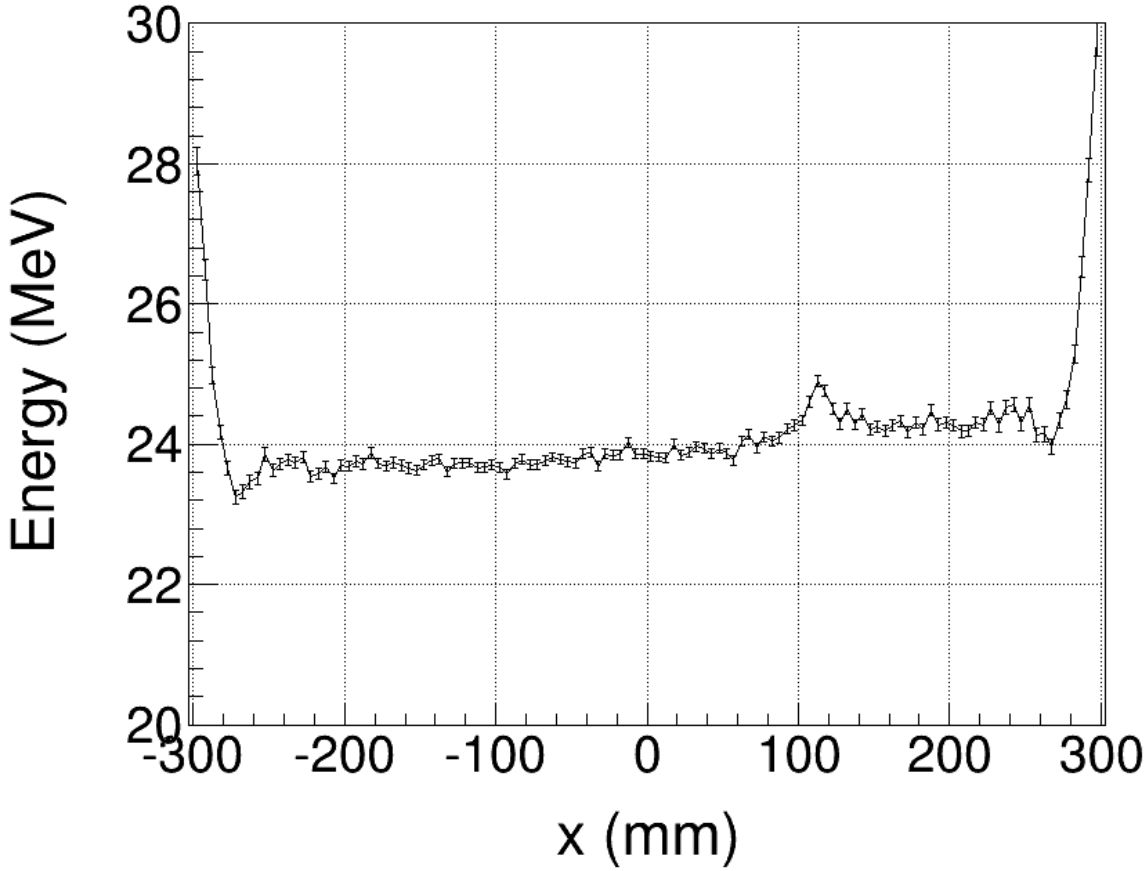

A position dependence is observed in E_C, indicating deviations from ideal exponential fluorescence attenuation.

E_C in All Layers of Proton MIPs

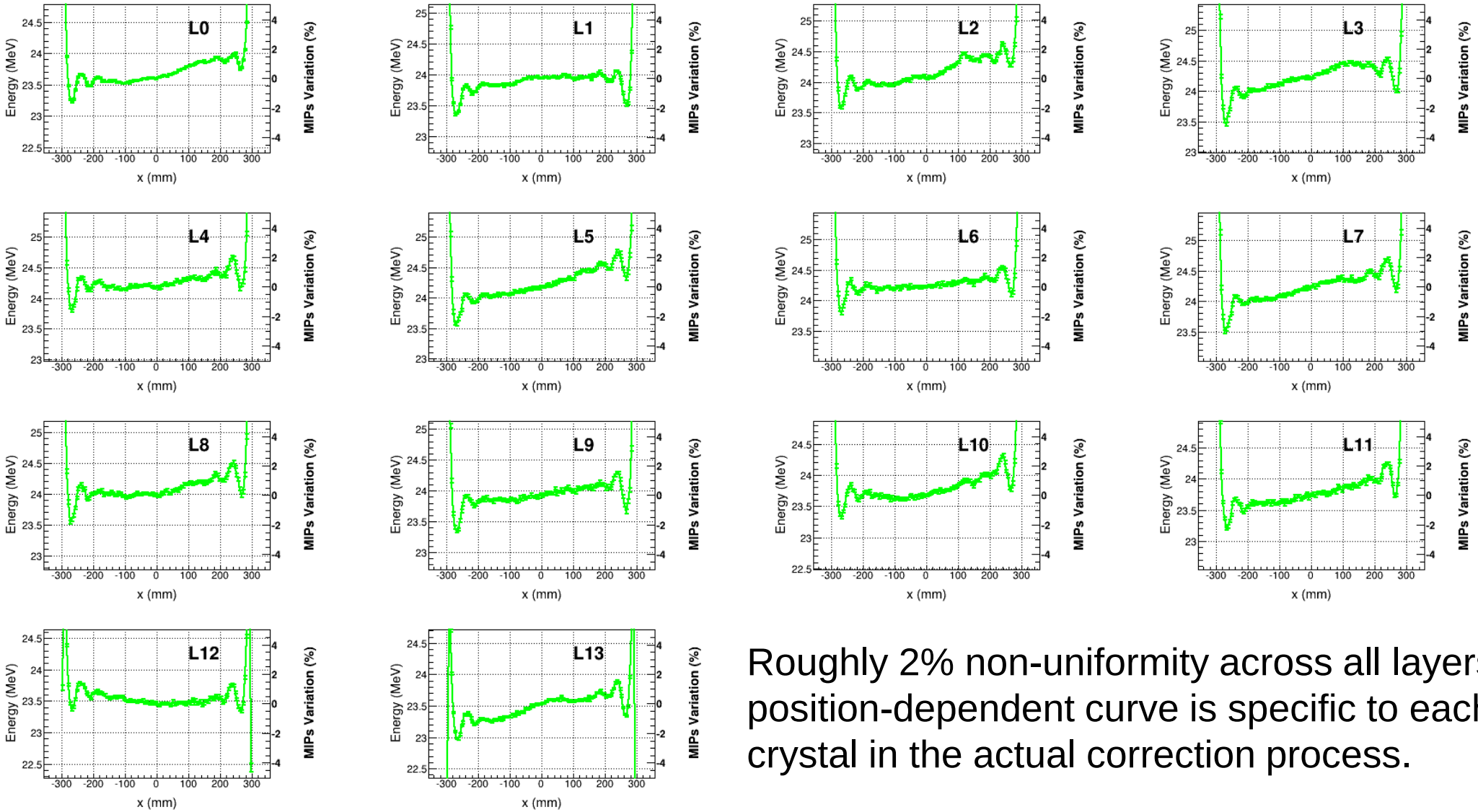

Roughly 2% non-uniformity across all layers, and the position-dependent curve is specific to each individual crystal in the actual correction process.

Helium MIPs

The positional uniformity of E_C has improved after correction compared to before the correction.

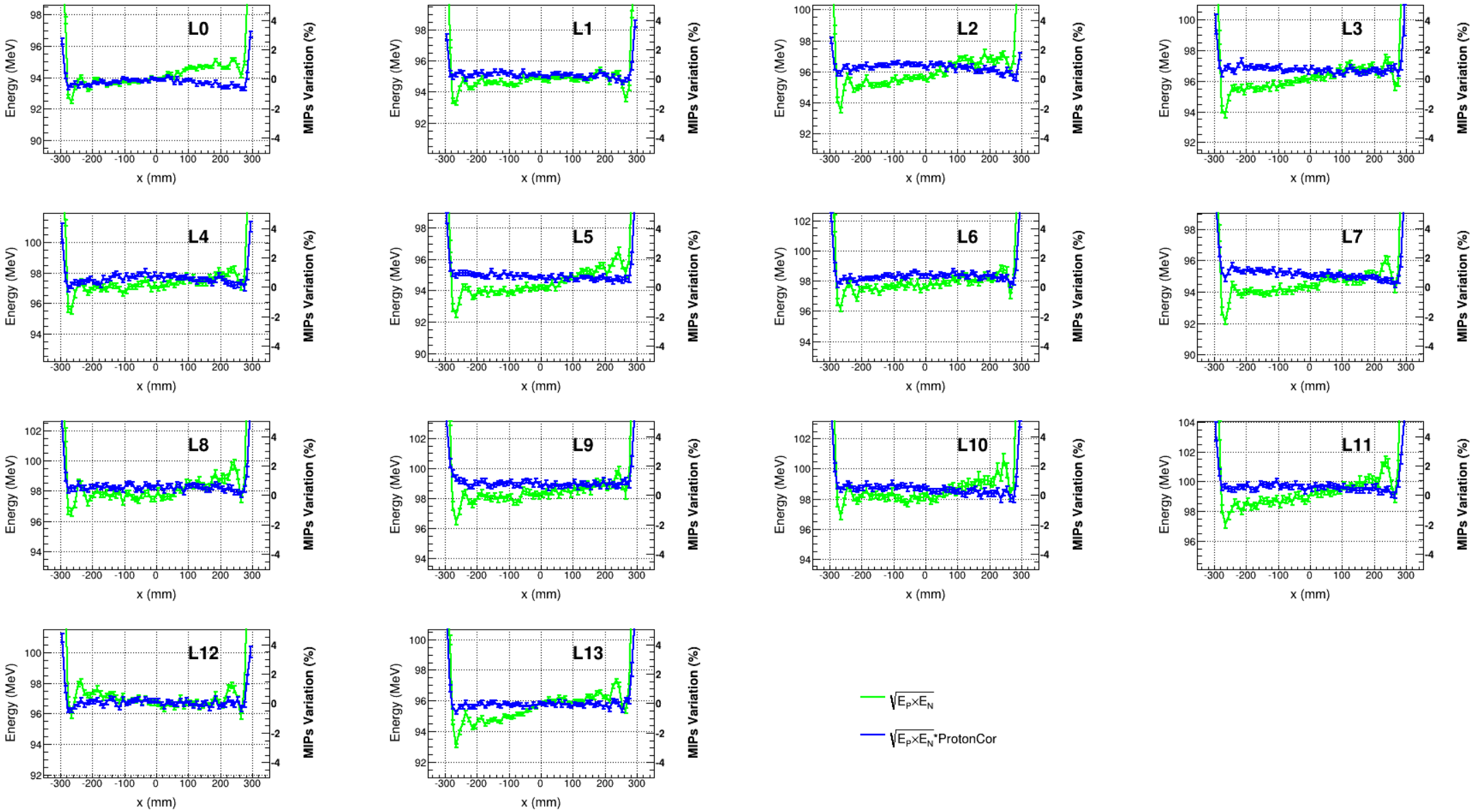

Carbon MIPs

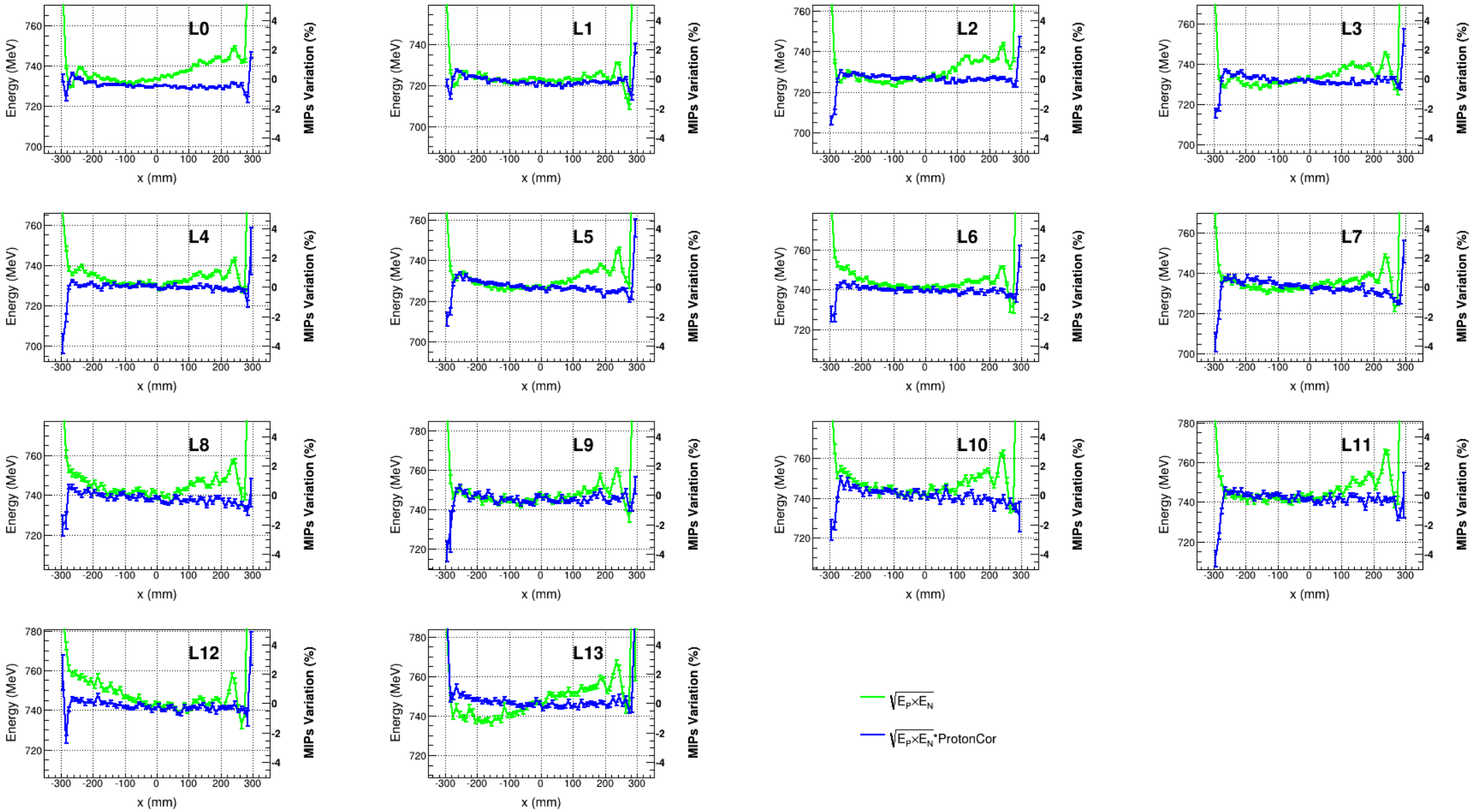
L0
L1
L2
L3
L4
L5
L6
L7
L8
L9
L10
L11
L12
L13
Energy (MeV)
MIPs Variation (%)
x (mm)
$\sqrt{E_P \times E_N}$
$\sqrt{E_P \times E_N}$*ProtonCor

An Example of E_P Correction

One point every 10 mm

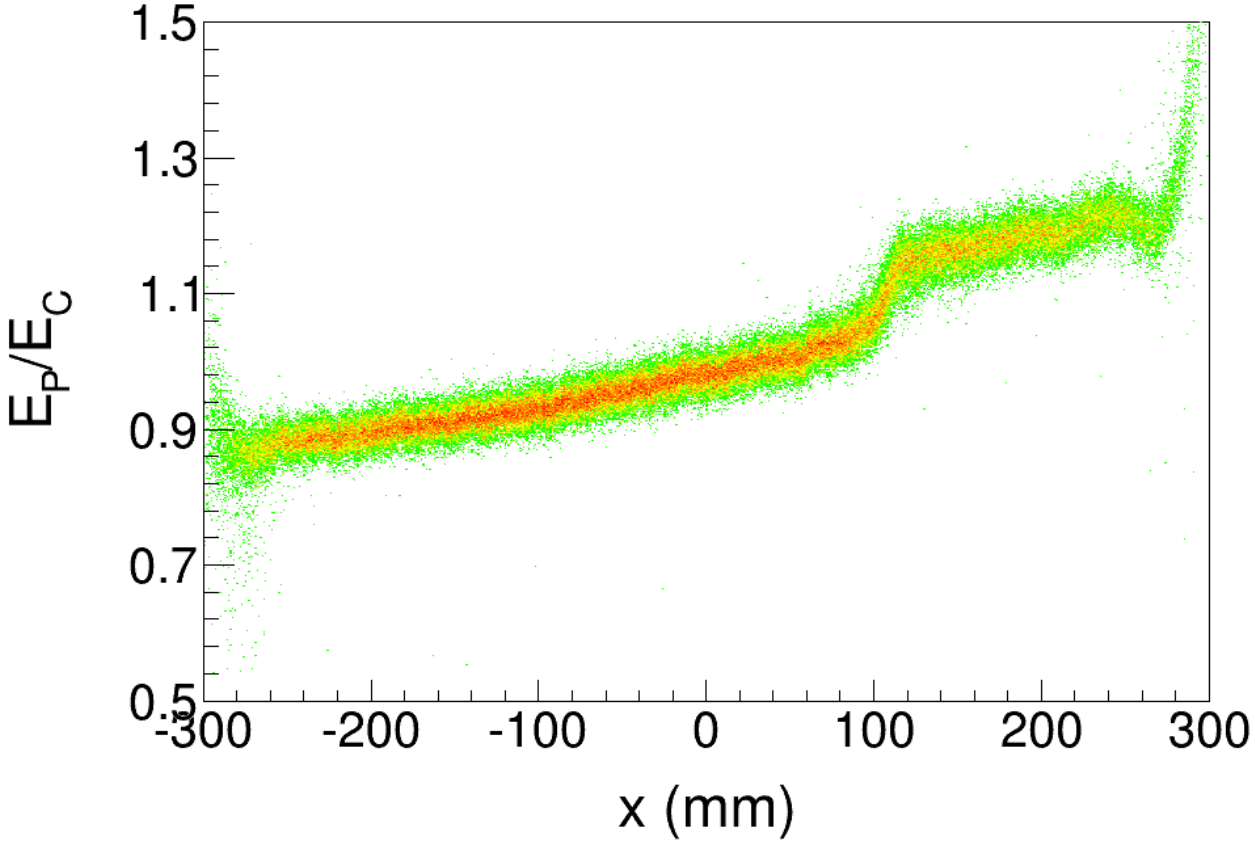

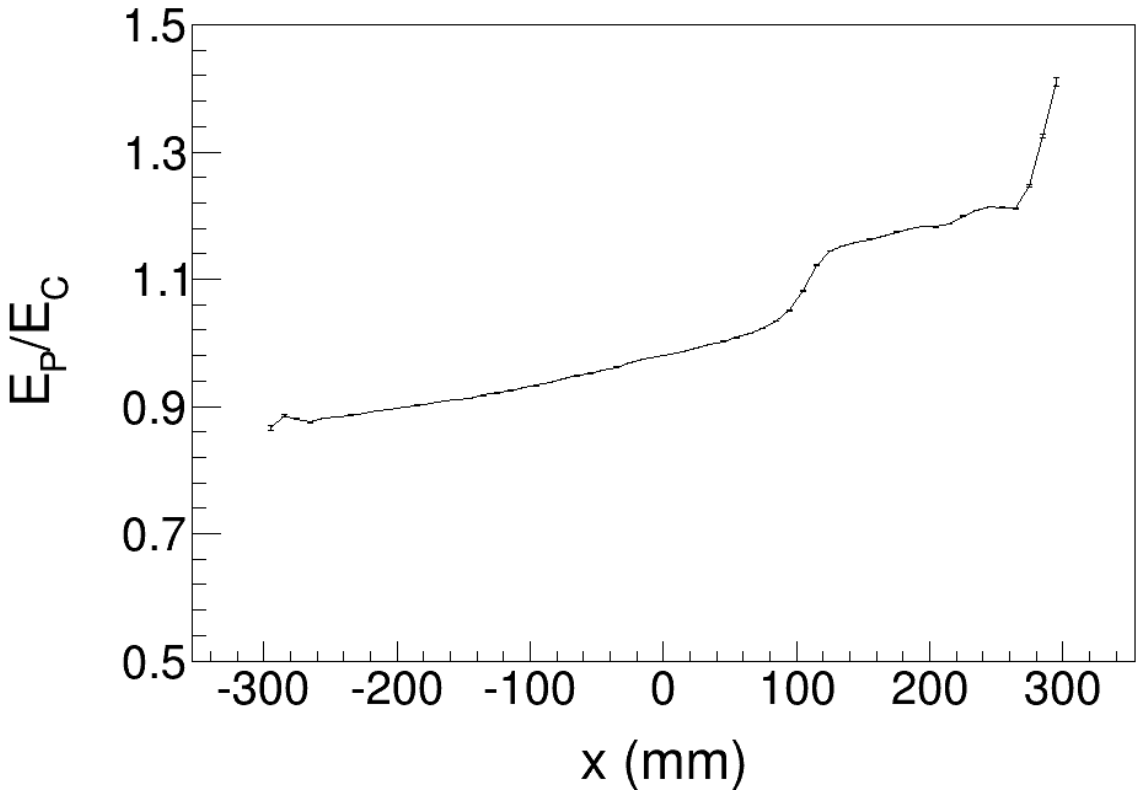

New Method

Smooth the temporal variation of the position-dependent coefficient

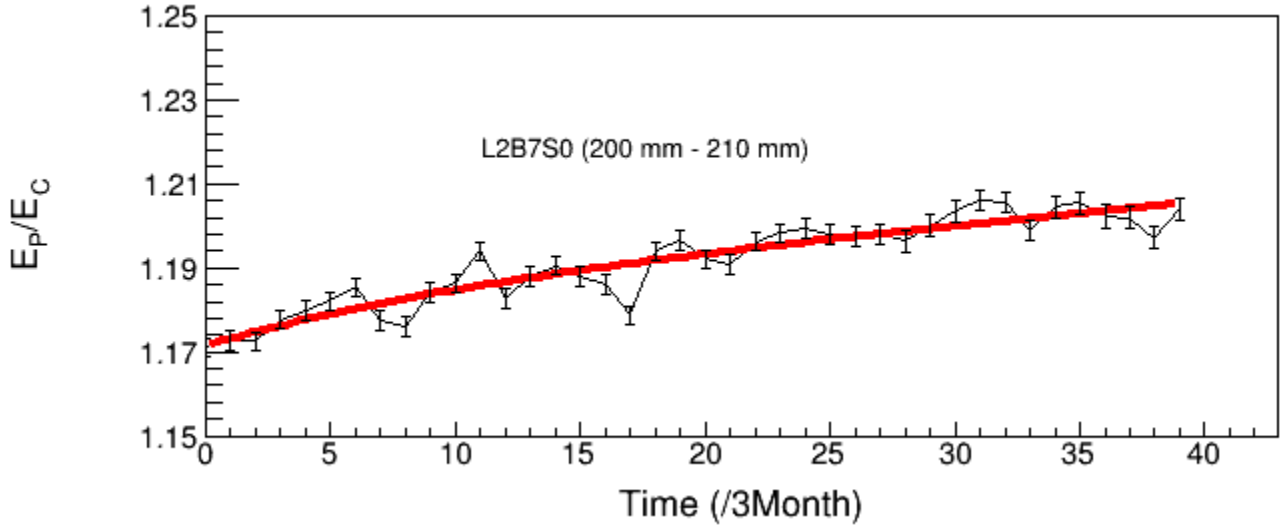

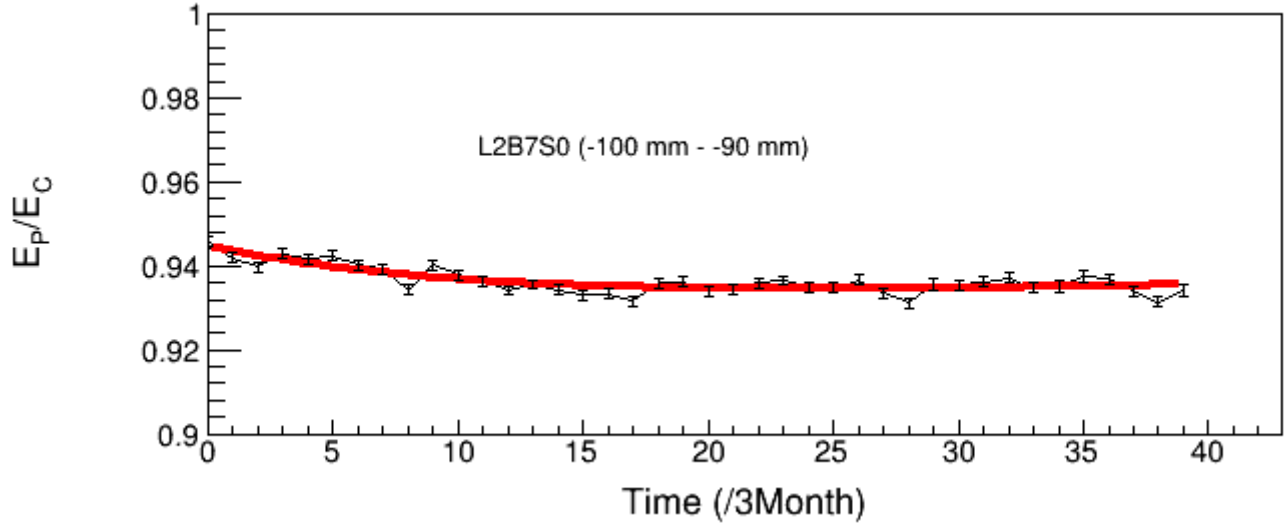

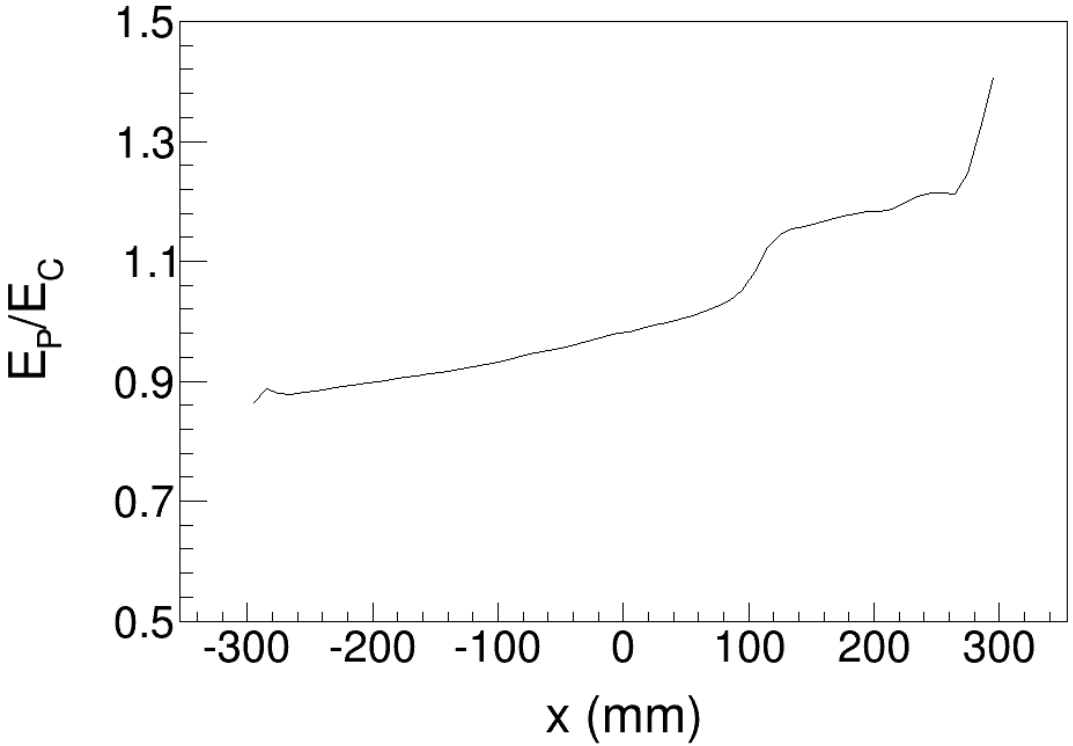

Comparison

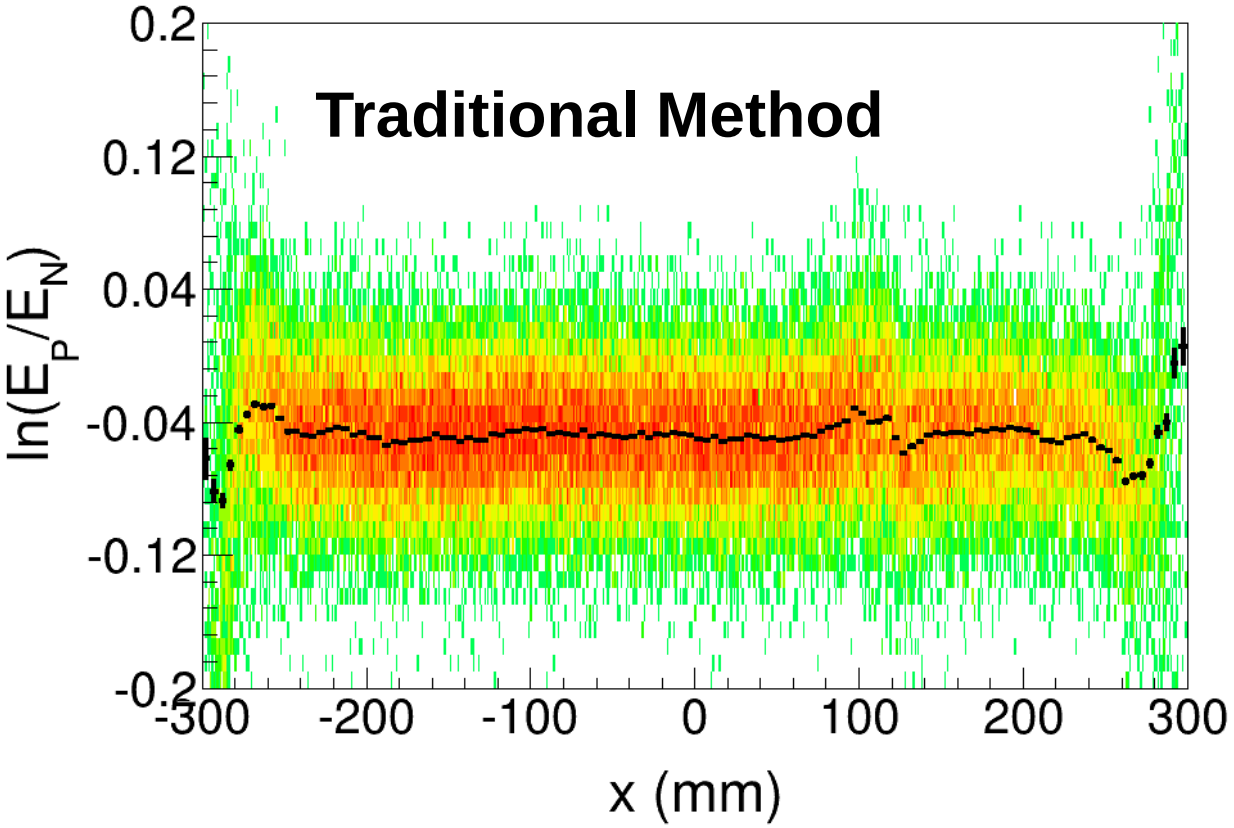

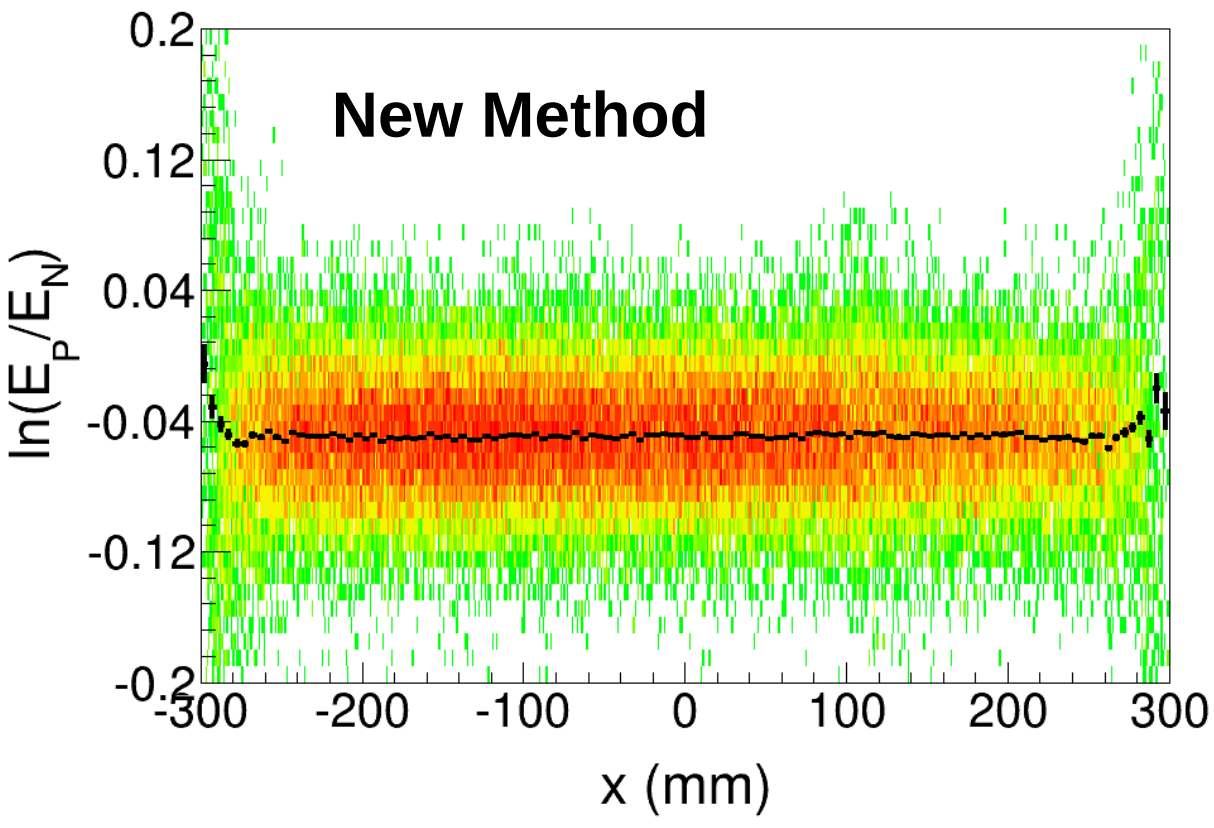

The new method reduces the energy position dependence in the reconstruction at both P and N ends

MIPs Calibration

Proton MIPs Calibration

- Most **abundant** component of cosmic rays
- **Daily updated** using proton MIPs for continuous calibration.

In-orbit Calibration: Proton MIPs within $\pm 20^{\circ}$ geographic latitude

Simulation of the Space Environment:
Primary component: Back-tracing simulation of incident protons within $\pm 20^{\circ}$ geographic latitude.
Secondary component: Based on AMS-01 measurements at low magnetic latitudes.

The input spectrum in the in-orbit simulation is not fully consistent with that of the actual space environment.

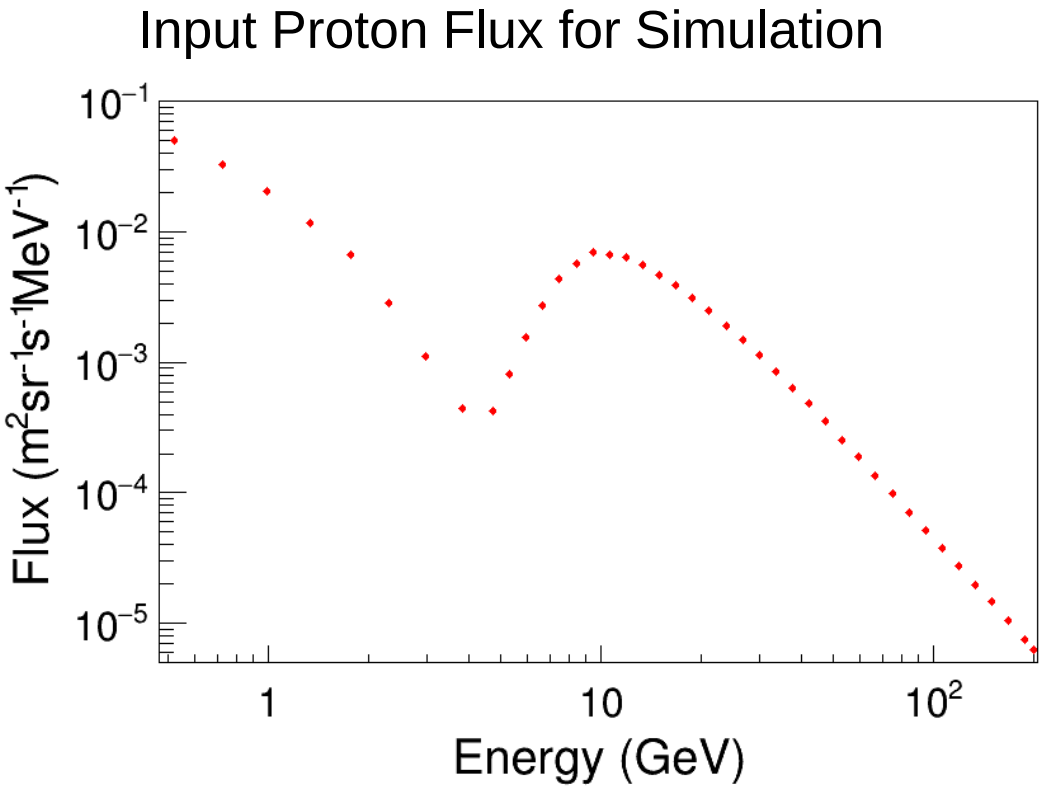

Proton MIPs Calibration

Simulation

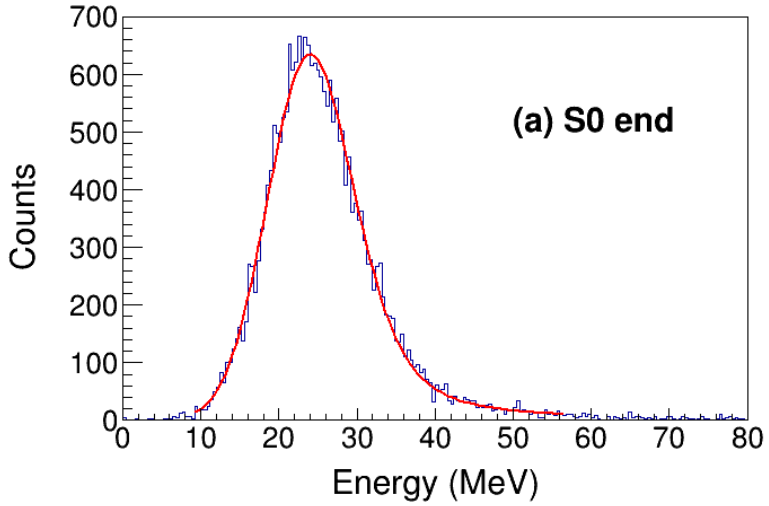

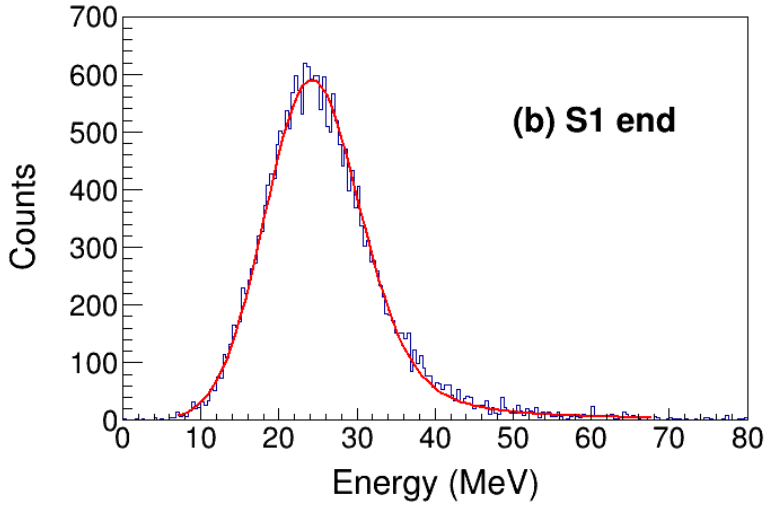

Flight Data

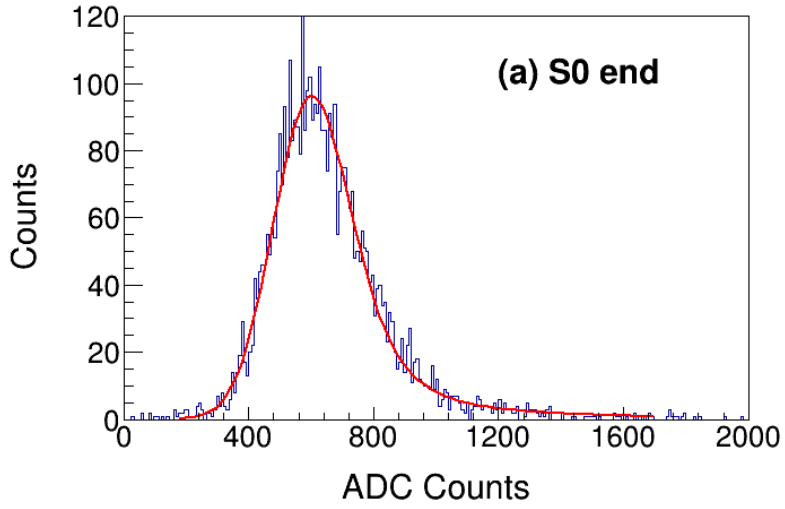

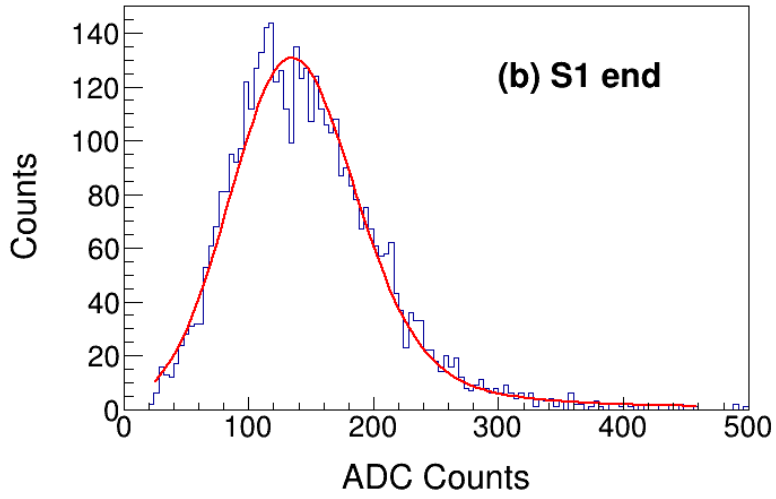

Matching the MIP peak in ADC from flight data with simulated energy deposition in MeV allows direct conversion from ADC counts to energy.

Proton MIPs Calibration

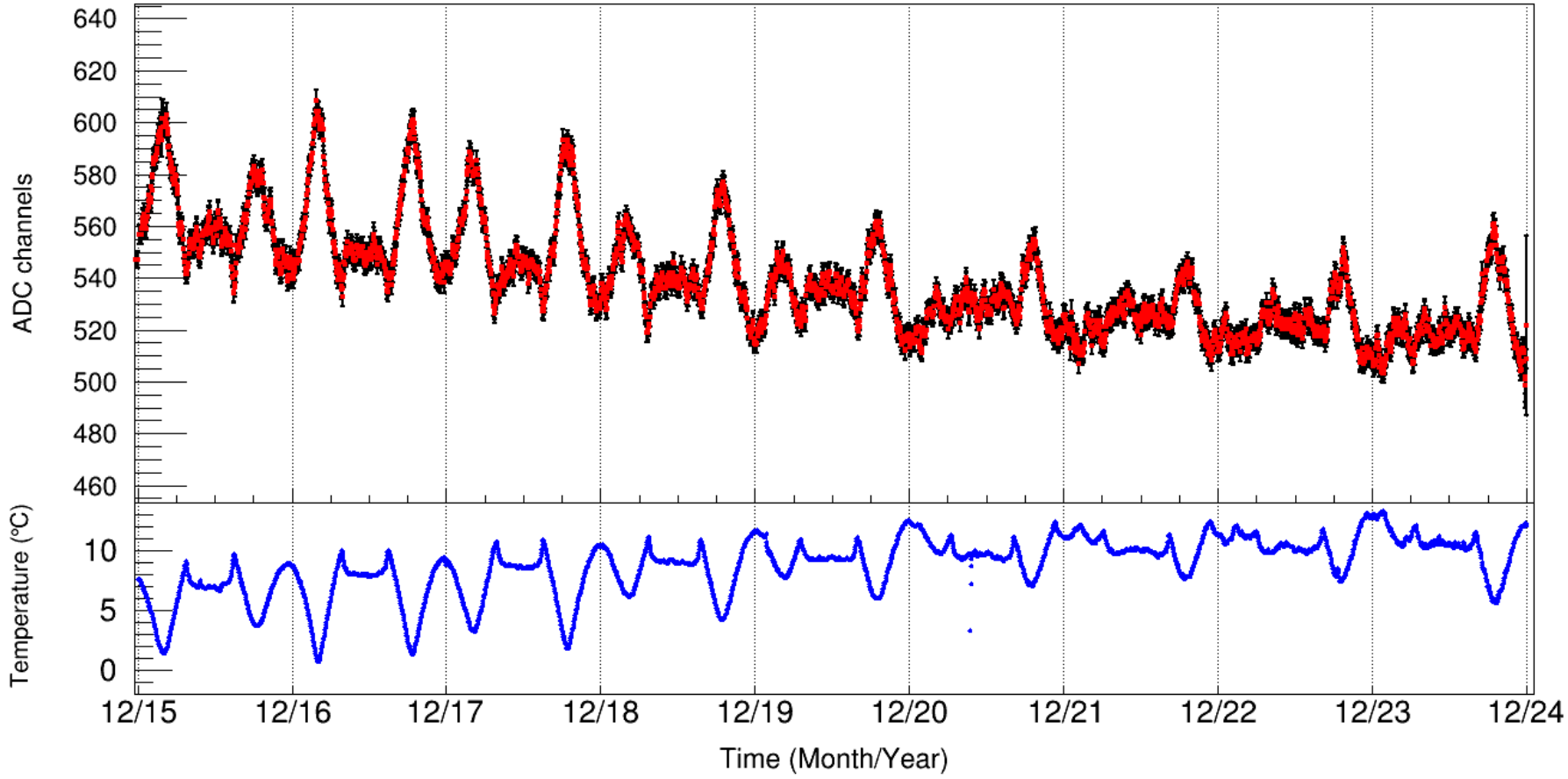

Proton MIPs are highly effective in correcting for temperature effects and thus have served as the fundamental benchmark for energy calibration.

Helium MIPs Calibration

Back-tracing simulation of incident helium particles within ±20° geographic latitude.

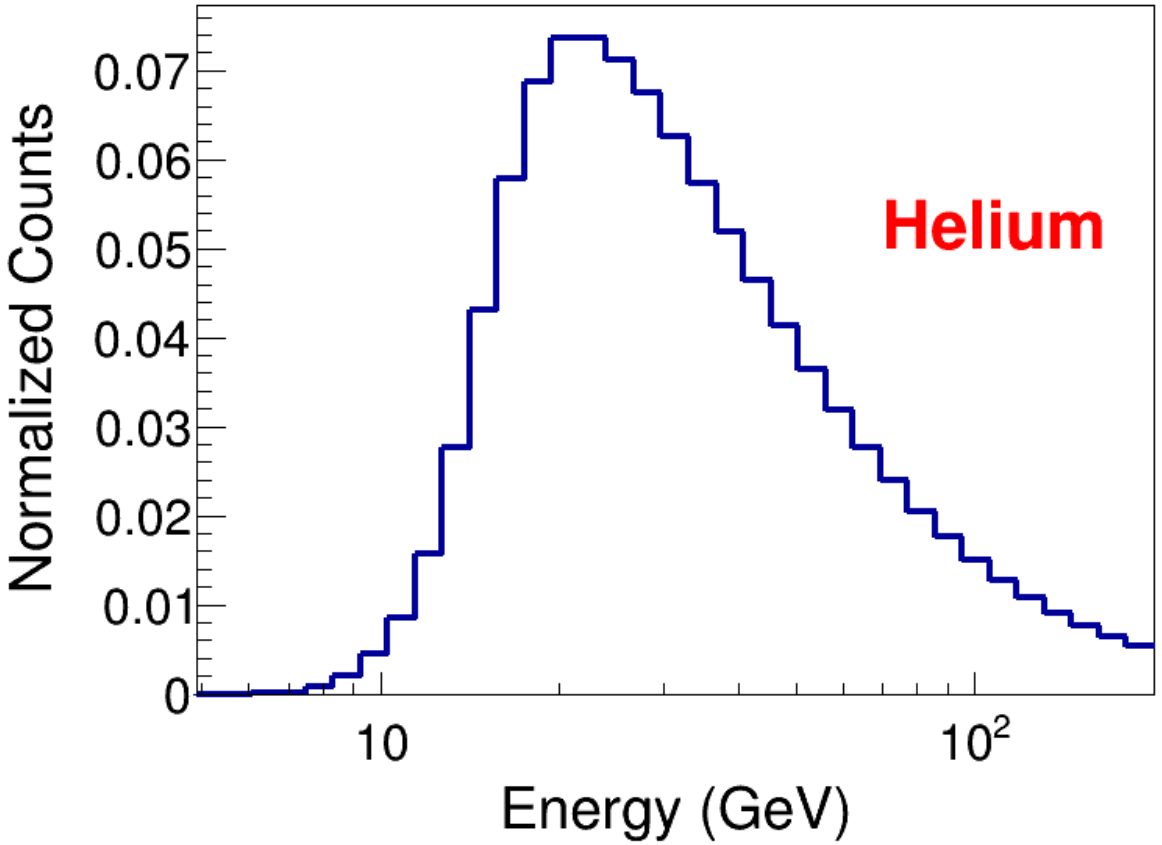

Why Helium MIPs?

- Primary particles → spectrum is stable
- Higher energy deposit (~4× protons)→ better signal-to-noise ratio

Further smooth and unify the energy scale

Helium MIPs at each Layer of the S0 end

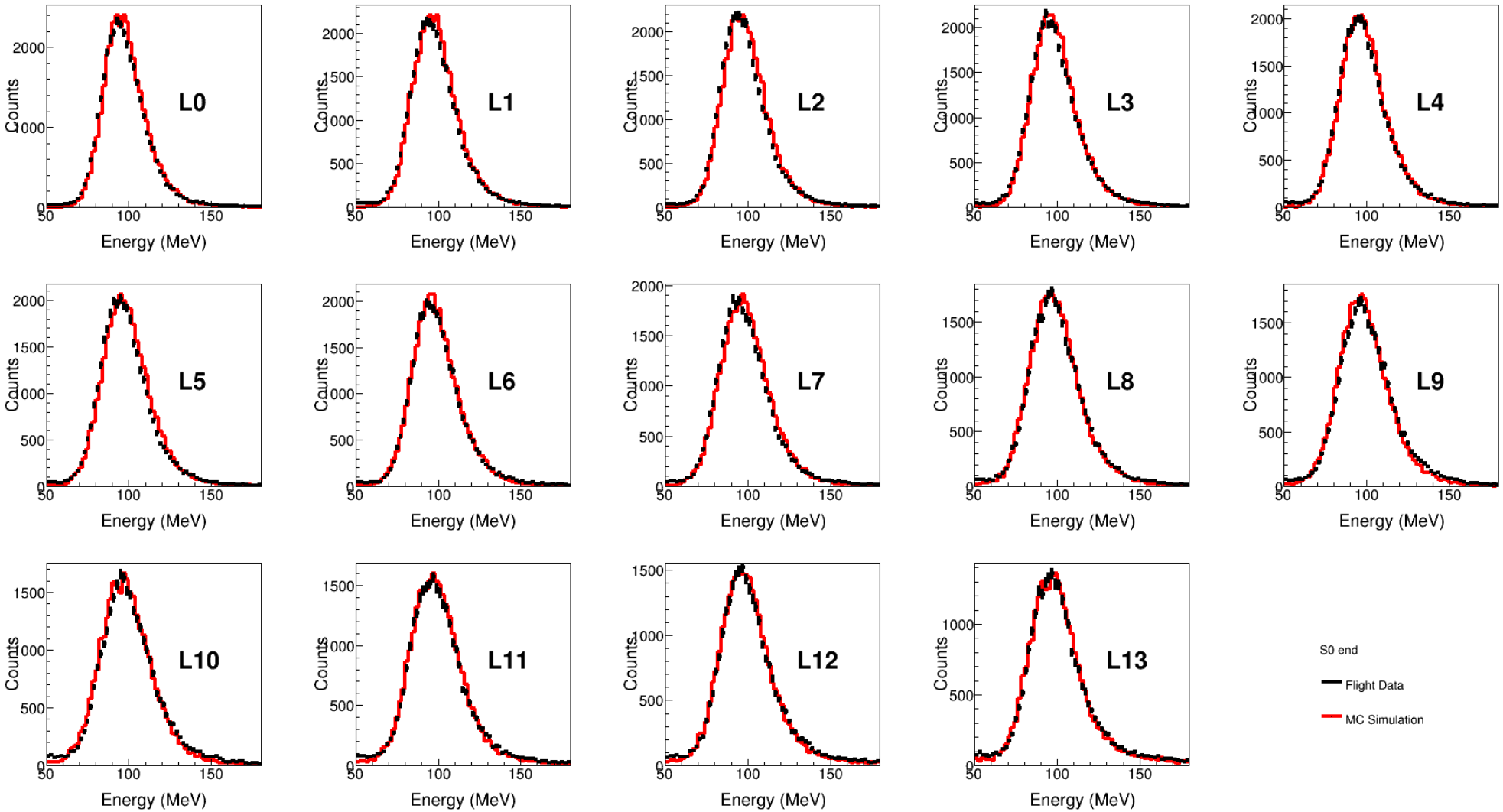

Helium MIPs at each Layer of the S1 end

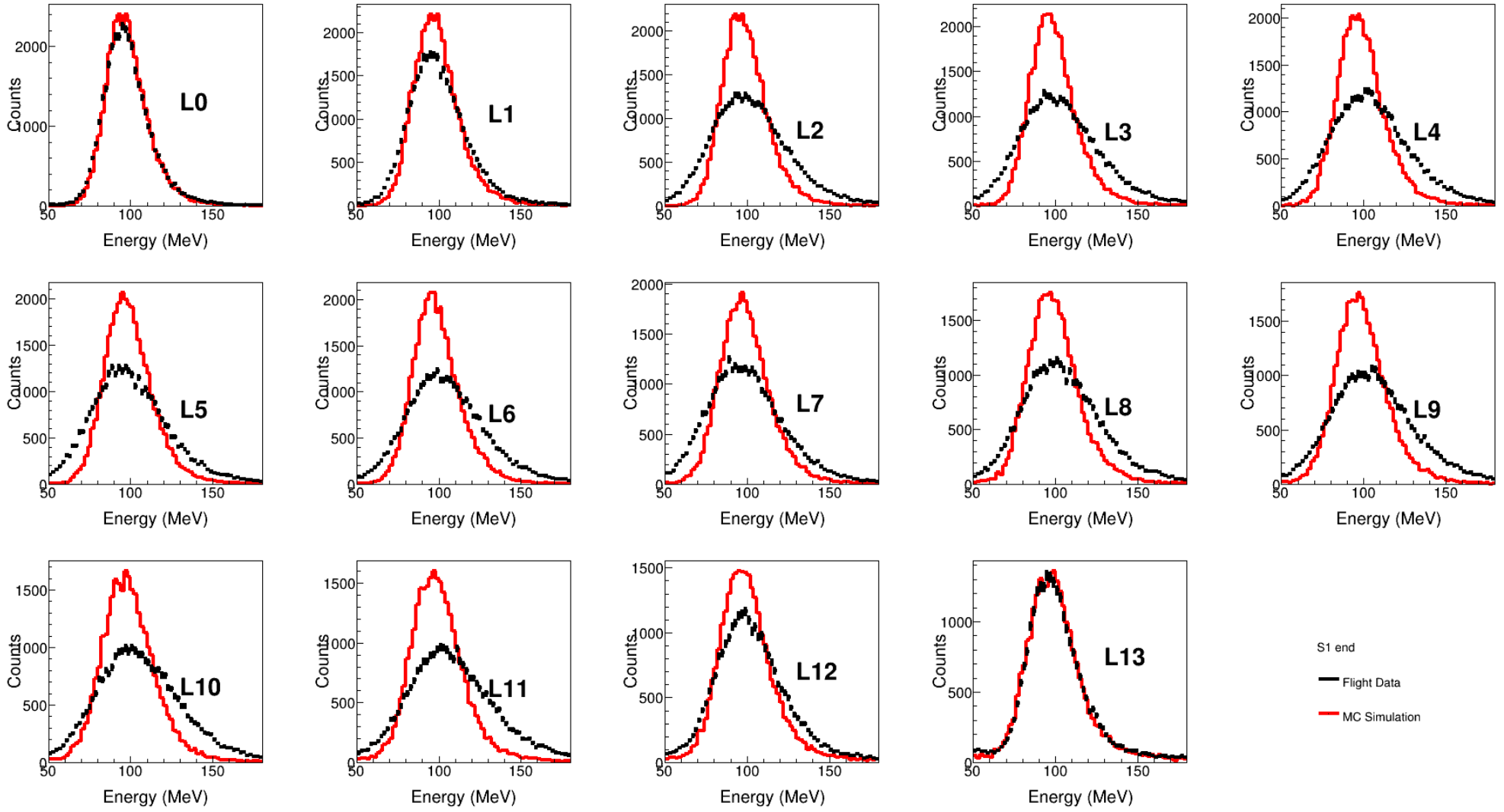

The digitization of the S1 end in the simulation data requires optimization

Helium MIPs Calibration

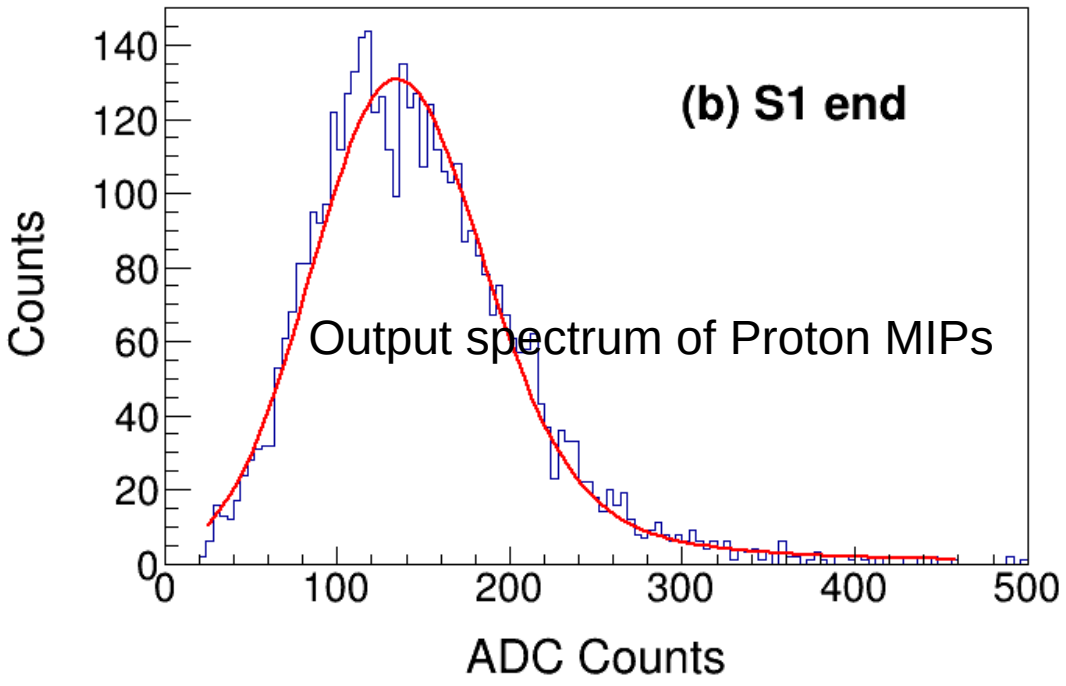

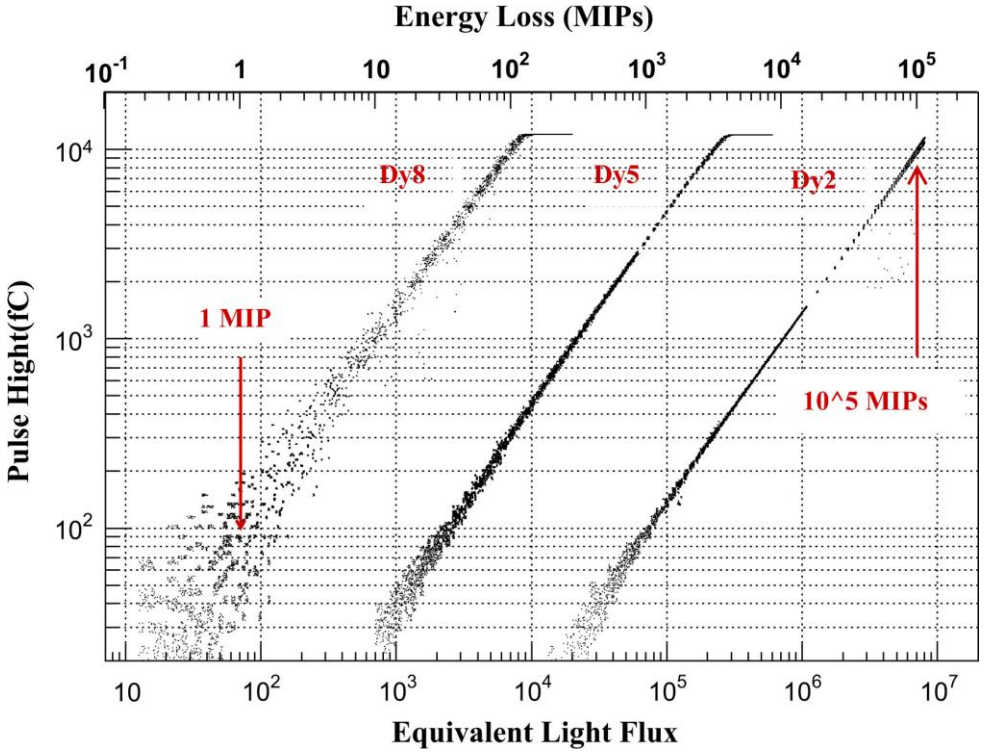

The proton MIP signal at the S1 end is relatively small and falls into the non-linear response region, likely due to a low signal-to-noise ratio.

$$C = \frac{E_{MIP}^{Proton}}{ADC_{MIP}^{Proton}} \Rightarrow C = \frac{E_{\mathrm{MIP}}^{\mathrm{Proton}}}{ADC_{\mathrm{MIP}}^{\mathrm{Proton}} \times MIPCor} = \frac{E_{\mathrm{MIP}}^{\mathrm{Proton}}}{ADC_{\mathrm{MIP}}^{\mathrm{Proton}} \times (E_{\mathrm{FD\ MIP}}^{\mathrm{Helium}} / E_{\mathrm{MC\ MIP}}^{\mathrm{Helium}})}$$

Helium MIPs Calibration

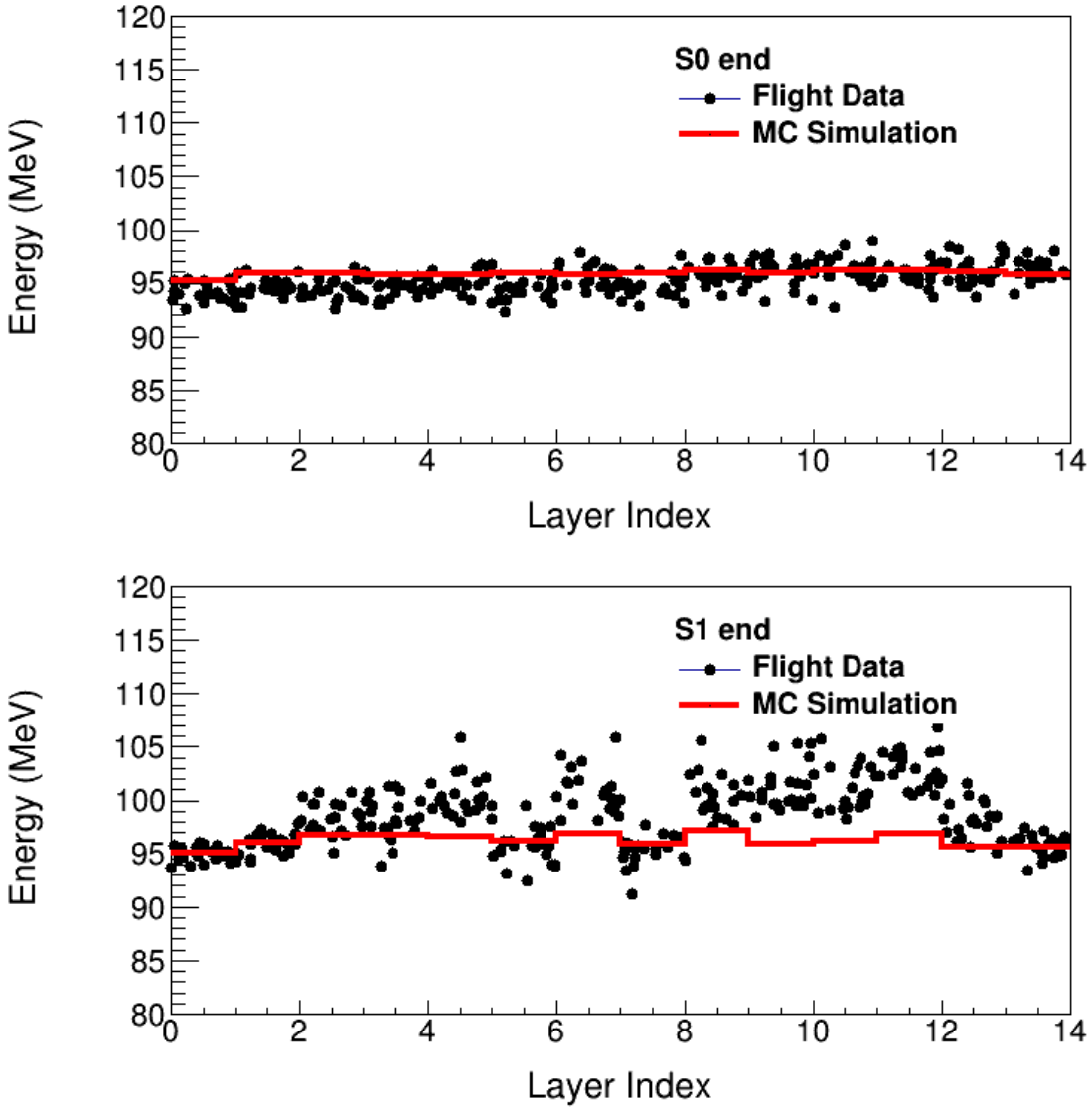

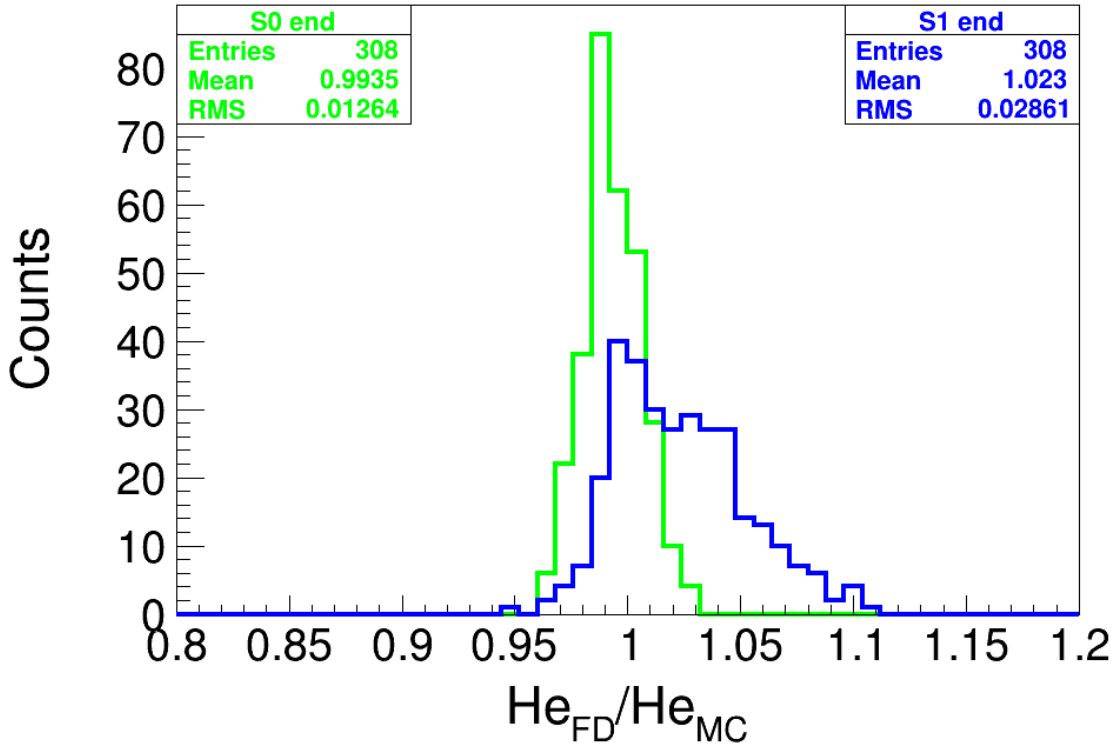

Compare the peak values of the Helium MIPs between flight data and simulation data.

Validation of Carbon MIPs - Total Energy Vs Time

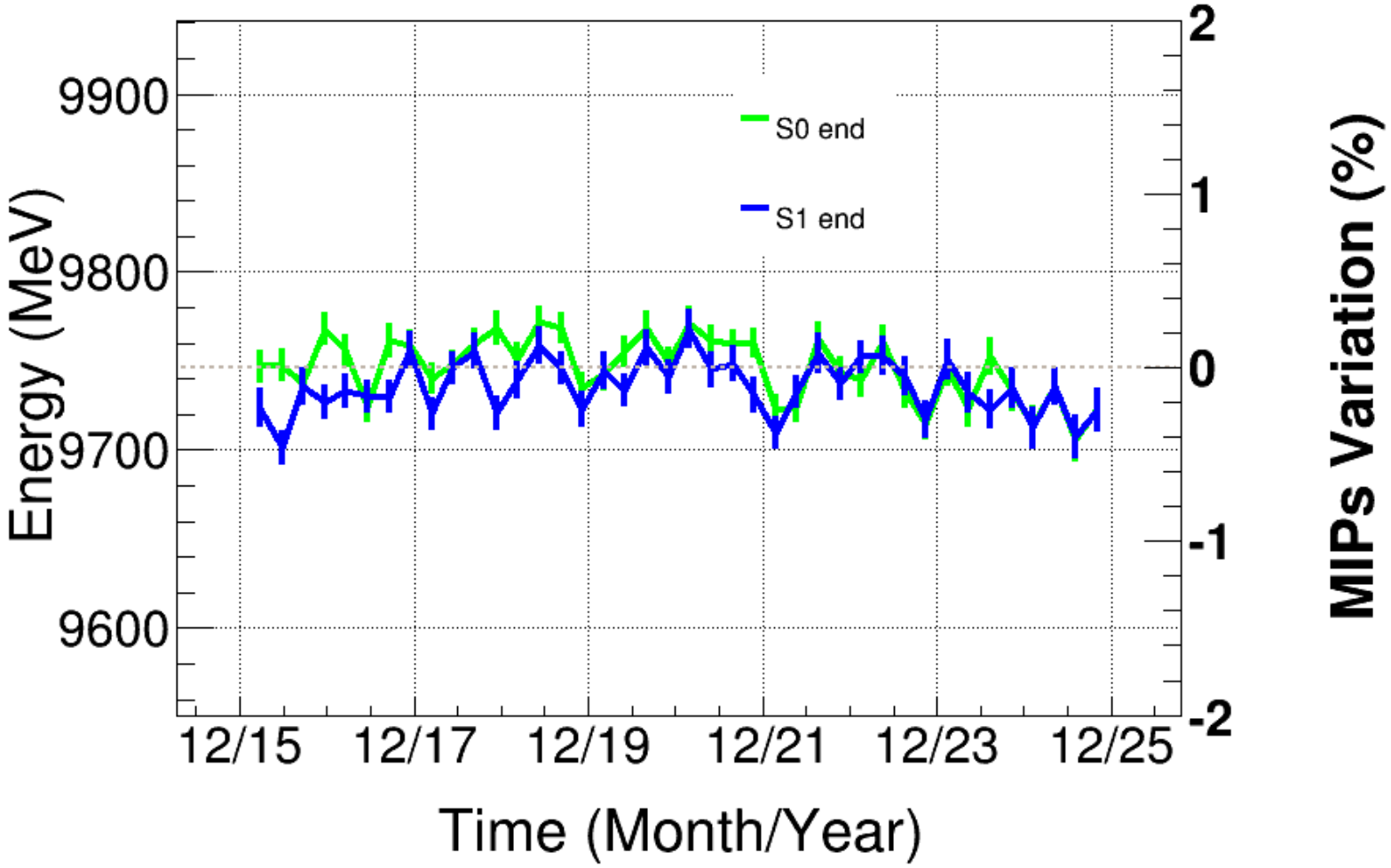

The Carbon MIP energy shows a temporal variation of less than 1%, and the energies measured at the two ends are highly consistent.

Layer Energy Vs Time

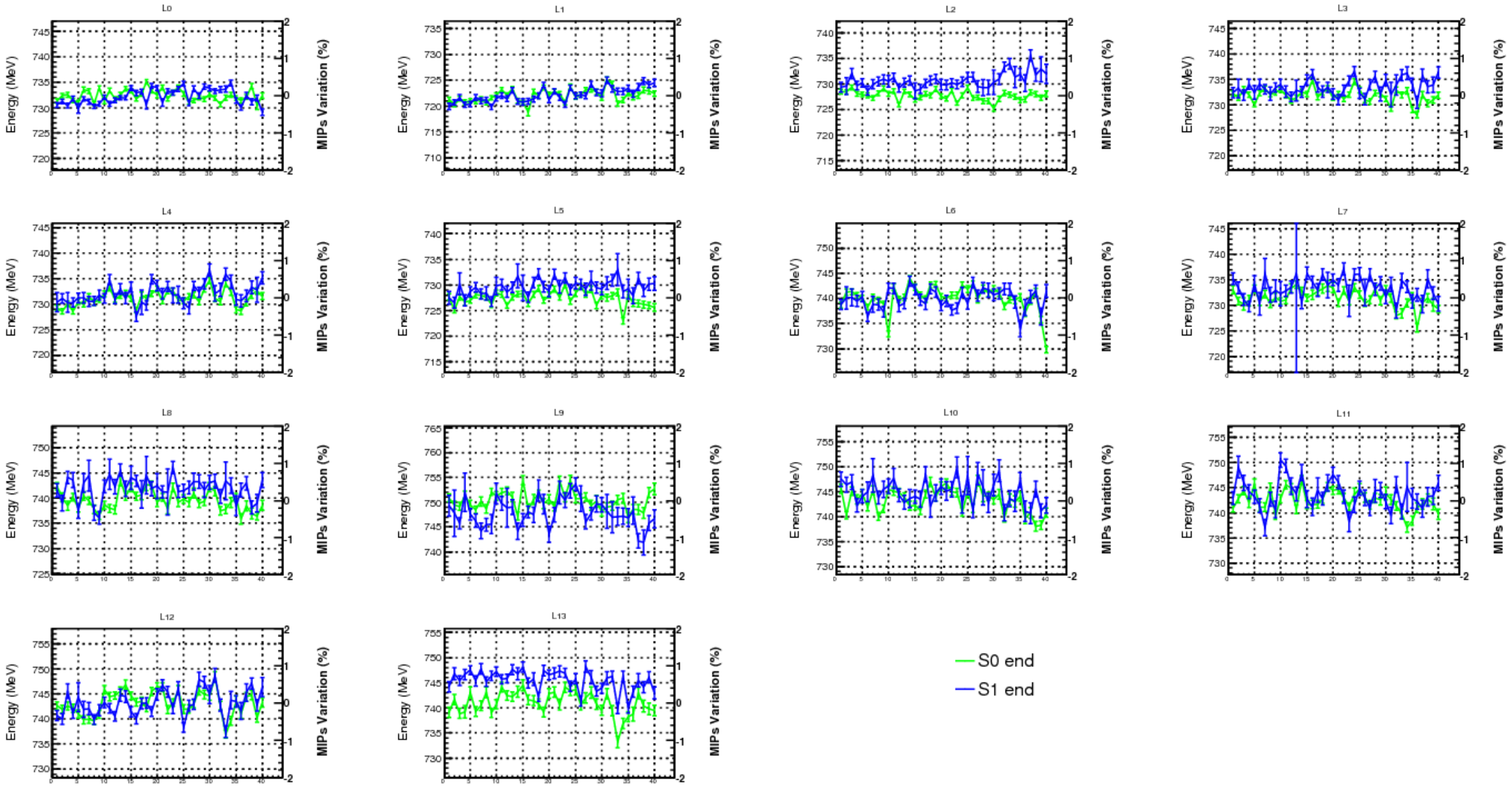

Dynode Ratio Calibration of PMTs

Traditional Method

The signal correlation of adjacent channels in a specific PMT.

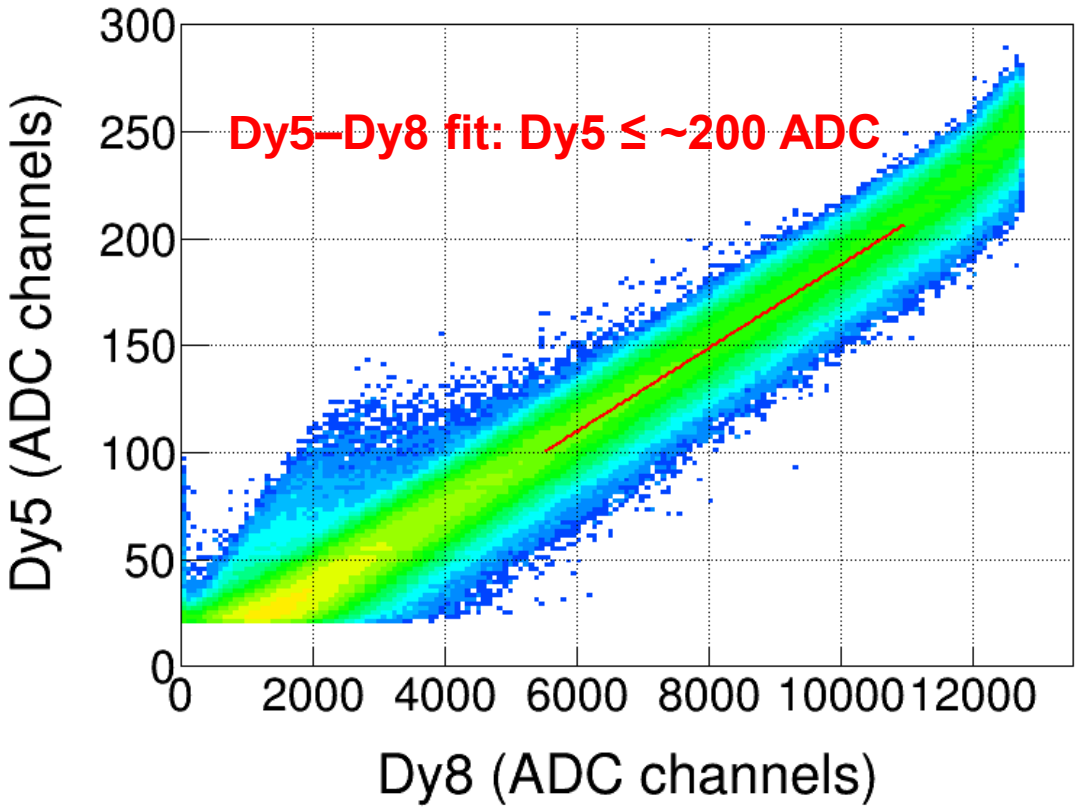

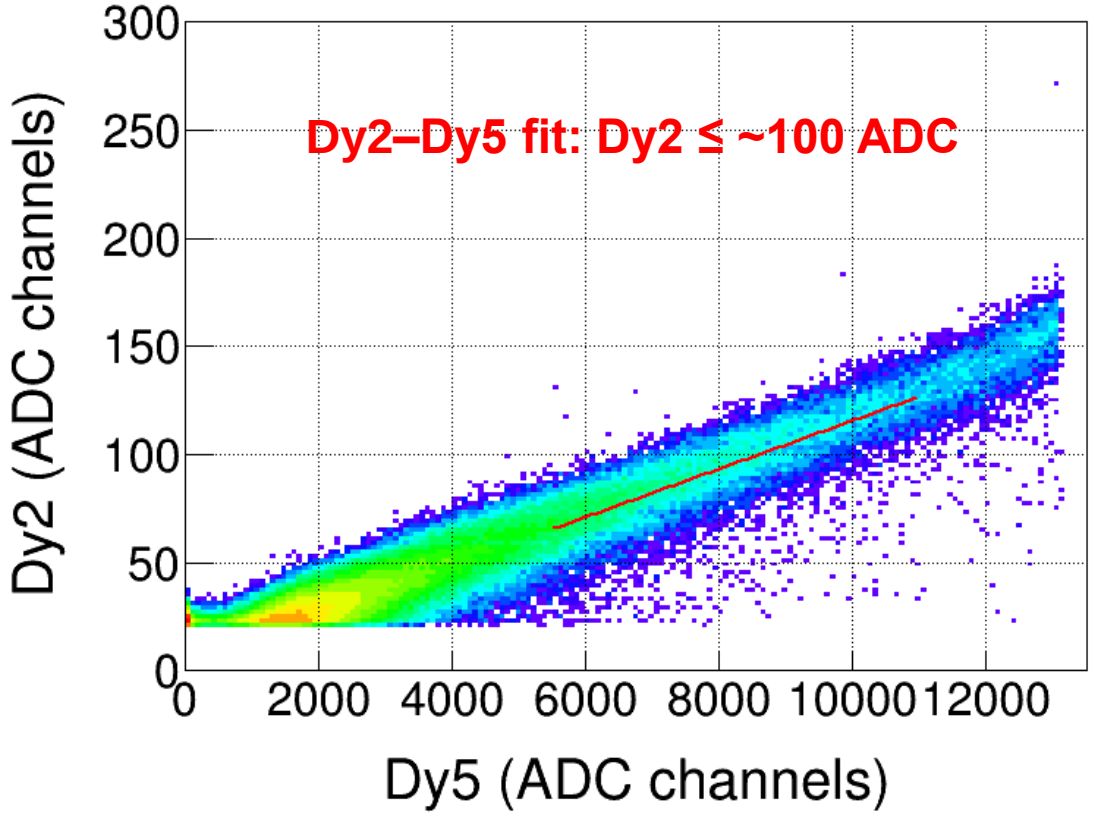

In energy reconstruction, the signal conversion between dynodes, derived from fits a few hundred ADC counts, must be extrapolated up to ~12,000 ADC counts.

New Method

$$\left(\frac{Dy5}{Dy2}\right)_P = \left(\frac{Dy5_P}{Dy5_N}\right) \times \left(\frac{Dy5_N}{Dy2_P}\right)$$

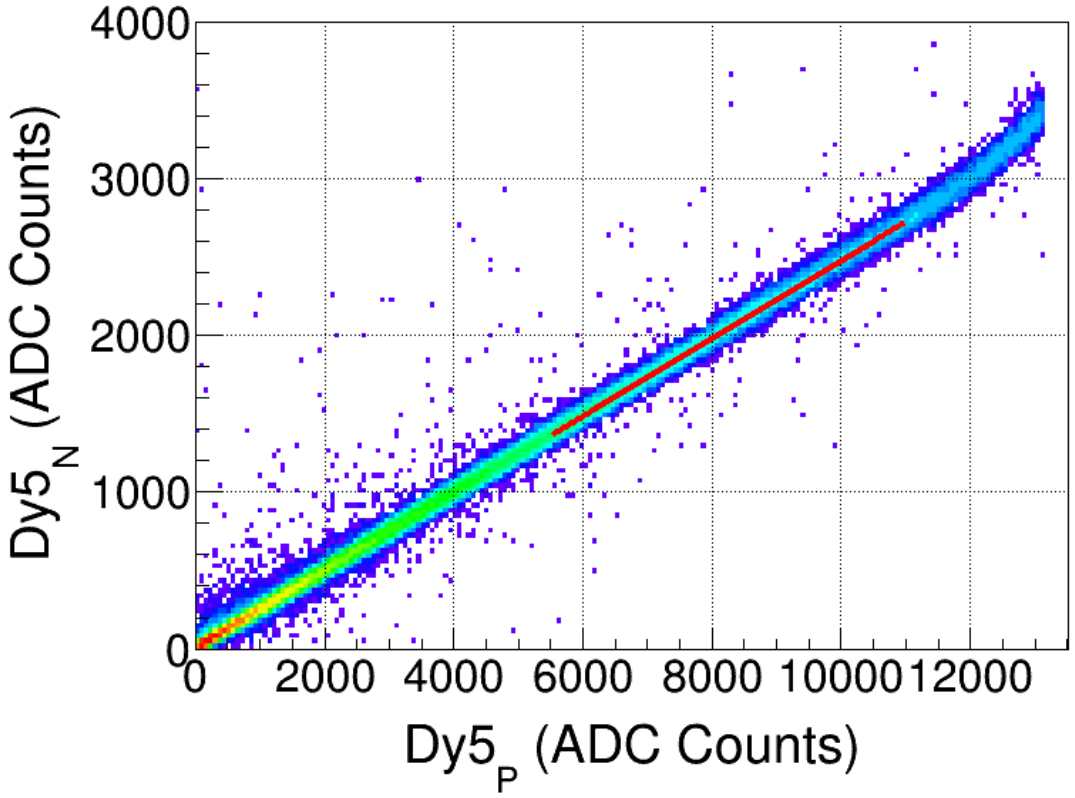

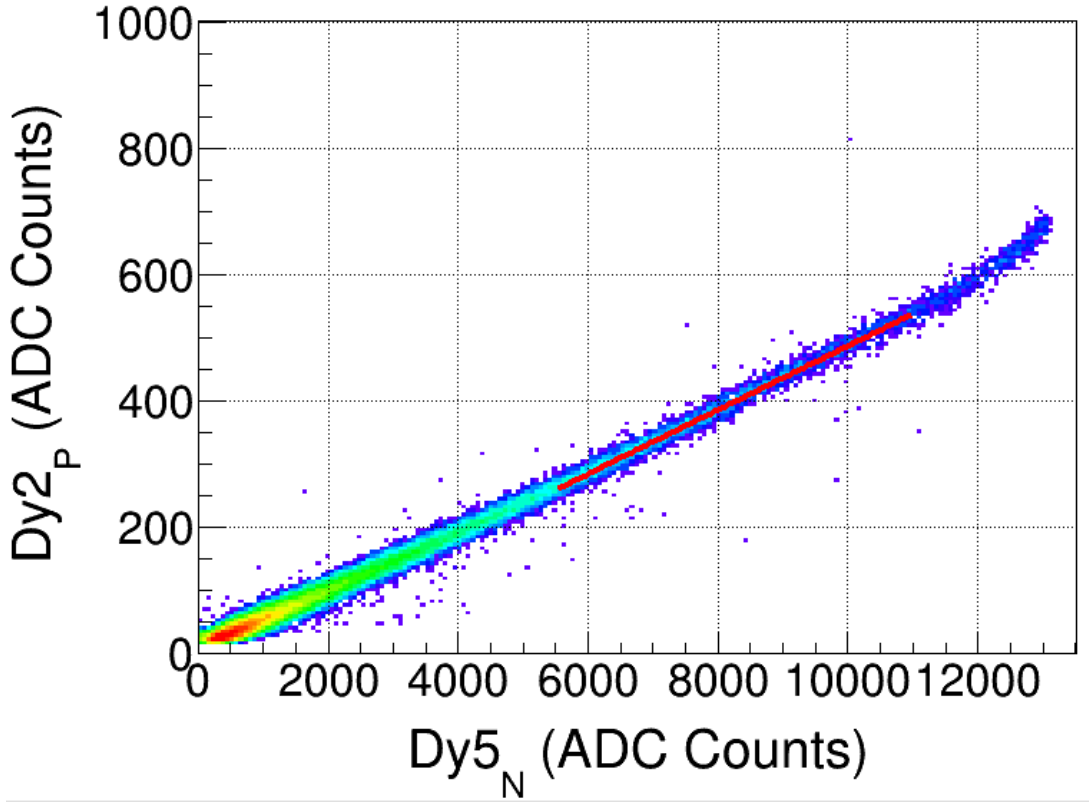

The opposite-end channel is used as an intermediary to extend the fitting range by combining ratios from channels with wider overlapping signal ranges.

New Method

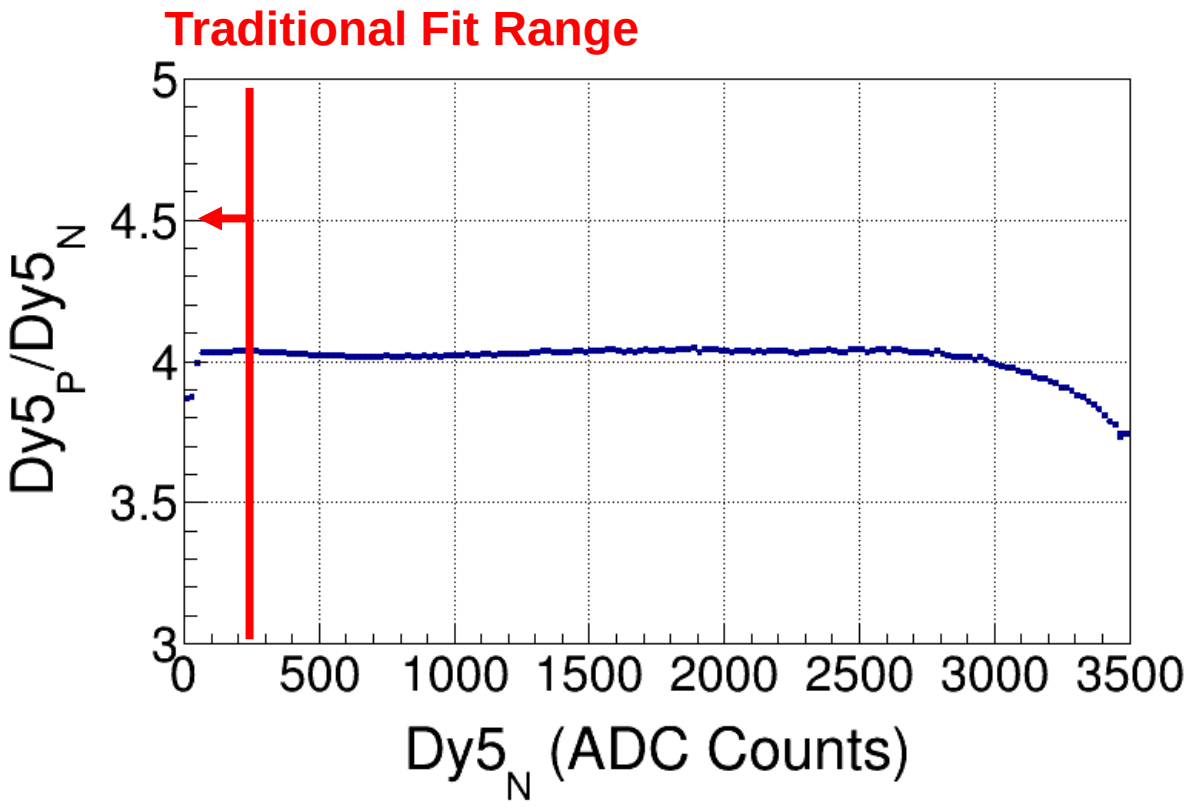

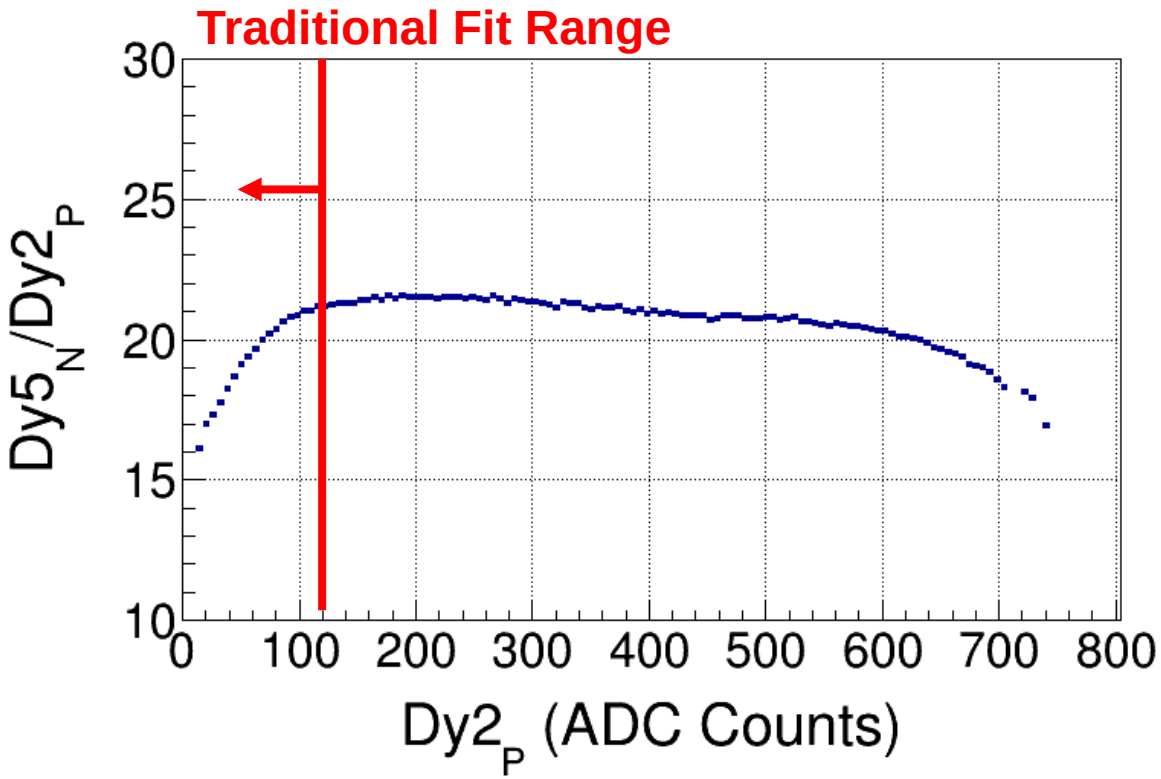

Especially for Dy2, this method extends the fitting range from ~100 to ~500 ADC counts compared with a direct Dy2–Dy5 fit, reducing low-signal nonlinearity.

New Method

$$(\frac{Dy8}{Dy5})_P = (\frac{Dy8_P}{Dy8_N}) \times (\frac{Dy8_N}{Dy5_P})$$
$$(\frac{Dy8}{Dy5})_N = (\frac{Dy8_N}{Dy5_P}) \times (\frac{Dy5_P}{Dy5_N})$$
$$(\frac{Dy5}{Dy2})_P = (\frac{Dy5_P}{Dy5_N}) \times (\frac{Dy5_N}{Dy2_P})$$
$$(\frac{Dy5}{Dy2})_N = (\frac{Dy5_N}{Dy2_P}) \times (\frac{Dy2_P}{Dy2_N})$$

The dynode ratios for all 616 PMTs in the BGO calorimeter can be obtained

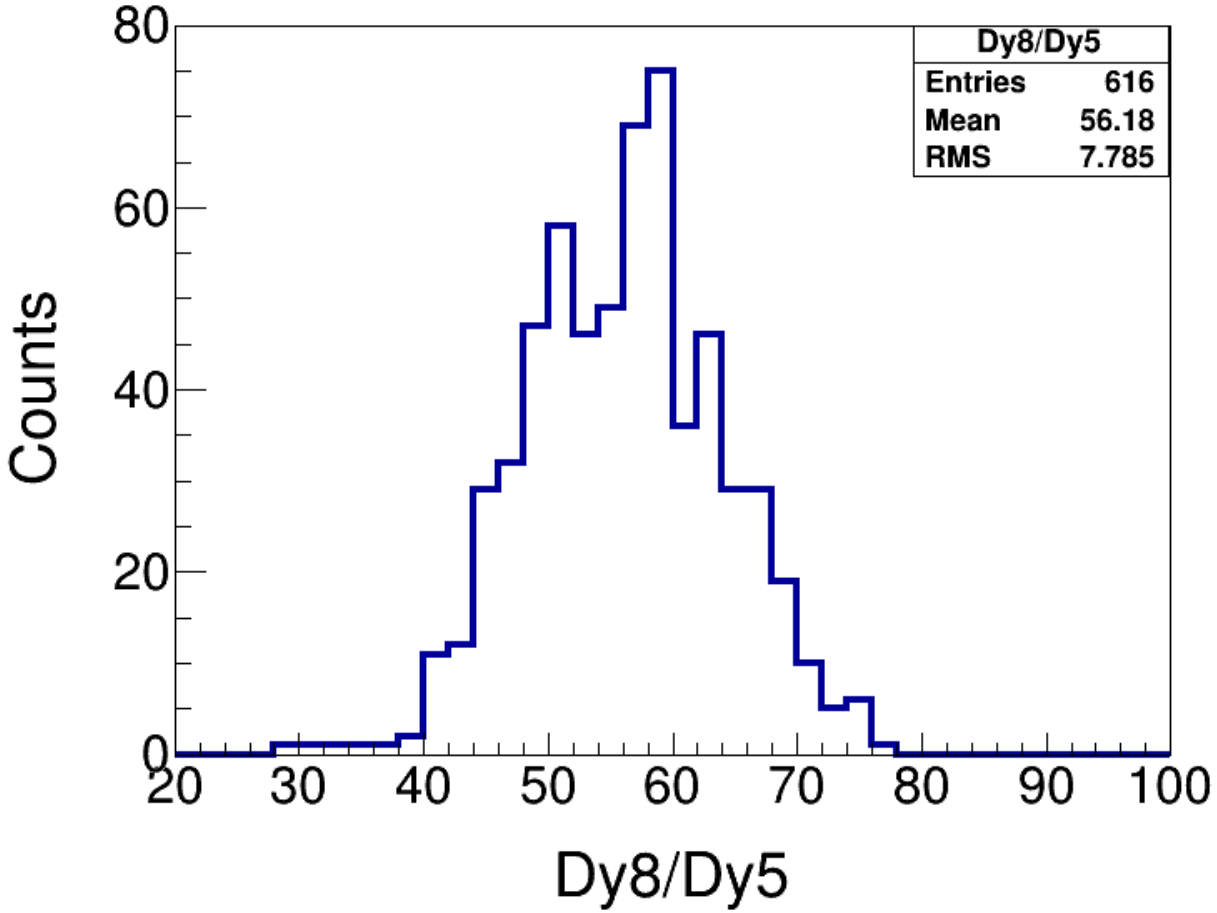

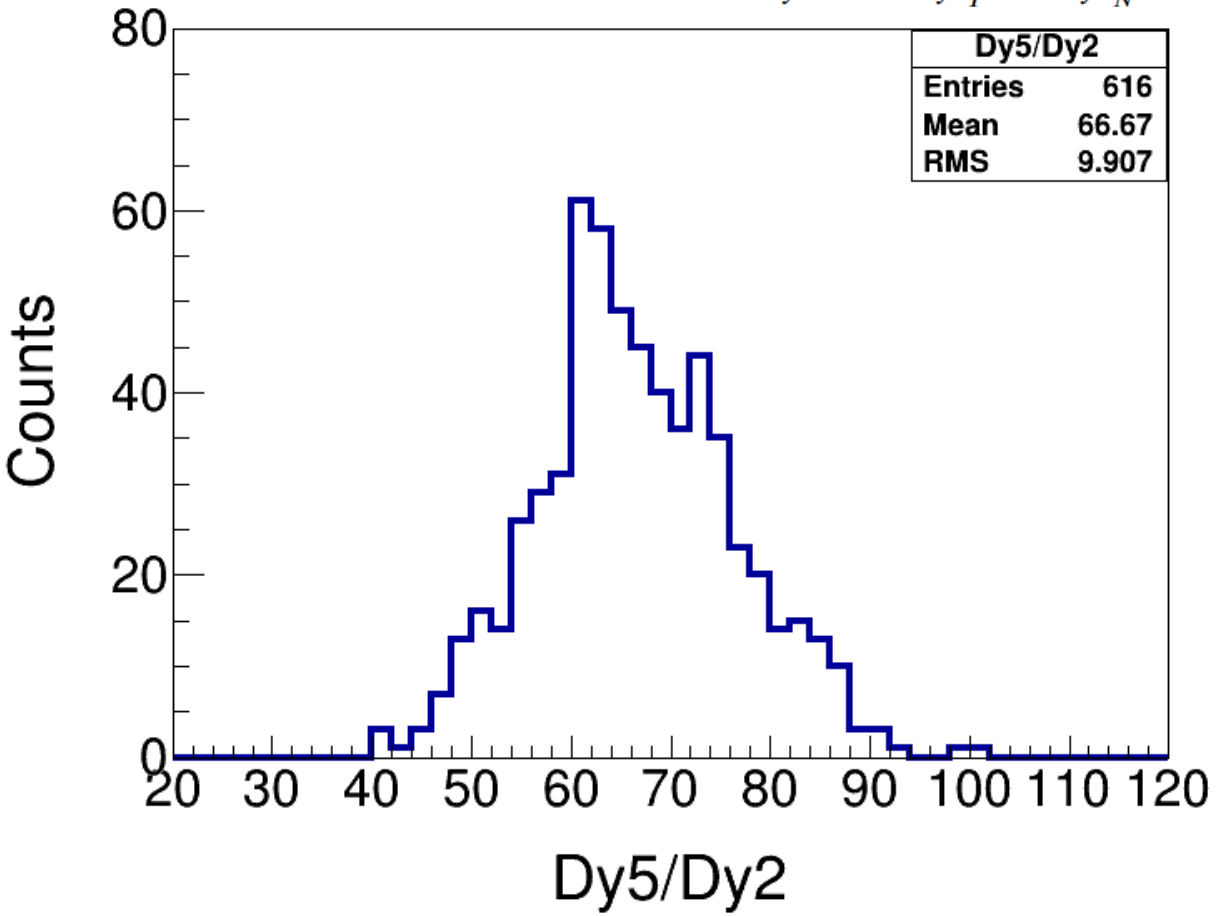

Stability

Variation of the dynode ratios for a specific PMT from January 1, 2016, to January 1, 2026.

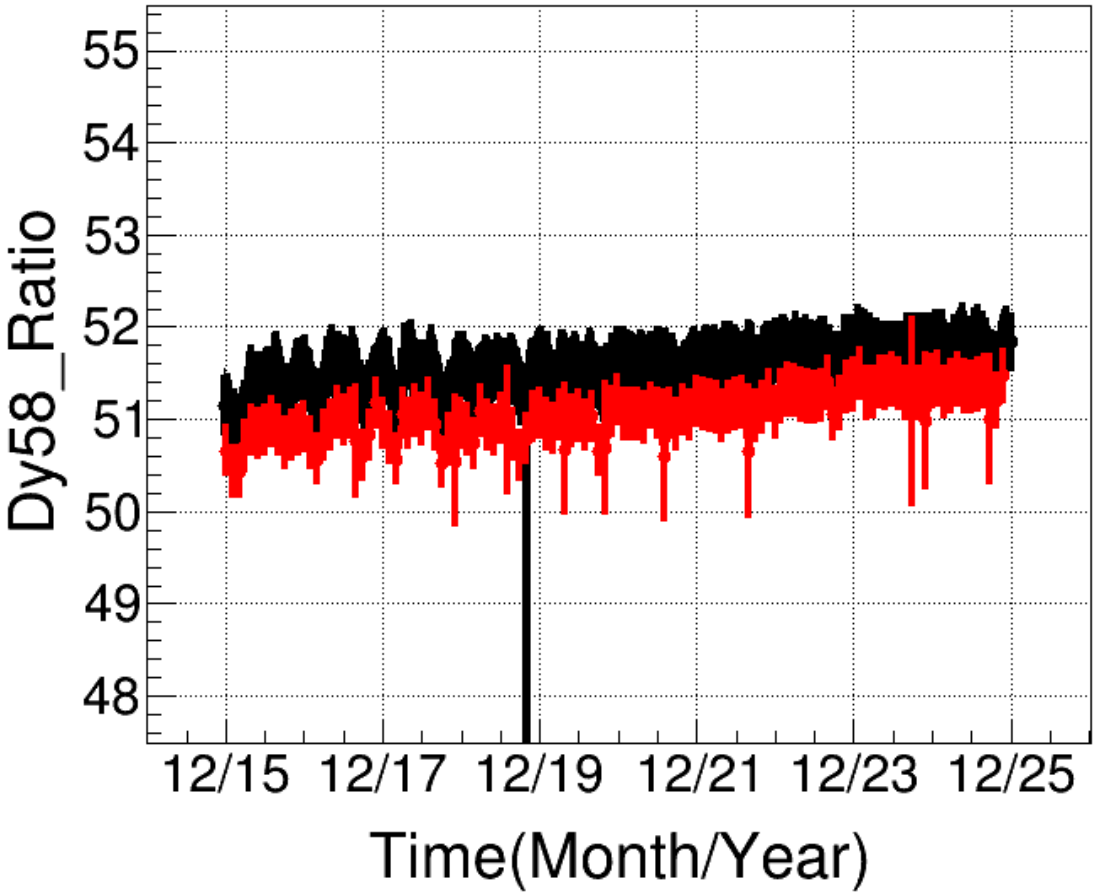

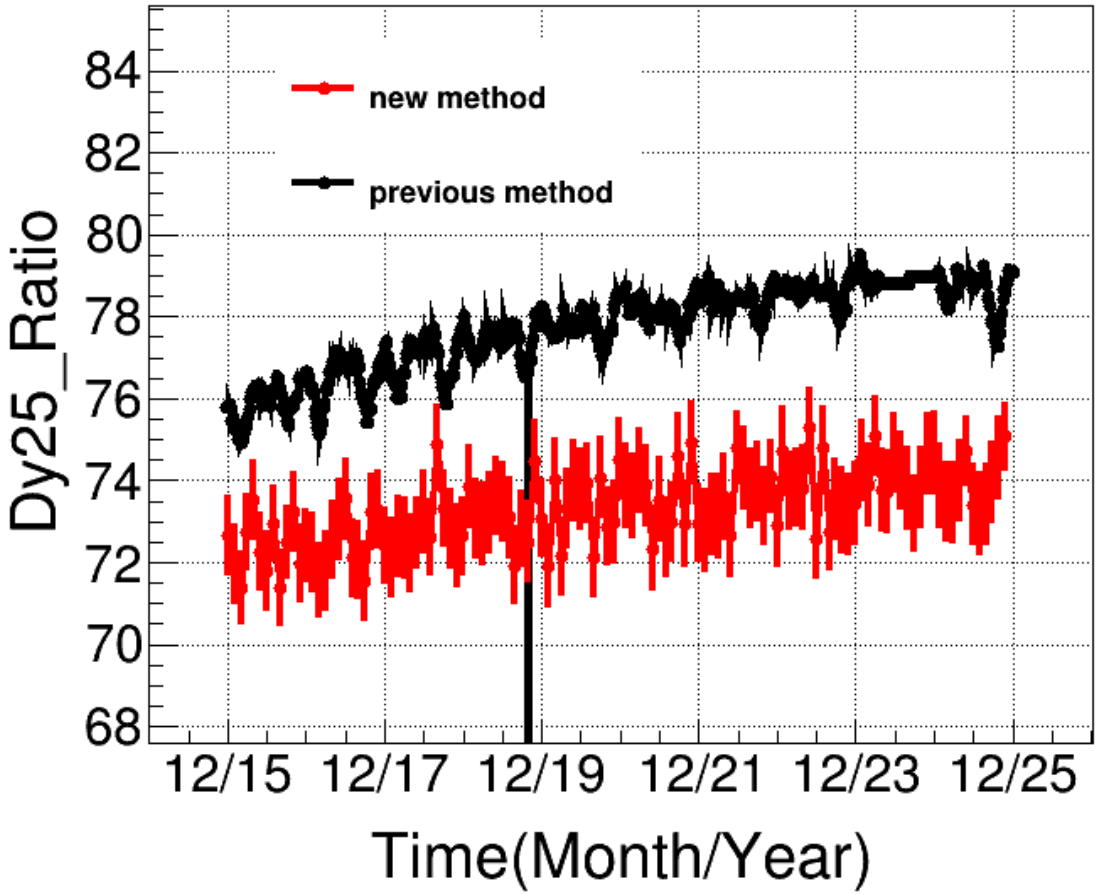

LED Test

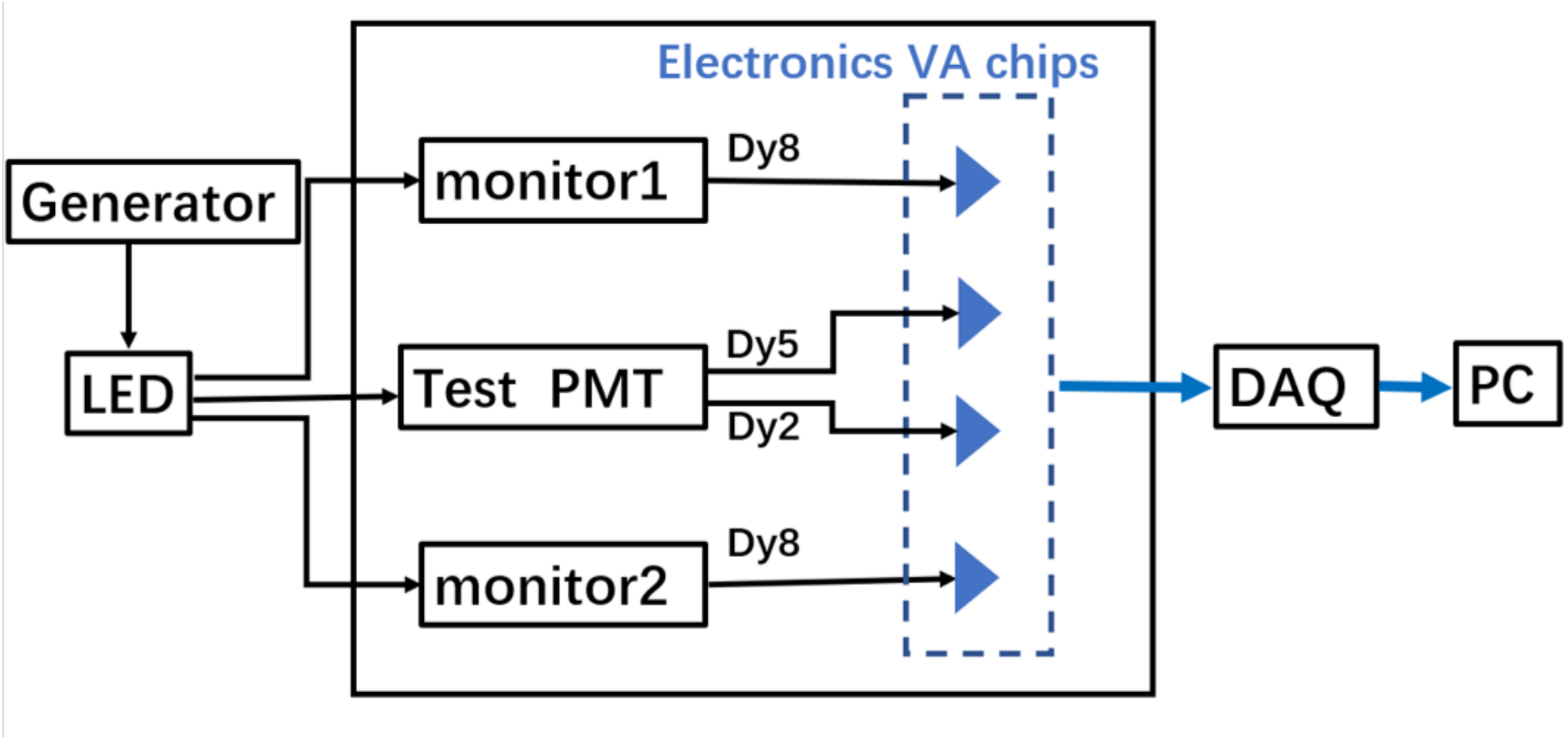

Two reference PMTs with different sensitivities (the output signal of Dy8 from monitor1, the output signal of Dy8 from monitor2) are used to verify the output signals from Dy2 and Dy5 of the test PMT. The light from a pulsed LED was split by fibers, which are able to cover all PMTs.

LED Test

Correlation between Dy5 and monitoring PMT (M1) signals.

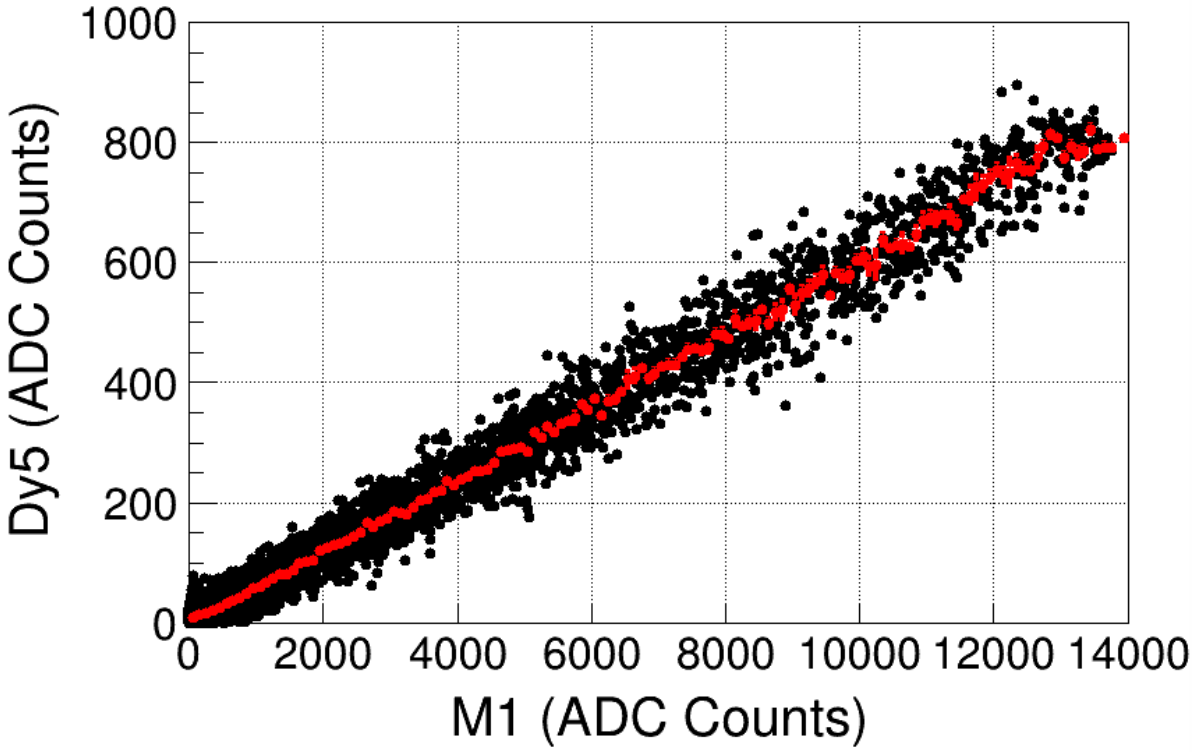

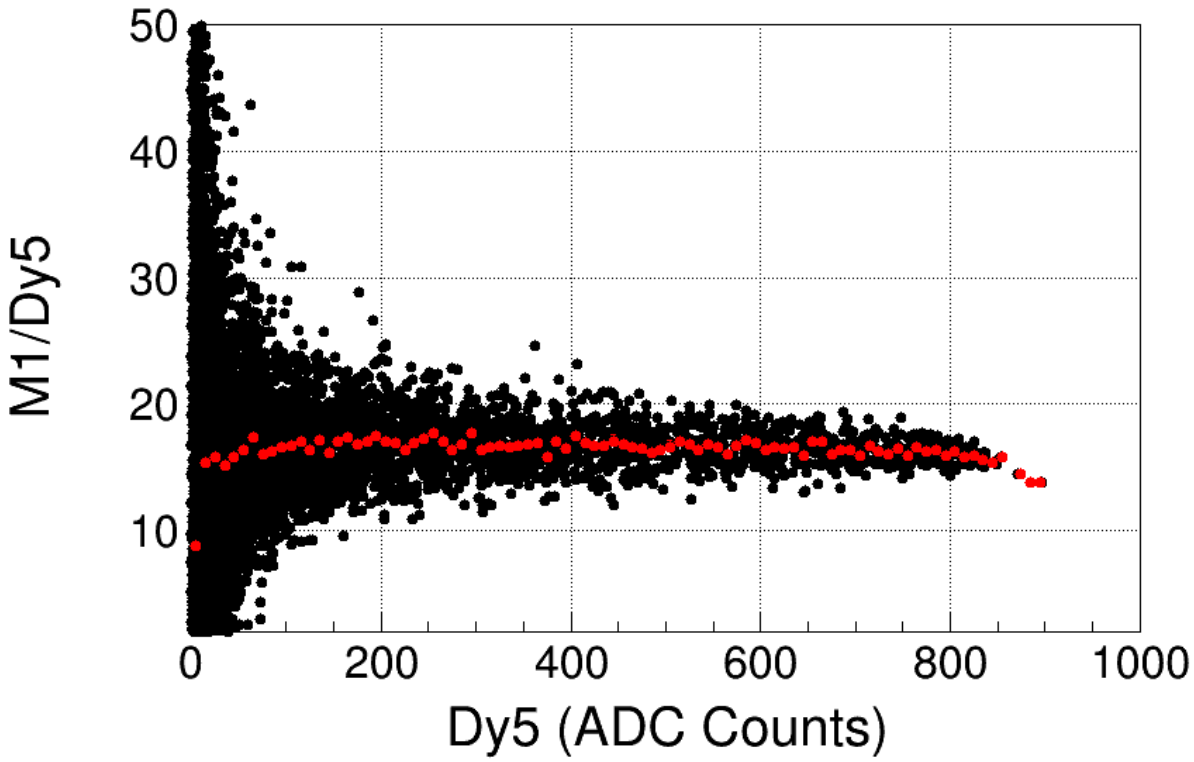

In the medium-to-high signal range, Dy5 and M1 exhibit good linear consistency, further confirming the reliability and effectiveness of Dy5 as an intermediary channel for dynode ratio calibration.

LED Test

Correlation between Dy2 and monitoring PMT (M2) signals.

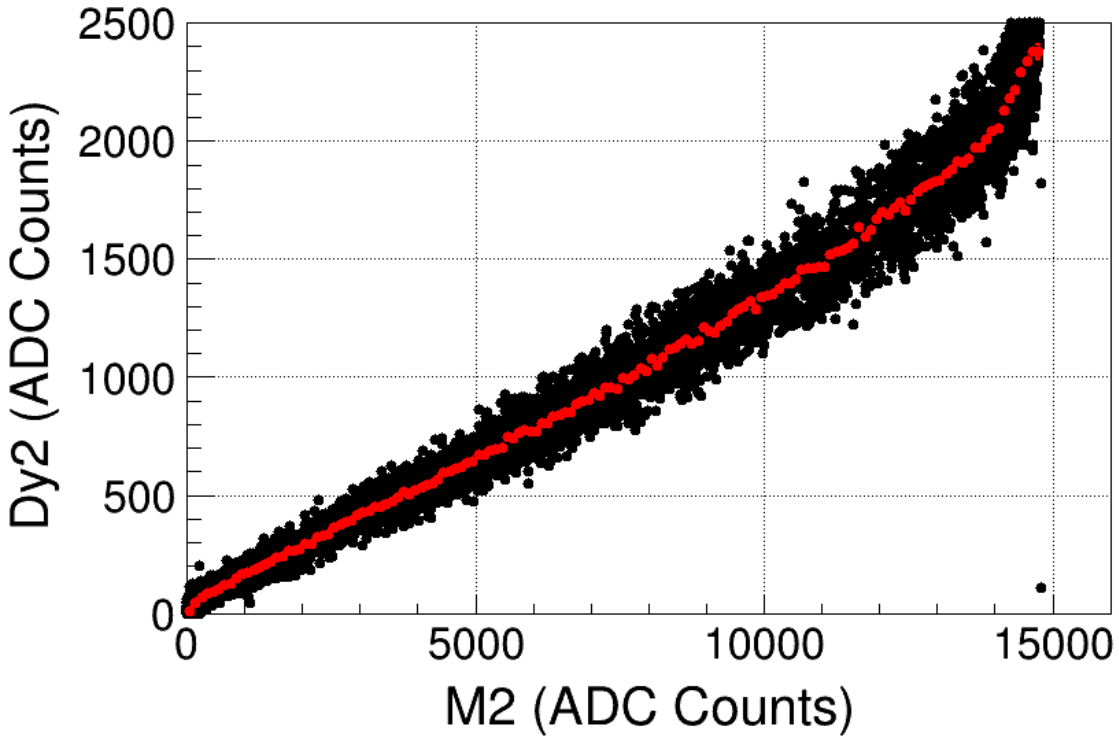

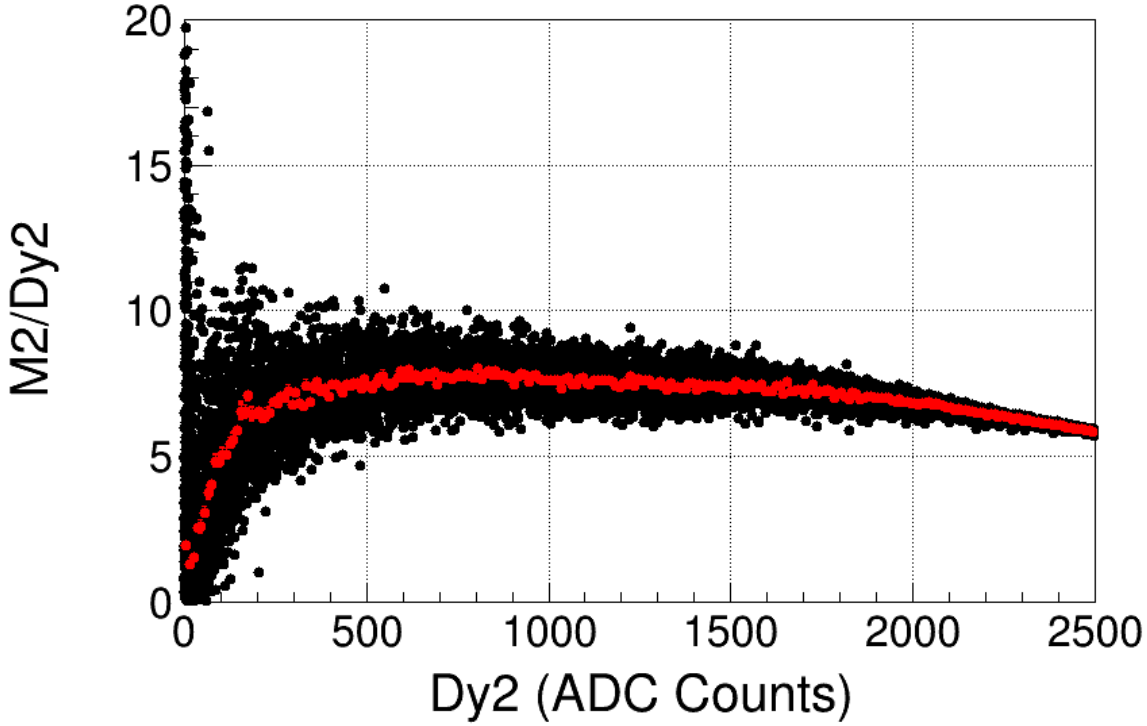

Dy2 and M2 also maintain a stable linear response in the medium-to-high signal region, but Dy2 exhibits stronger nonlinearity at low signals, consistent with in-flight observations.

The Response to High-Energy Cosmic-Ray Electron Candidates

PN Consistency

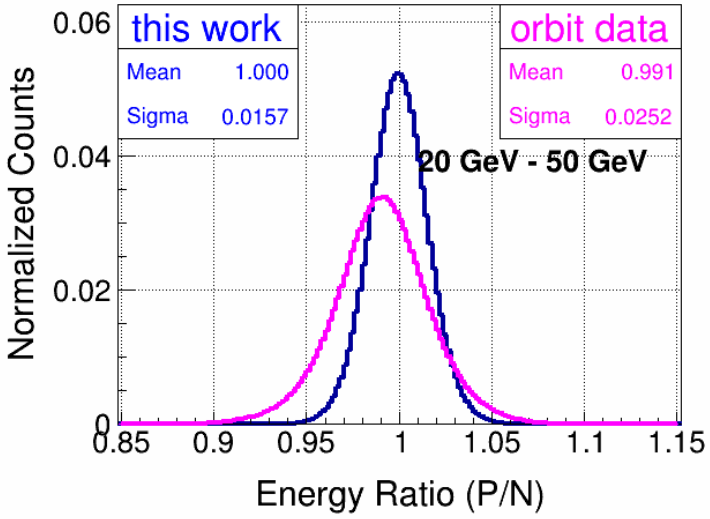

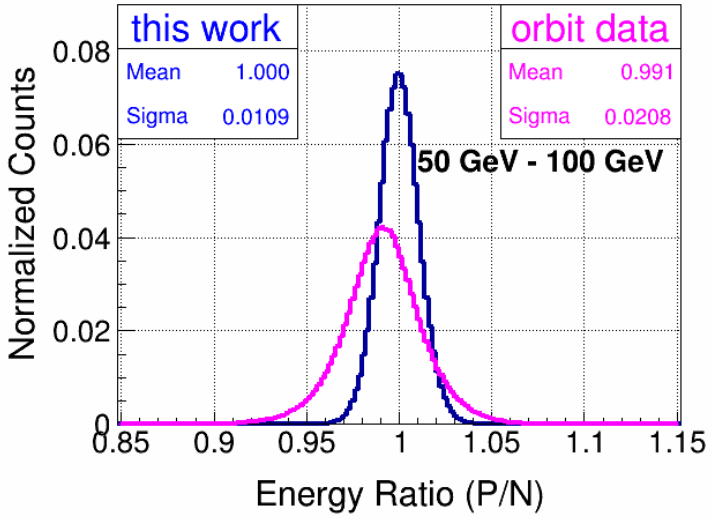

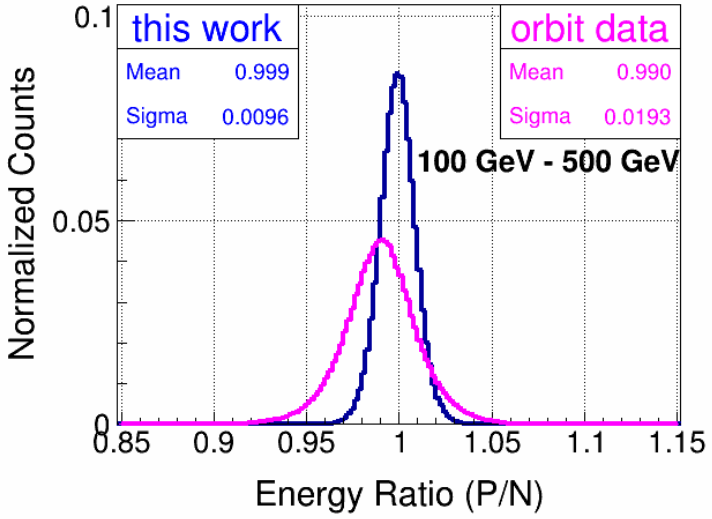

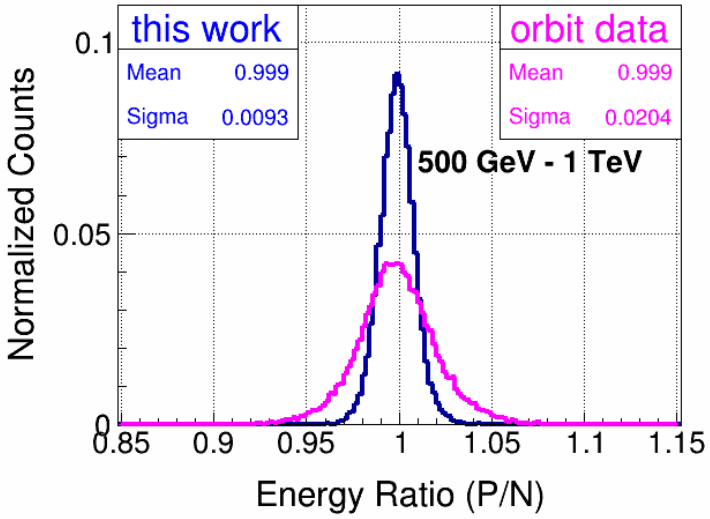

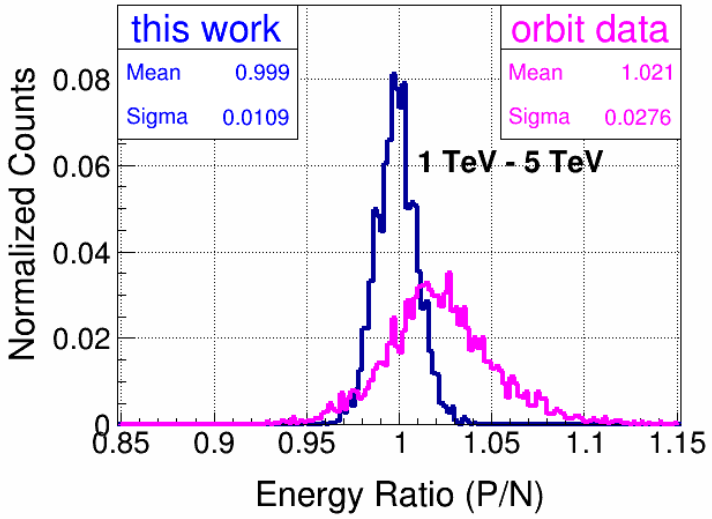

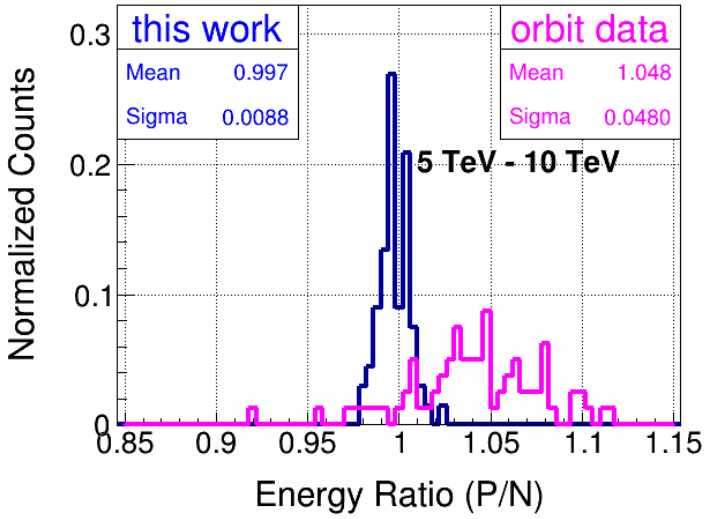

Stability of P/N

Electron Candidates Above 200 GeV

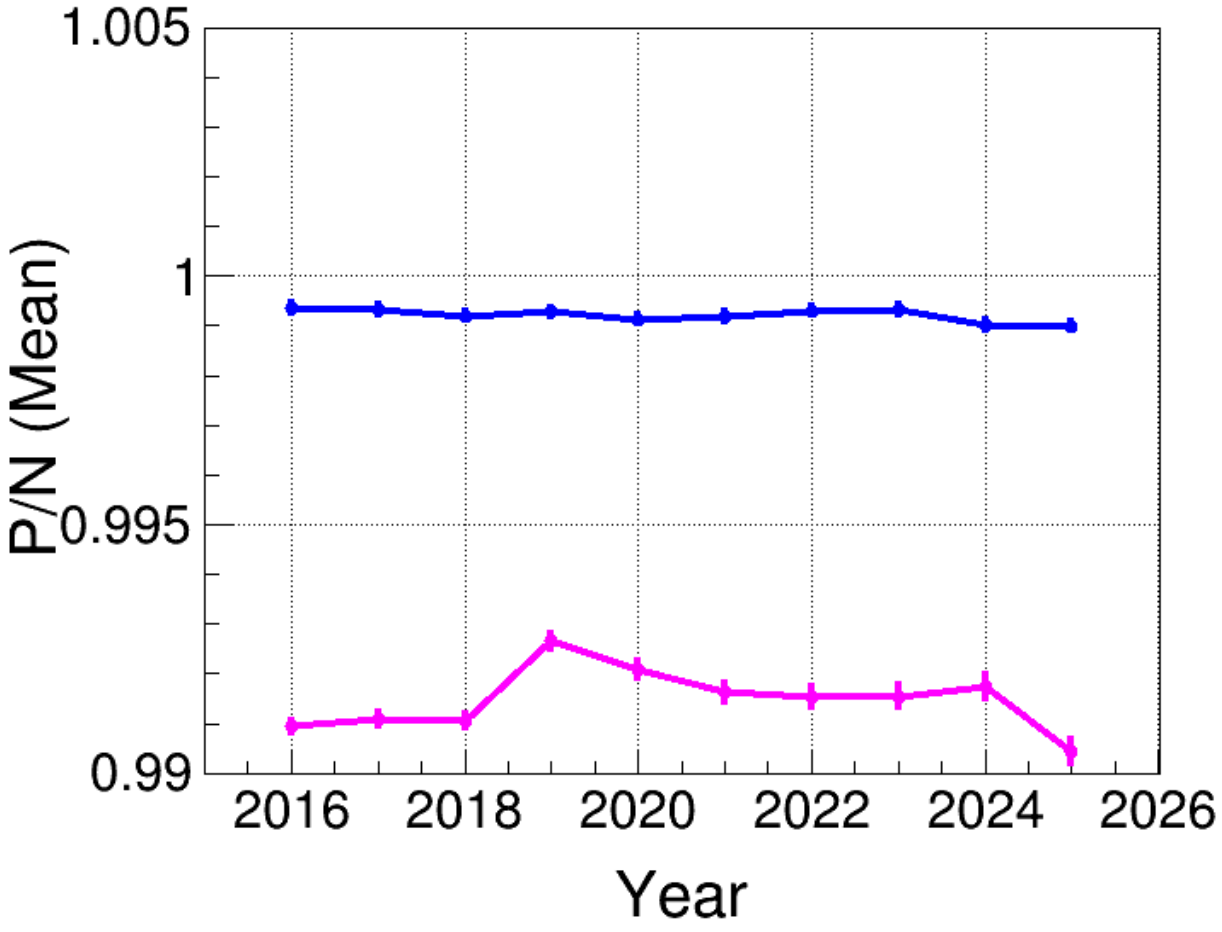

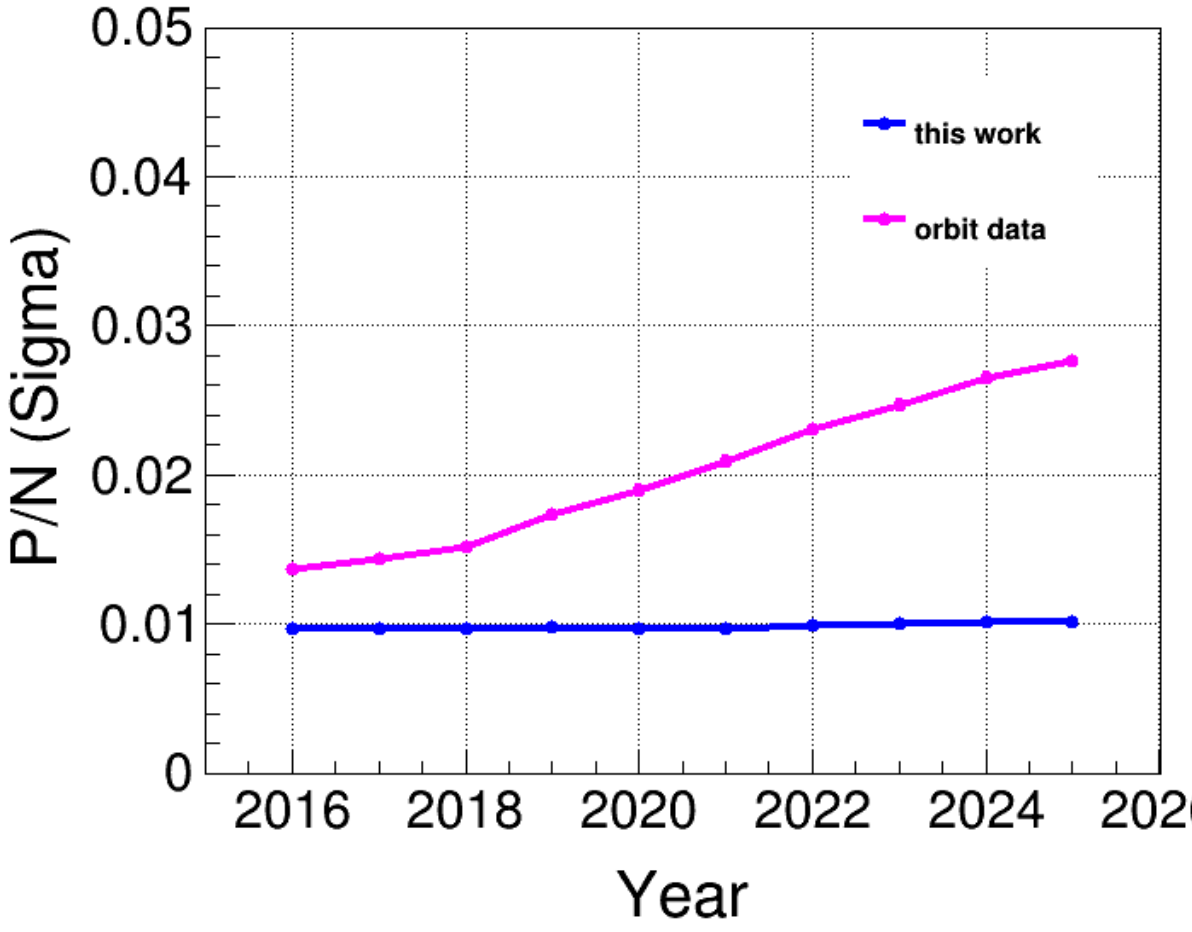

Even/Odd Consistency

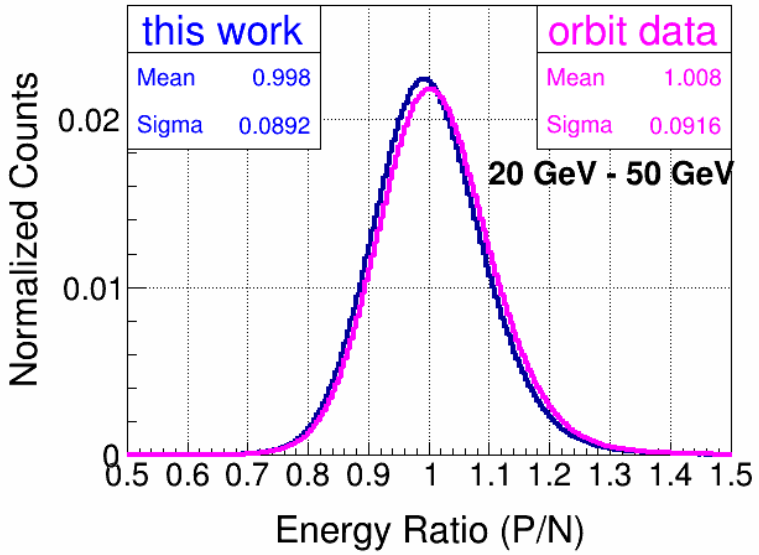

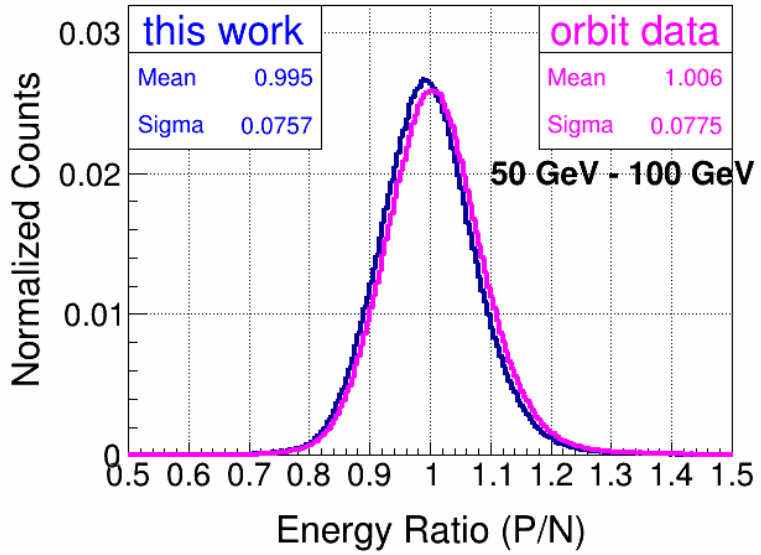

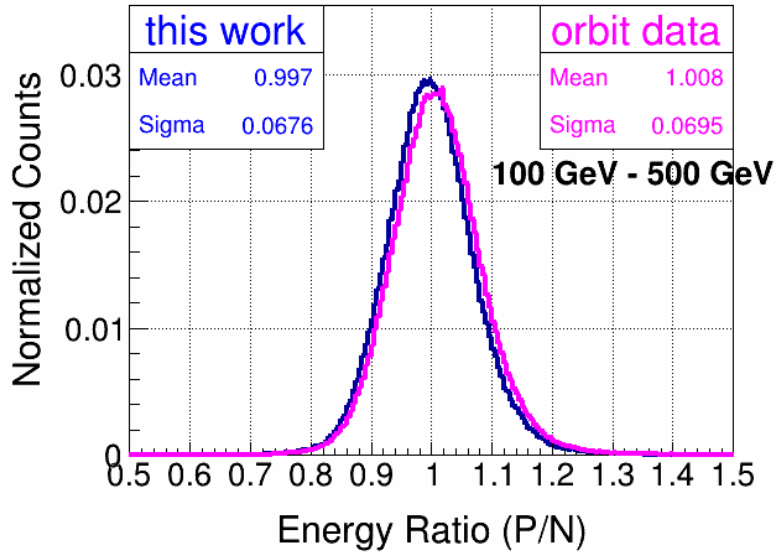

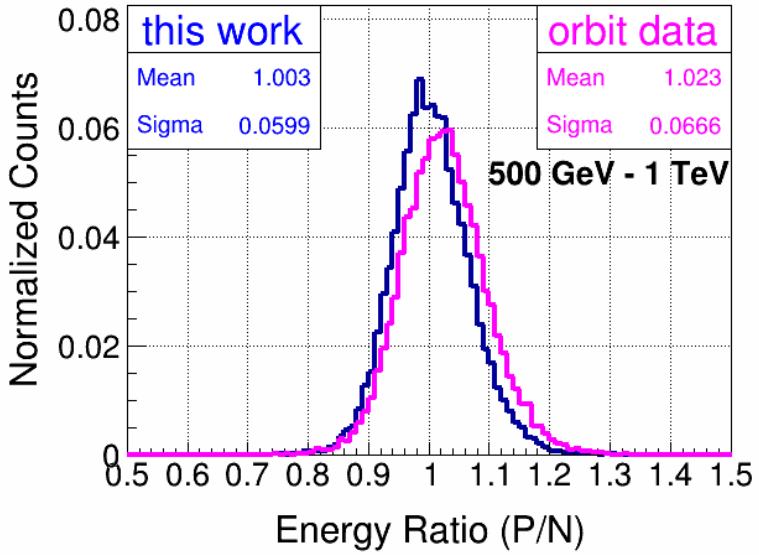

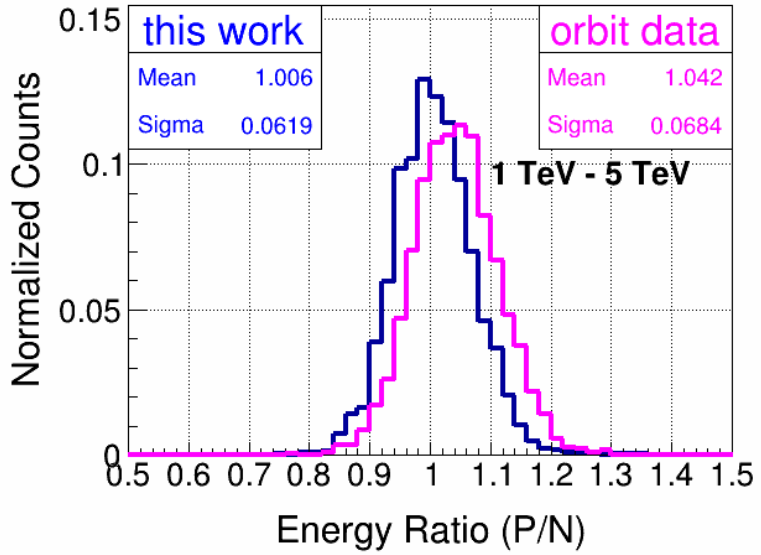

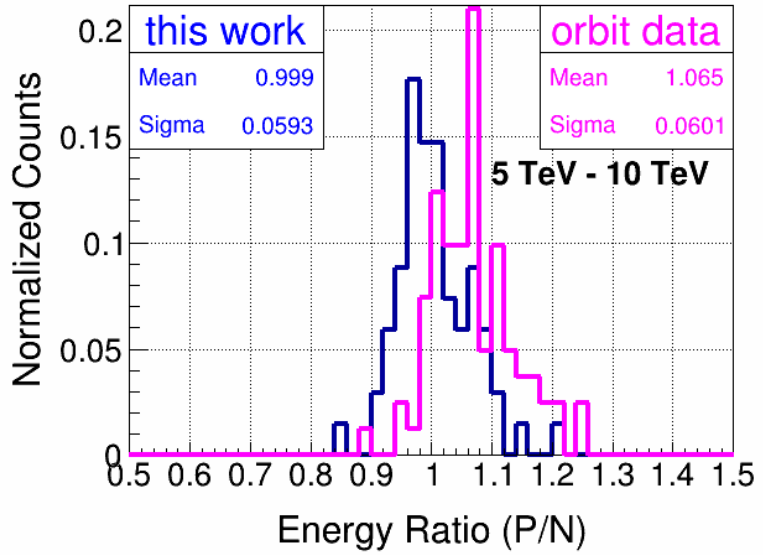

Stability of Even/Odd

Electron Candidates Above 200 GeV

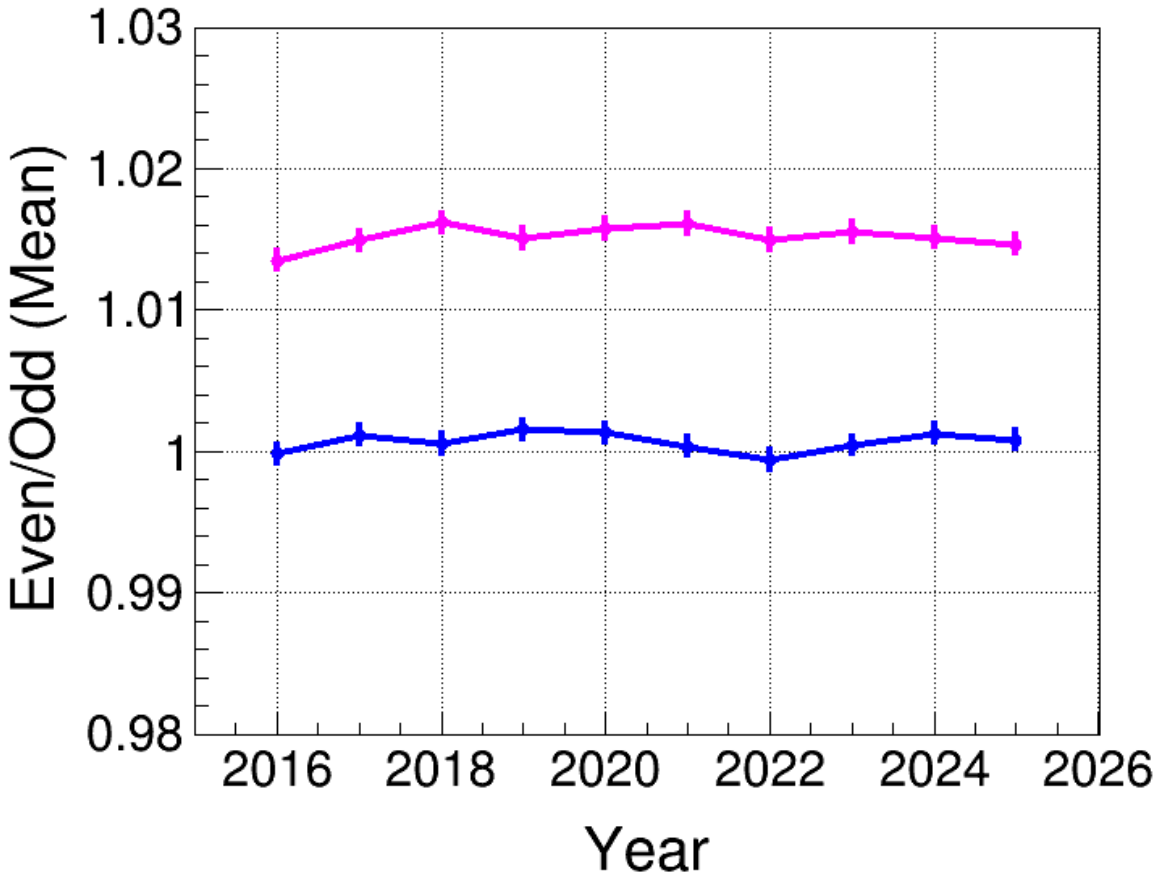

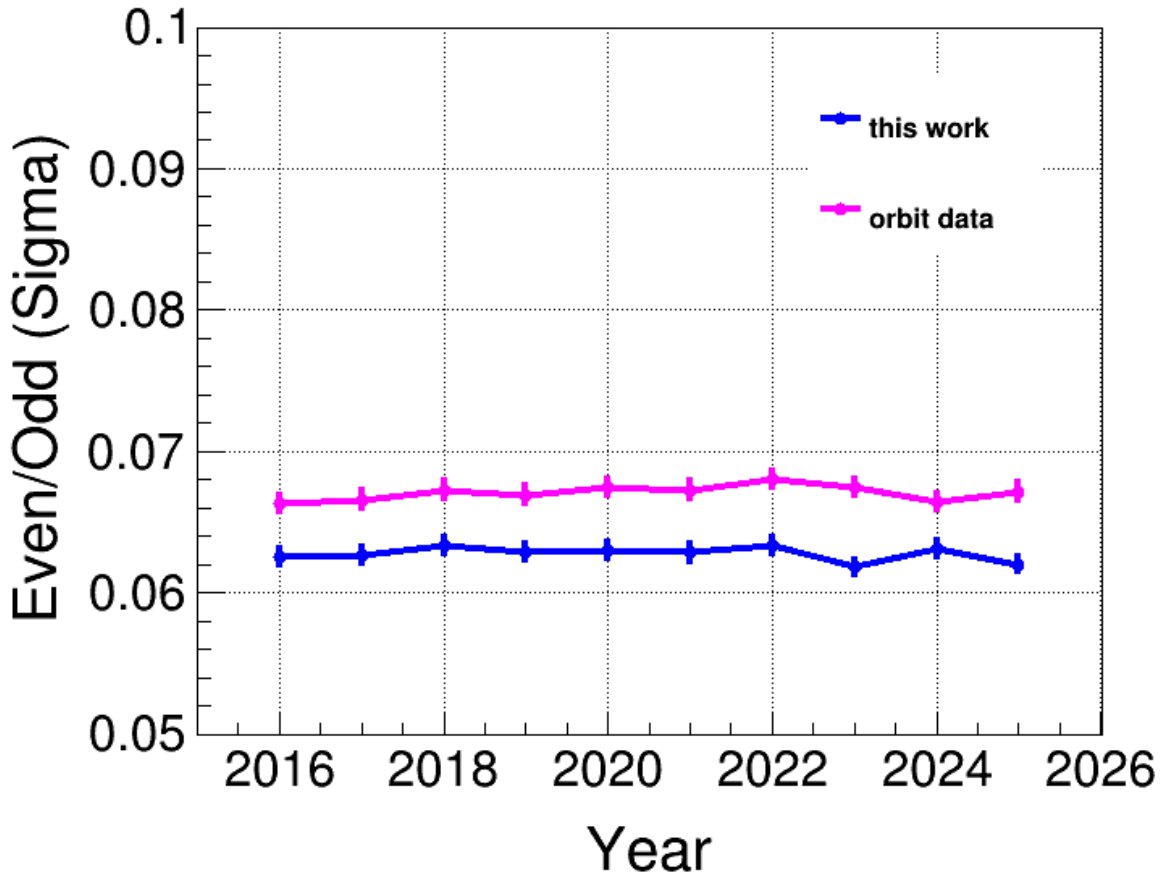

Shower maximum crystal

The Crystal with the Maximum Energy Deposition in the BGO Calorimeter for Electron Candidates

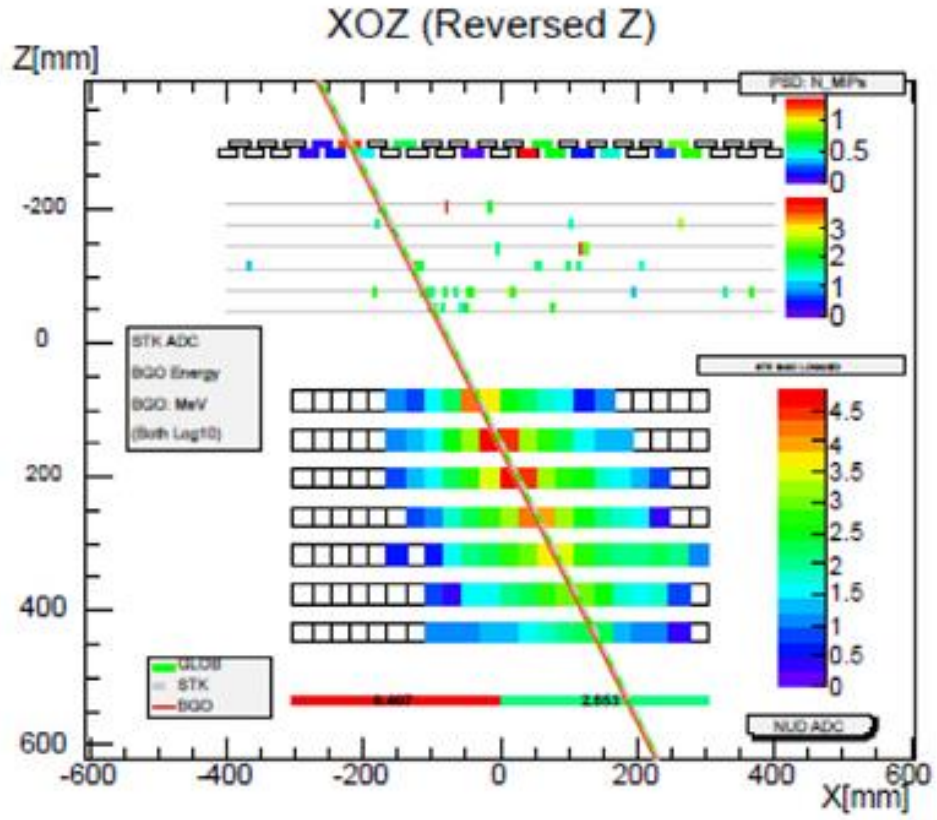

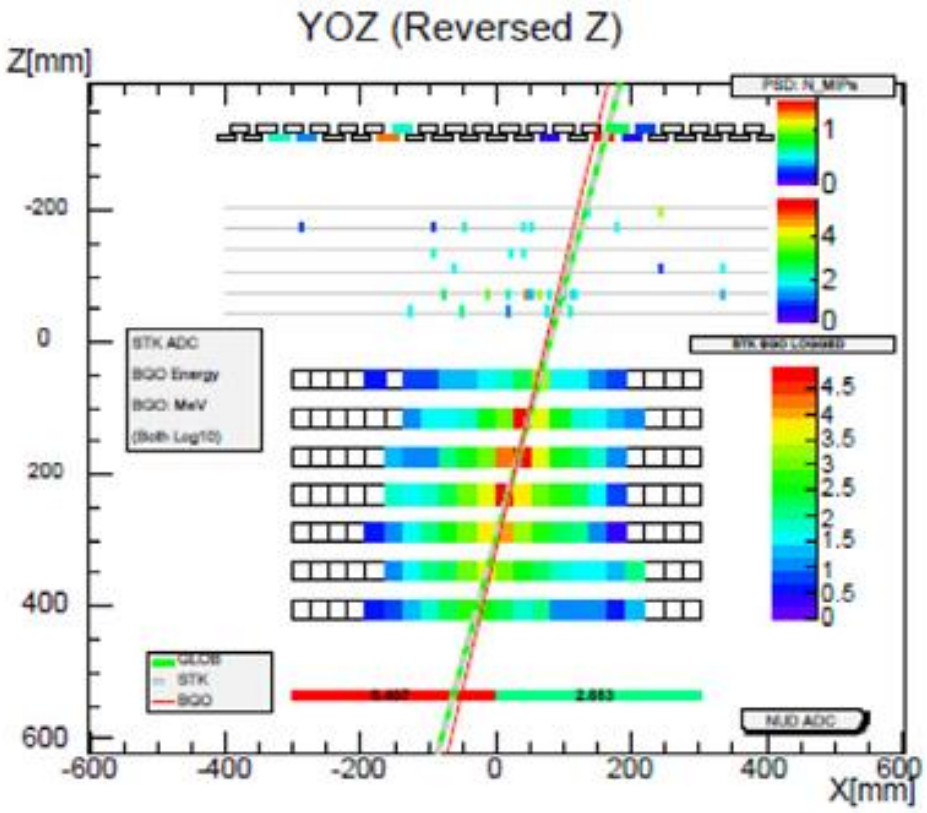

Shower maximum crystal

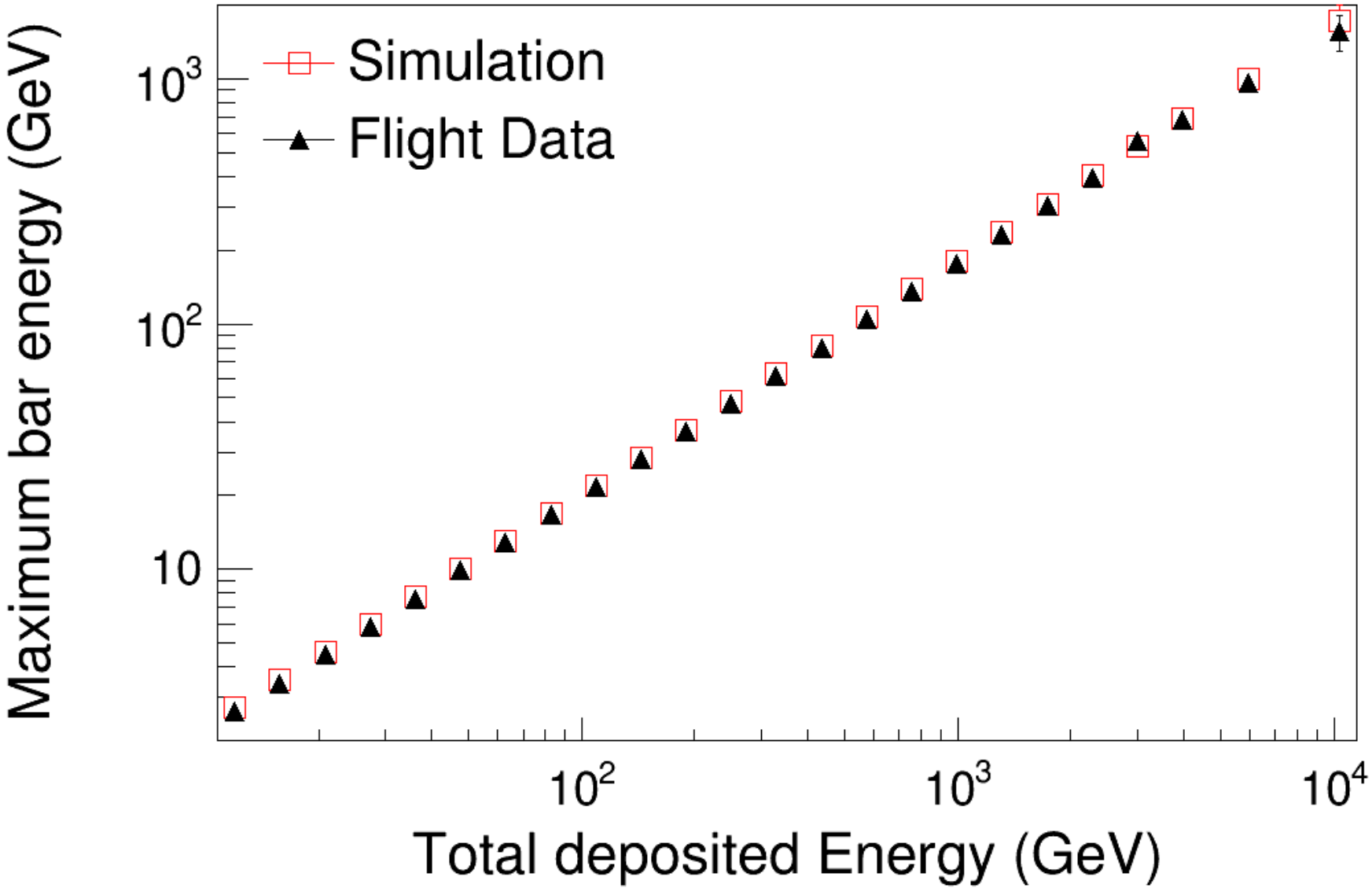

Statistical Stability of Electron Candidates

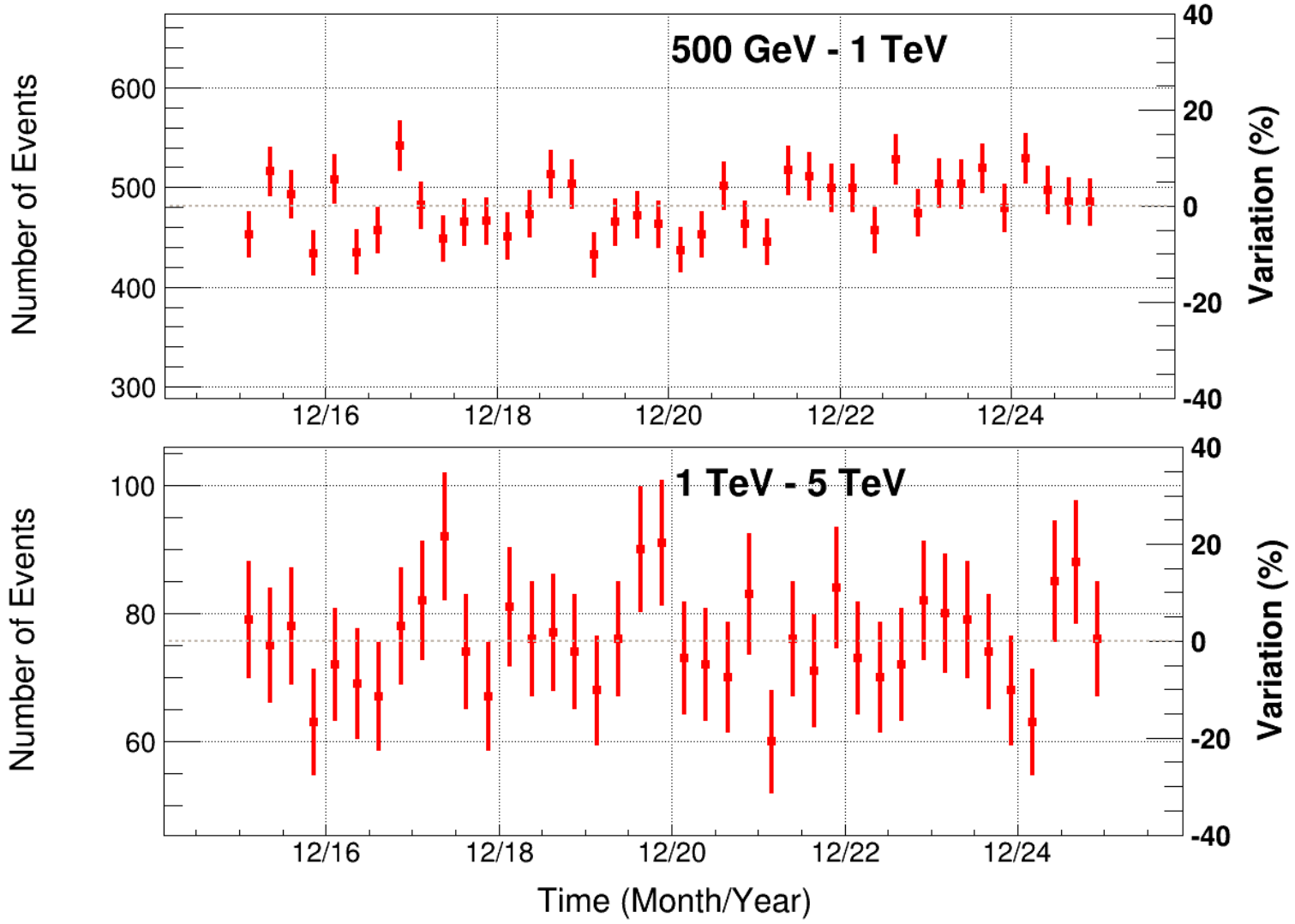

The event rates (3 months) fluctuate randomly around a stable average without systematic drift, indicating a stable detector response over years of operation.

High-Energy Electron Candidates

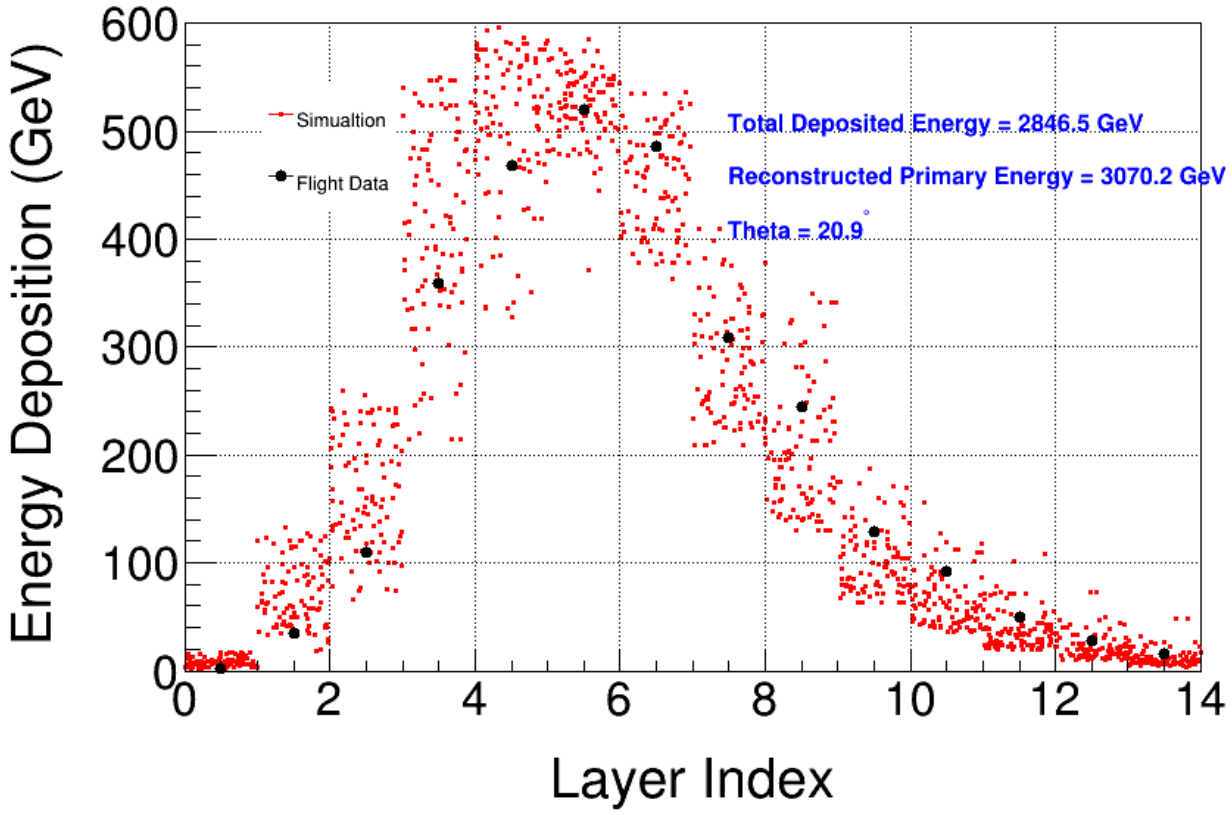

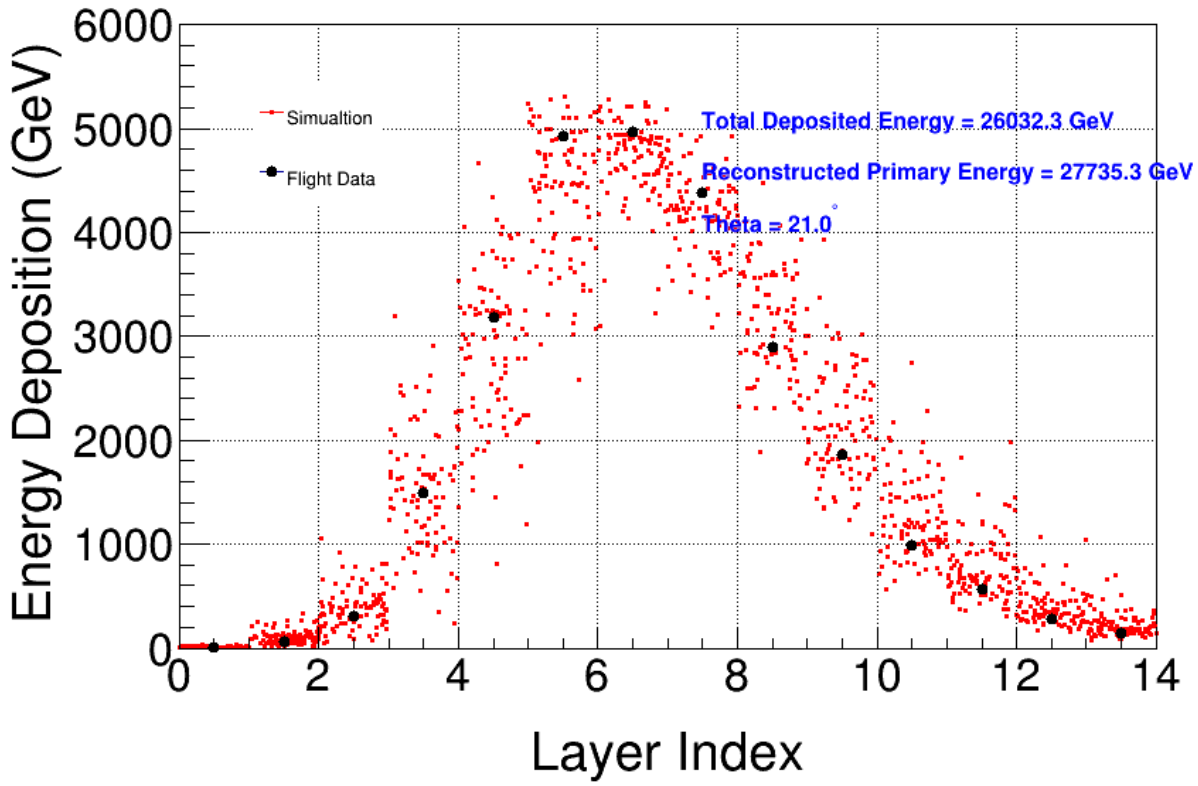

The longitudinal energy deposition distribution of the electron candidate event across layers, with the simulation data representing 100 electrons having the same energy and incident direction as the flight data.

Thanks!

BACKUP

Calibration of Fluorescence Attenuation Effect

Dy5 Method Vs Dy8 Method

Electron Candidates Above 200 GeV In a Specific BGO Bar

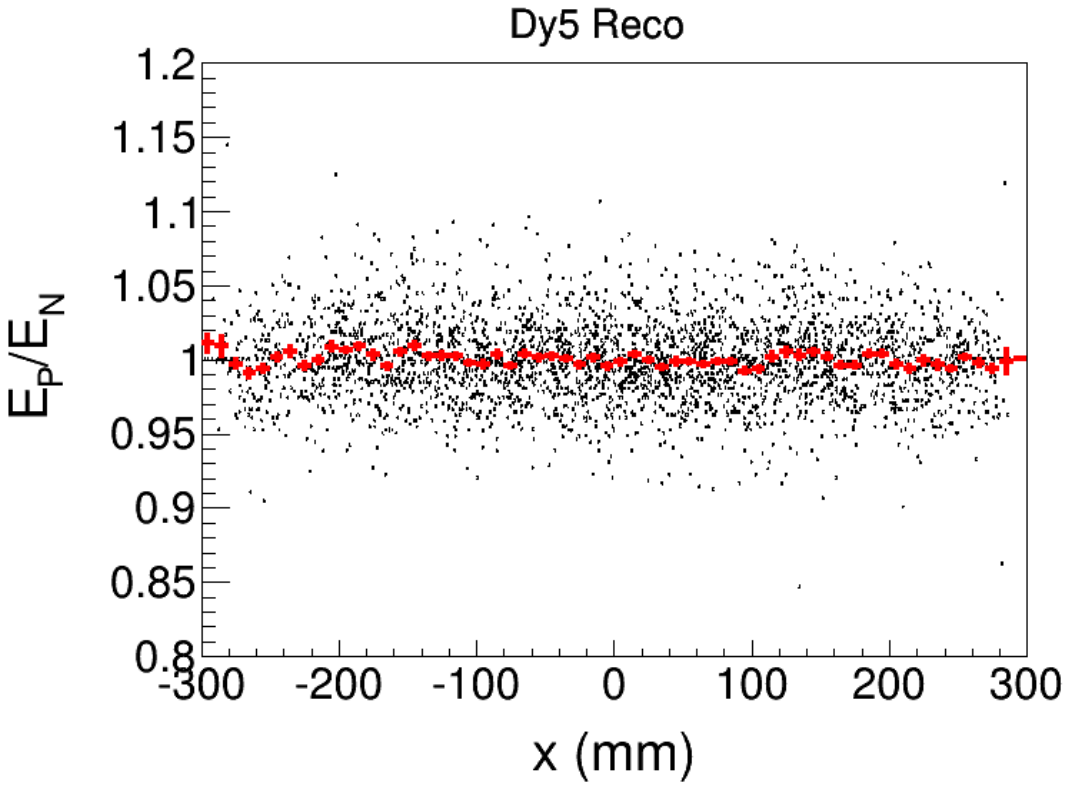

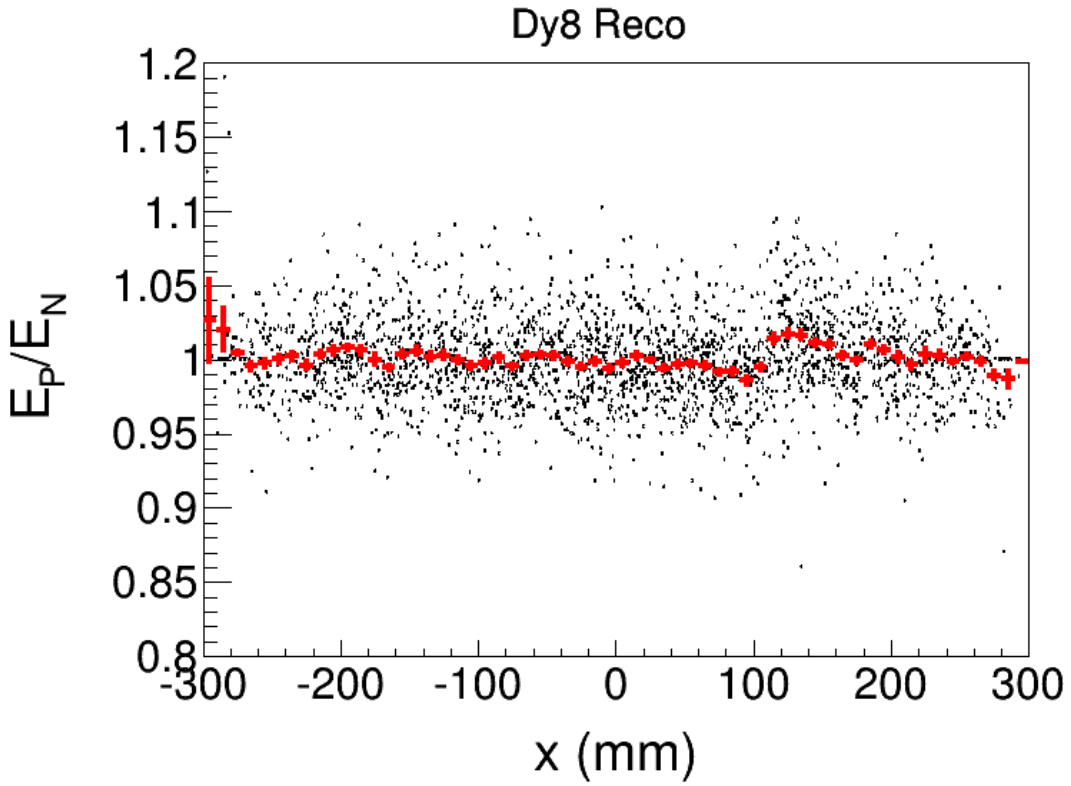

This may be due to the lower signal-to-noise ratio of Dy8, leading to larger fluctuations and degraded resolution. Therefore, Dy8 is not suitable for attenuation calibration.

10 mm Vs 5 mm

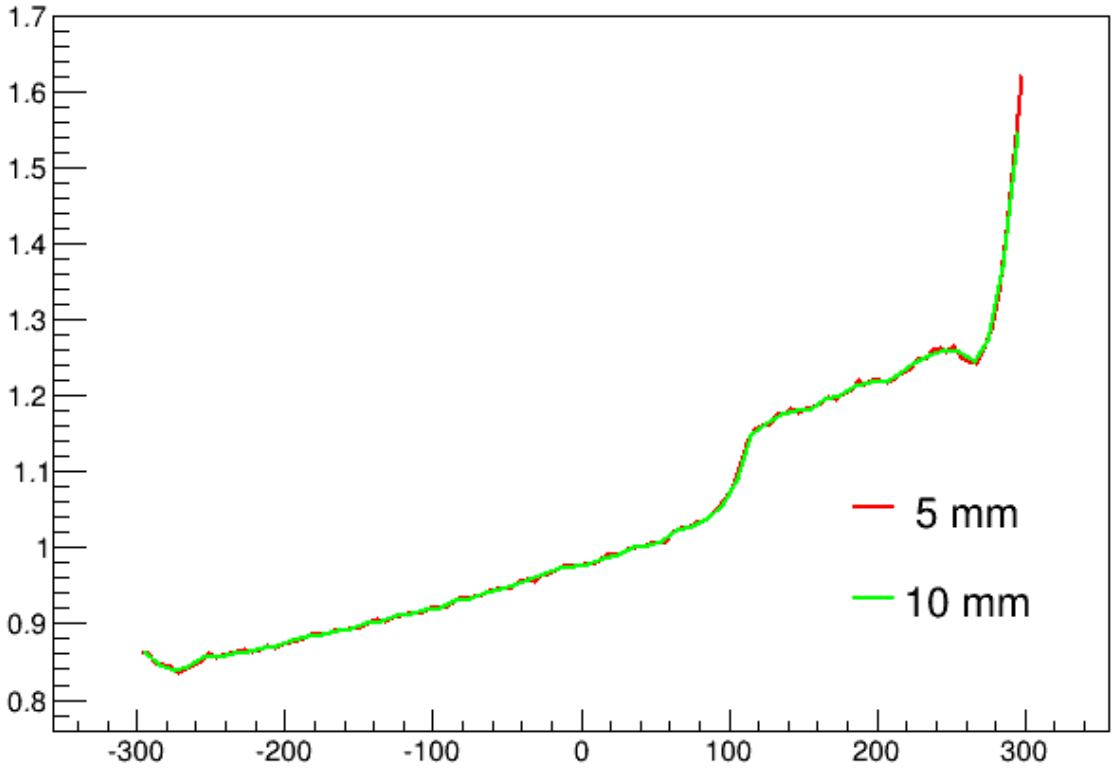
1.7
1.6
1.5
1.4
1.3
1.2
1.1
1
0.9
0.8
-300
-200
-100
0
100
200
300
5 mm
10 mm

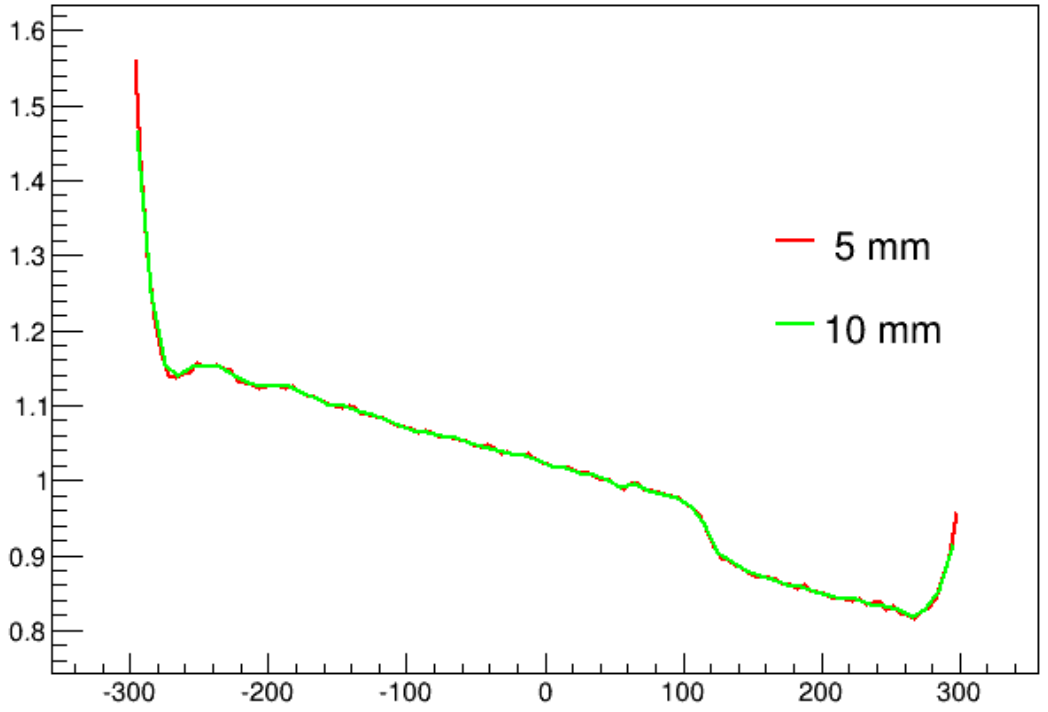
1.6
1.5
1.4
1.3
1.2
1.1
1
0.9
0.8
-300
-200
-100
0
100
200
300
5 mm
10 mm

DAC Calibration

Layer 5 and Layer 7

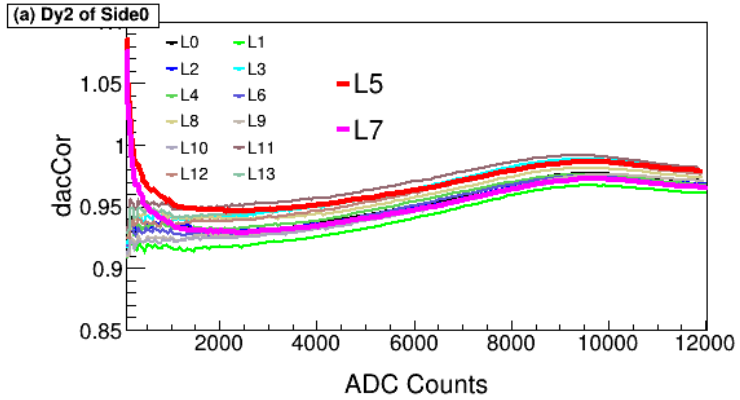

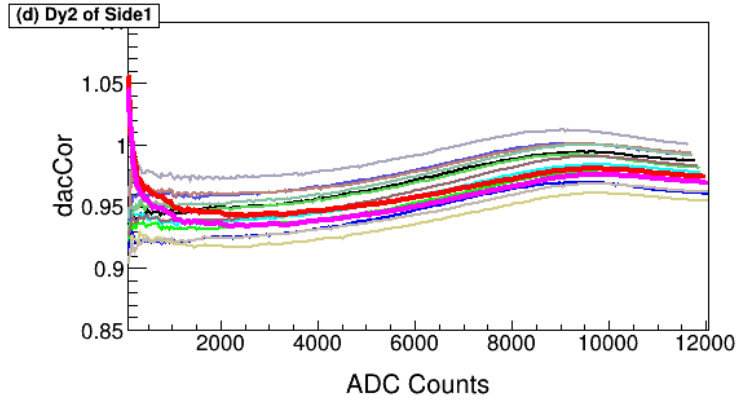

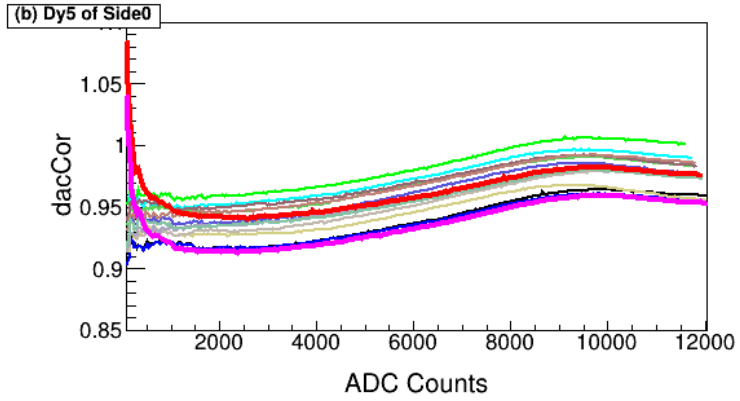

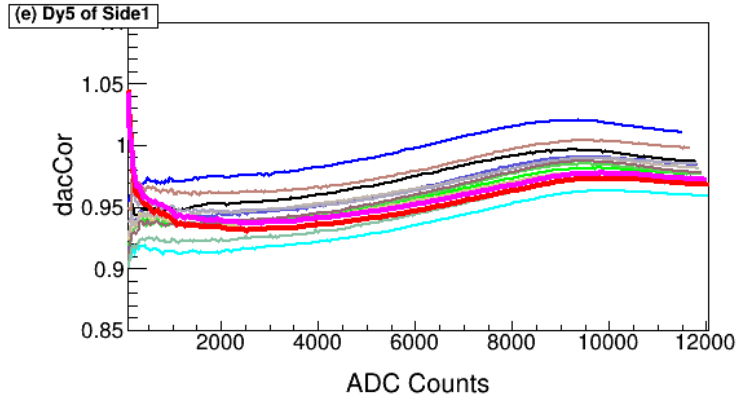

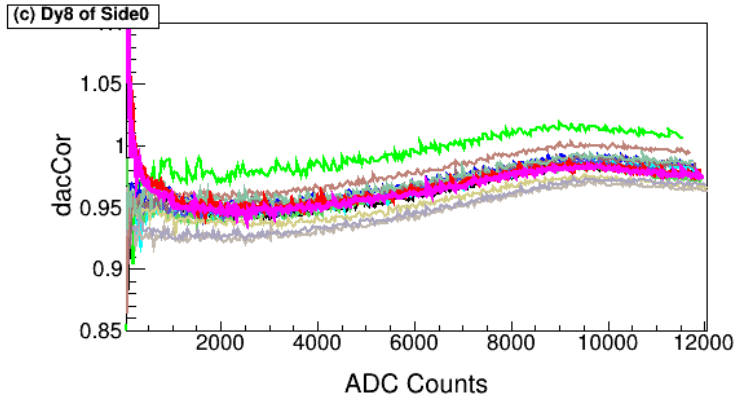

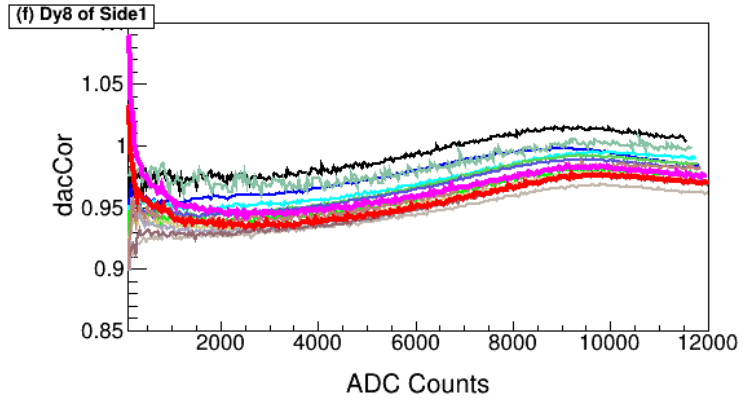

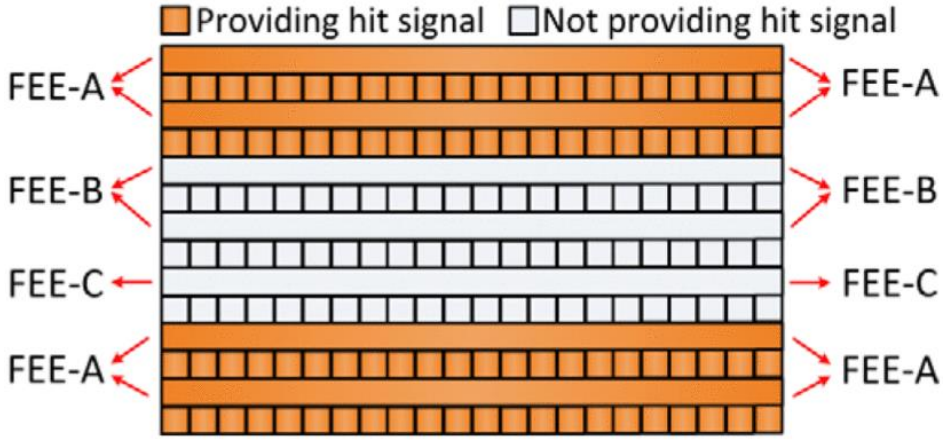

Helium MIP

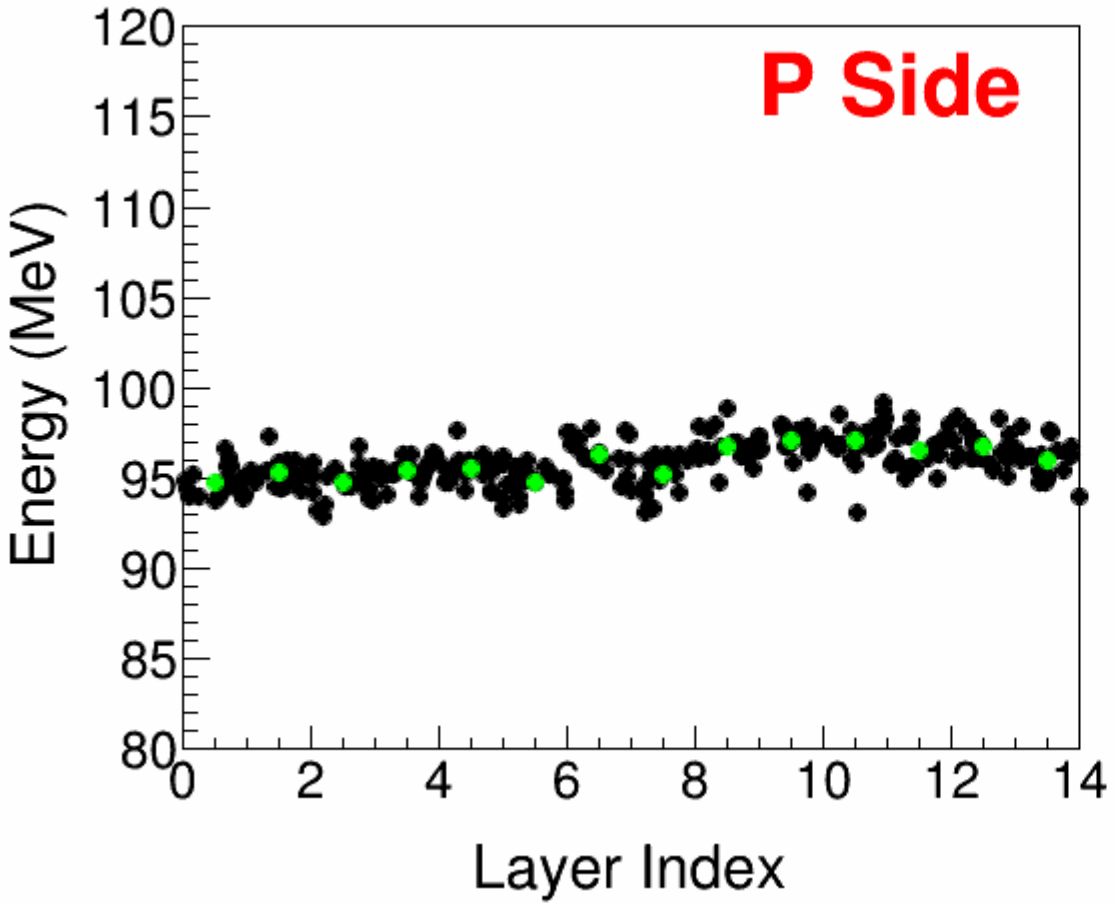
P Side
Energy (MeV)
Layer Index
120
115
110
105
100
95
90
85
80
0
2
4
6
8
10
12
14

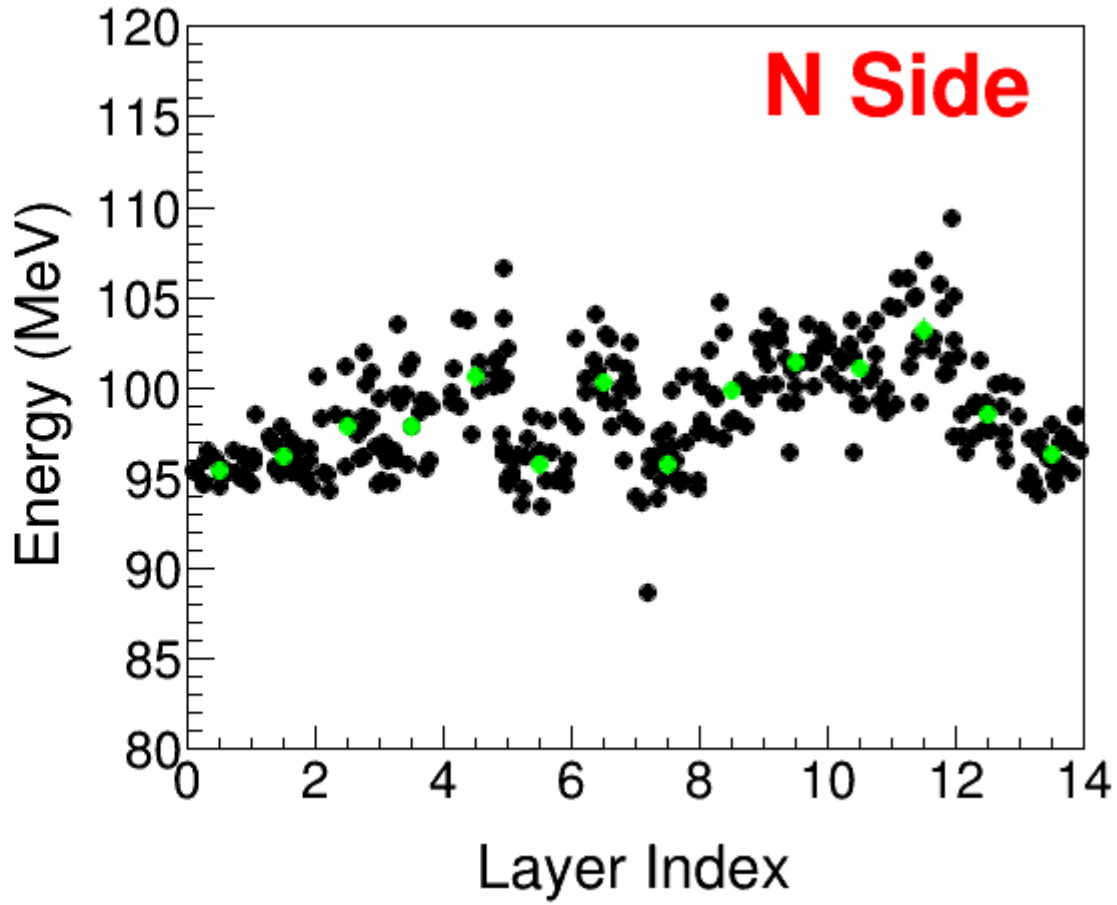
N Side
Energy (MeV)
Layer Index
120
115
110
105
100
95
90
85
80
0
2
4
6
8
10
12
14

MIPs Calibration

Helium MIPs Calibration

A Specific Bar

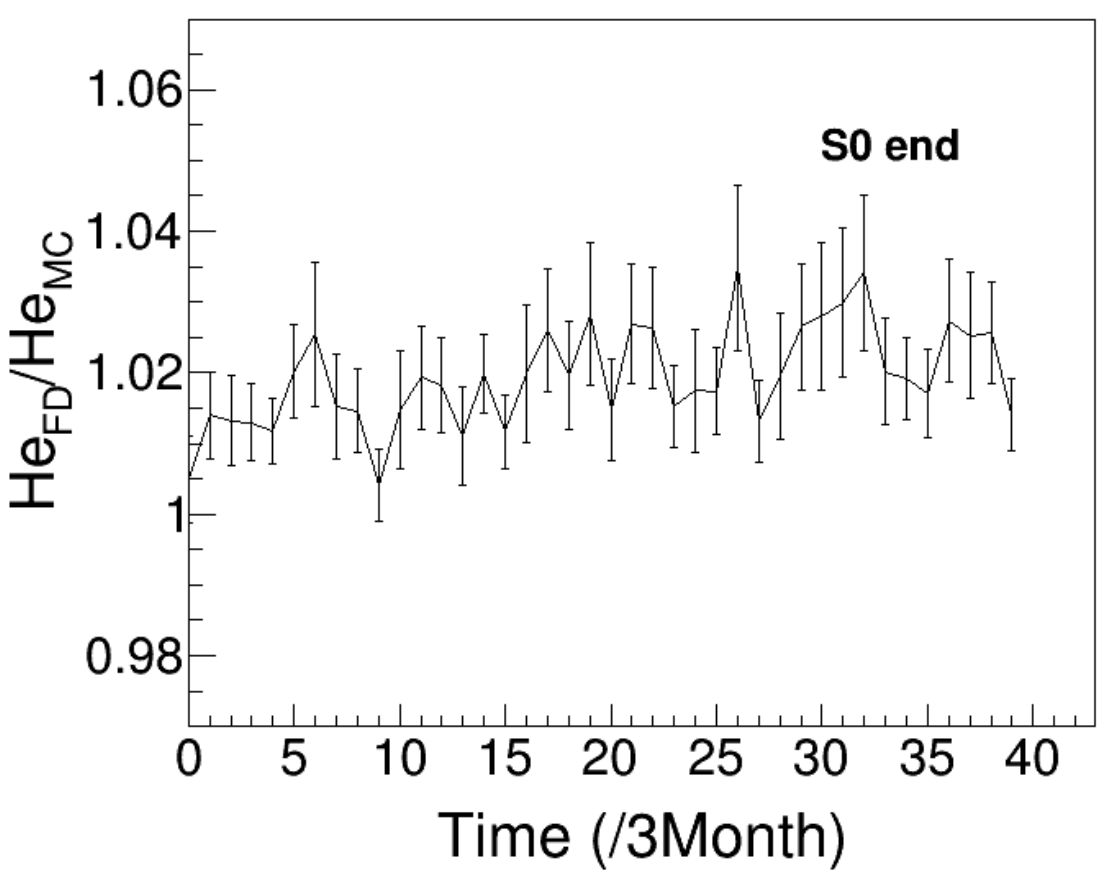

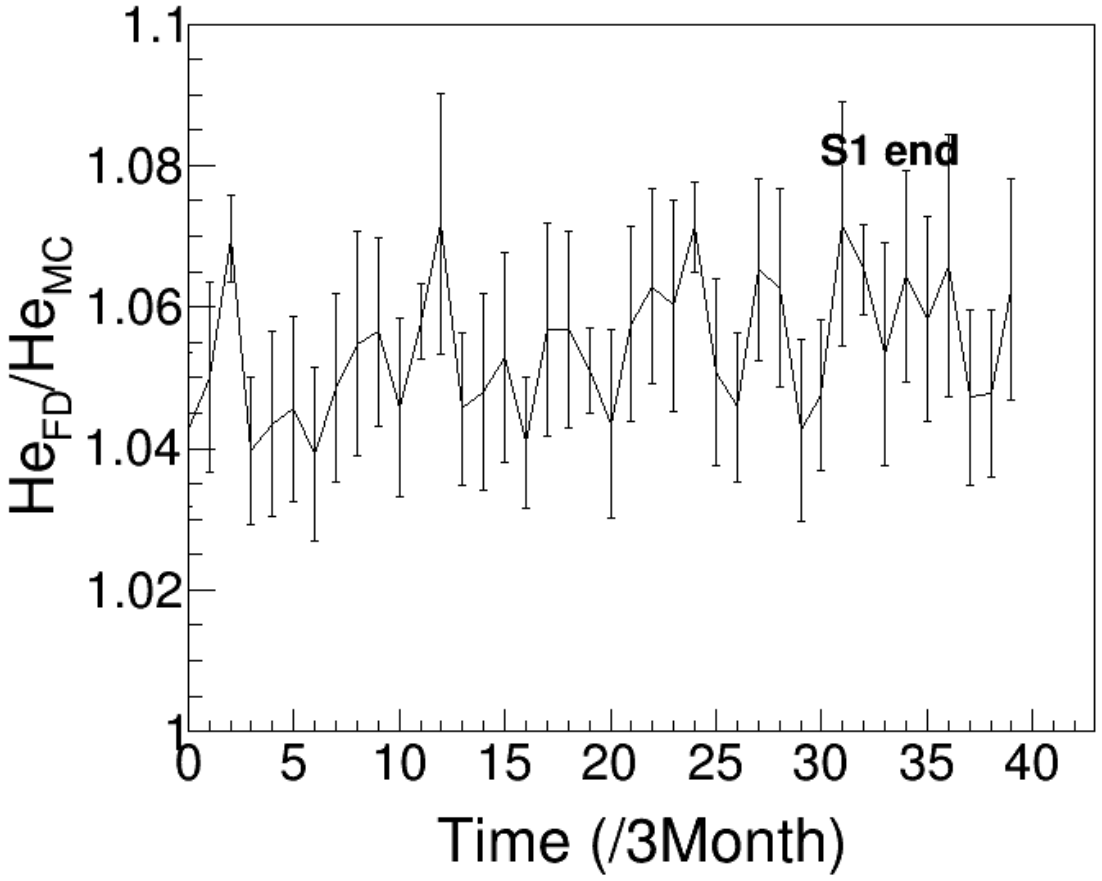

In practice, the $\mathbf{He_{MC}}$ value is replaced by the first-layer value derived from flight data collected during the initial three-month period.